DISS. ETH N. 27276

Managing Lake Kivu: moving from a steady-state to a dynamic modelling approach

A thesis submitted to attain the degree of

DOCTOR OF SCIENCES of ETH ZURICH

(Dr. sc. ETH Zurich)

presented by

FABIAN BÄRENBOLD

MSc in Environmental Sciences and Engineering, EPFL

born on 02.02.1988

citizen of Roggliswil, LU

accepted on the recommendation of

Prof. Dr. Rolf Kipfer, examiner

Dr. Martin Schmid, co-examiner

Prof. Dr. Bernhard Wehrli, co-examiner

Prof. Dr. Werner Aeschbach, co-examiner

2021

Table of content

Summary

Lake Kivu is a deep, meromictic lake in the East-African Rift Valley on the border between Rwanda and the Democratic Republic of the Congo (DRC). It is well-known for its huge reservoir of dissolved carbon dioxide and methane in the permanently stratified deep waters. The reason for this unusual gas reservoir is the intrusion of warm, saline, gas-rich and dense groundwater into the deep water of Lake Kivu. Besides providing carbon dioxide, the deep inflow of dense groundwater also maintains a strong density stratification, which prevents turbulent mixing. Consequently, the diffusive upward transport of carbon dioxide and methane, which is at least partially of biogenic origin, is very weak. For the surrounding population and their countries, the gas reservoir is a potential risk and a natural resource at the same time. Although the gases in the lake are currently still far away from saturation (below 55 %), an extreme mixing event could potentially bring deep water to the surface, where it would outgas and asphyxiate animals and humans in the surroundings. In contrast to the potential risk, the methane in Lake Kivu also represents a valuable energy resource for both Rwanda and the DRC.

In 2003, gas measurements indicated an increase of methane concentrations in the deep water of Lake Kivu by around 15 % within 30 years. This is a very fast increase for a lake whose deep water has a residence time of 800 – 1000 years, and therefore, these concerning findings greatly influenced the topics of this dissertation. Firstly, in spite of the increase in methane concentrations, there had been a lack of reliable gas measurements since 2003. Secondly, the one-dimensional lake model, which had previously been used to assess changes in gas concentrations and stratification, largely relied on a steady-state assumption. The model was therefore not adequate for the long-term transient simulation of scenarios with fast changing methane concentrations due to natural increase or large-scale gas extraction.

In the first part of this dissertation, we developed a measurement system for dissolved gases in Lake Kivu, involving a mobile mass spectrometer, which is designed to prevent gas loss during the sampling process. We successfully used the measurement system to assess carbon dioxide and methane concentrations in Lake Kivu as part of an intercomparison study with two other research groups. The results of this study indicate that methane concentrations have been close to a steady-state since at least 1974 and thus suggest that there is no increasing risk of a spontaneous gas eruption. In addition to measuring carbon dioxide and methane, we adjusted an existing measurement technique for dissolved noble gases to collect gas samples in the gas-

rich waters of Lake Kivu. The analysis of these measurements shows that atmospheric noble gases neon and krypton, and the light argon isotope ^{36}Ar are depleted by 50 – 70 % in the stratified deep waters. We argue that this depletion is most probably not caused by ebullition from the lake, but rather by the inflow of noble gas depleted groundwater. Furthermore, elevated noble gas ratios $^{3}He/^{4}He$ and $^{40}Ar/^{36}Ar$ corroborate the influence of magmatic gases on Lake Kivu.

In the second part of the dissertation, we developed and calibrated a one-dimensional lake model for Lake Kivu. In contrast to the previous model, the new model dynamically calculates mixing and the stratification depth of inflowing groundwater. It is therefore appropriate for the simulation of a changing lake over much longer timescales than before. The main finding of our simulation results is the fact that the currently observed density stratification and gas profiles are compatible with a simulation, which is initiated with a completely homogeneous and gas-free lake around 2000 years ago. This result confirms that the groundwater sources are the main driver of today's stratification and gas profiles.

Zusammenfassung

Der Kivusee ist ein tiefer, meromiktischer See im ostafrikanischen Graben, der auf der Grenze zwischen Ruanda und der Demokratischen Republik Kongo (DR Kongo) liegt. Er ist weltweit bekannt für sein enormes Vorkommen an Kohlendioxid und Methan, das gelöst im stabil geschichteten Tiefenwasser lagert. Der Grund für dieses ungewöhnliche Gasvorkommen ist der Zufluss von warmem, salz- und kohlendioxidreichem und daher dichtem Grundwasser direkt ins Tiefenwasser des Kivusees. Dieser Zufluss von dichtem Grundwasser sorgt für eine sehr stabile Dichteschichtung, die turbulente Mischung verhindert und den vertikalen Transport von Kohlendioxid und vornehmlich biologisch produziertem Methan praktisch unterbindet. Für die angrenzenden Länder und deren Bevölkerung ist das Gasvorkommen ein potentielles Risiko. Auch wenn der Gasdruck im See momentan noch weit von der Sättigung entfernt ist (unterhalb von 55 %), könnte ein ausserordentliches Mischereignis gasreiches Tiefenwasser an die Oberfläche bringen. Durch den fehlenden Wasserdruck an der Oberfläche würde ein grosser Teil der Gase entweichen und könnte für die in der Nähe des Sees lebenden Menschen und Tiere den Erstickungstod bedeuten. Im Gegensatz zur potentiellen Gefahr durch Ausgasen ist das Methanvorkommen aber auch eine wertvolle Energieressource für Ruanda und DR Kongo.

Im Jahr 2003 deuteten Gasmessungen darauf hin, dass die Methankonzentrationen im Tiefenwasser des Kivusees innerhalb von 30 Jahren um ungefähr 15 % angestiegen waren. Da die Aufenthaltszeit des Tiefenwassers im Kivusee bei 800 bis 1000 Jahren liegt, kann ein solcher Anstieg innerhalb eines Jahrhunderts zu gefährlich hohen Gaskonzentrationen führen. Dieser schnelle Anstieg hat die Themen der vorliegenden Dissertation stark beeinflusst. Erstens gibt es trotz des starken Methananstiegs seit 2003 keine neuen verlässlichen Gasmessungen im Kivusee. Und zweitens geht das eindimensionale Computermodell, das zum Simulieren der Veränderungen der Dichteschichtung und der Gaskonzentrationen im Kivusee angewandt wird, davon aus, dass sich die Gaskonzentrationen im Kivusee nahezu im Gleichgewicht befinden. Dieses Modell ist darum nicht gut geeignet, um längerfristige Szenarien mit schnell ansteigenden Methankonzentrationen (durch natürliche Produktion oder künstliche Gasextraktion) zu simulieren.

Im ersten Teil dieser Dissertation haben wir ein Messsystem entwickelt, das mittels Massenspektrometrie im Wasser gelöste Gase misst, ohne dass die Proben dabei Gas verlieren. Im Rahmen einer Vergleichsstudie mit zwei anderen Forschungsgruppen haben wir dieses Messsystem erfolgreich für die Bestimmung der Kohlendioxid- und Methankonzentrationen im

See verwendet. Unsere Resultate legen nahe, dass die Gaskonzentrationen seit mindestens 1974 nicht messbar angestiegen sind und deshalb heute keine erhöhte Gefahr durch Ausgasen besteht. Neben Kohlendioxid und Methan haben wir auch die Konzentrationen von gelösten Edelgasen mittels einer an gasreiches Wasser angepassten Methode zur in-situ Probenahme bestimmt. Unsere Messungen im Tiefenwasser zeigen, dass die atmosphärischen Edelgase Neon und Krypton und das atmosphärische Argon-Isotop ^{36}Ar im Vergleich zu luftgesättigtem Wasser zu ungefähr 50 – 70 % abgereichert sind. Die wahrscheinlichste Erklärung für diese unübliche Edelgas-Abreicherung ist nicht Ausgasen im See, sondern dass die magmatisch beeinflussten Grundwasserzuflüsse im Tiefenwasser ebenfalls abgereichert sind an Edelgasen. Der Einfluss von magmatischen Fluiden im Kivusee wird durch die erhöhten Edelgas-Isotopenverhältnisse $^{3}He/^{4}He$ and $^{40}Ar/^{36}Ar$ erhärtet.

Im zweiten Teil der Dissertation haben wir ein neues eindimensionales Computermodell für den Kivusee entwickelt und kalibriert. Im Gegensatz zum vorherigen Modell werden Mischungsprozesse und die Einschichttiefe von Grundwasserquellen dynamisch berechnet. Das neue Modell ist deshalb gut geeignet, um Simulationen eines sich verändernden Sees über lange Zeitskalen zu rechnen. Unsere Simulationsresultate zeigen, dass die momentan beobachtete Dichteschichtung und die Profile der Gaskonzentrationen kompatibel sind mit einer Simulation, die mit einem komplett homogenen und gasfreien See vor 2000 Jahren beginnt. Dieses Ergebnis bestätigt, dass die heutige Schichtung und Gasprofile ein Resultat der seit langer Zeit aktiven Grundwasserquellen im Kivusee sind.

Chapter 1

General Introduction

Lake Kivu

Lake Kivu is a large (2386 km^2) and deep (485 m) lake on the border between Rwanda and the Democratic Republic of the Congo (DRC) in Central-East-Africa, right at the feet of the Virunga volcano chain (Figure 1.1). It is famous worldwide for high carbon dioxide (CO_2) and methane (CH_4) concentrations of up to ~100 and ~20 mmol L^{-1} in the permanently stratified deep waters (Tietze, 1978; Schmid et al., 2005; Bärenbold et al., 2020a). The high gas concentrations can only be maintained due to the hydrostatic pressure and the strong density stratification, which prevents seasonal mixing in the deep waters.

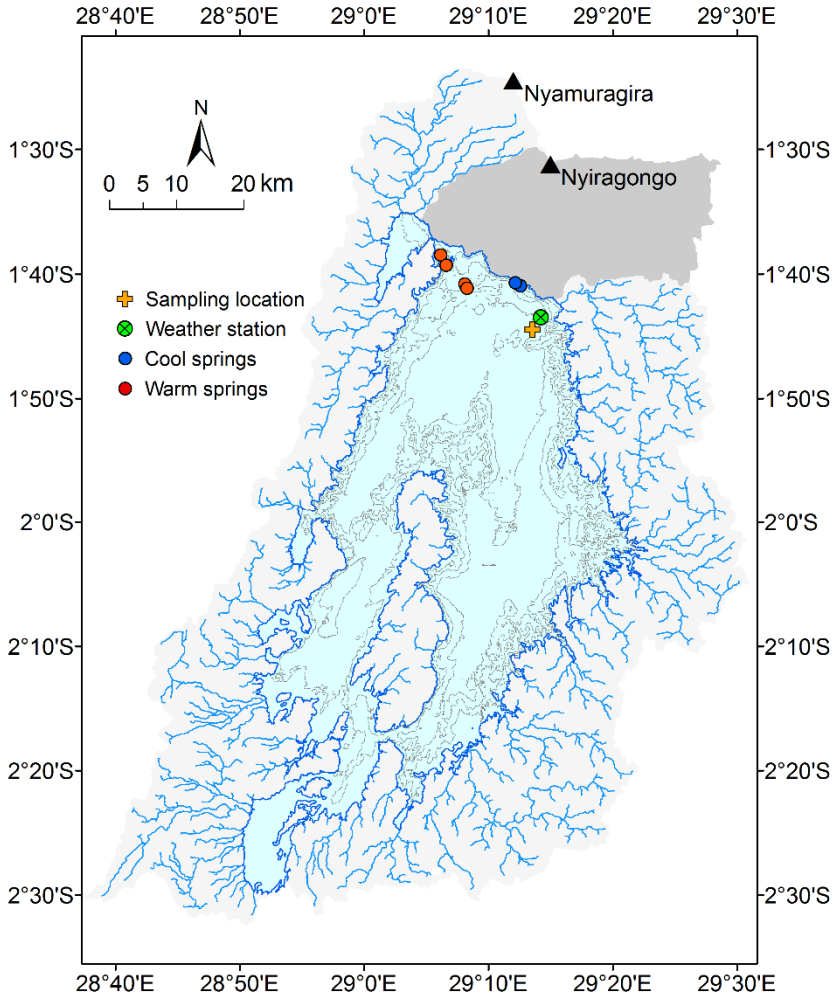

Figure 1.1. Map of Lake Kivu with contour lines every 100 m and tributaries. The region near to the Nyiragongo volcano does not have surface tributaries, but instead rainwater infiltrates and feeds groundwater aquifers. The inflow locations of cool and warm springs are indicated according to Ross et al., 2015a.

Geographically, Lake Kivu is part of the Western Branch of the East-African Rift System (EARS), which started to develop ~12 Mio. years BP (Chorowicz, 2005). After having a much lower lake level (~300 m below current level) and draining to the north into Lake Edward for a long time (Wood and Scholz, 2017), Lake Kivu underwent major changes ~10 - 12 ka BP. These changes include the blocking of its northern outflow by the Virunga volcano chain, and a lake level rise due to a wetter climate (Wood and Scholz, 2017) with subsequent drainage via the Ruzizi River to the south into Lake Tanganyika (Felton et al., 2007). It is believed that since ~3 ka BP, hydrothermal groundwater is entering the lake (Votava et al., 2017), and providing warm, saline and CO_2-rich water (Ross et al., 2015a), which subsequently stratifies close to the bottom of the lake. In addition to the hydrothermal groundwater, Ross et al. (2015a) also discovered two cooler, less saline sources in the upper part of the lake at ~100 – 190 and 250 m, respectively. The existence of hydrothermal springs, along with cooler sources at ~180 and ~250 m was already proposed before by Schmid et al., 2005 based on numerical modelling.

Lake Kivu's enormous gas reservoir is a direct consequence of the inflowing hydrothermal groundwater because the groundwater i) provides CO_2, and ii) maintains the density stratify-cation, which prevents seasonal mixing below a depth of ~60 m. This situation leads to very long residence times in the deep water (800 – 1000 years according to Schmid et al., 2005). Because of the long residence time, CO_2 and mainly biologically produced CH_4 can accumulate in the deep water of Lake Kivu either until they reach a steady-state between inflow, production and upward transport, or until an unusually deep mixing takes place and releases the gases to the atmosphere. Such gas eruptions have happened in the past at gas-rich lakes Nyos (Kling et al., 1987) and Monoun (Sigurdsson et al., 1987) with 1746 and 37 casualties due to asphyxiation, respectively. Sediment cores from Lake Kivu show that deep mixing events have happened several times in the last 3 ka, with the latest event around 1000 years ago (Ross et al., 2015b; Votava et al., 2017; Uveges et al., 2020). In addition, up to 9 smaller mixing events are believed to have happened during the last 2000 years (R. Hecky, pers. comm.).

Besides representing a potential risk, the CH_4 reservoir in Lake Kivu is a valuable resource for the neighboring countries Rwanda and DRC. Since 2015, the first large-scale methane extraction plant is in operation. "KivuWatt Limited", which is a subsidiary of the US-based company ContourGlobal, draws water from 350 m, extracts the CH_4 in a degassing chamber just below the lake surface, and reinjects the almost CH_4-free water at 240 m. The cleaned CH_4 gas is subsequently used to provide 26 MW of electricity to the Rwandan grid. According to projections, several hundreds of MW could be installed in the future (Expert Working Group on Lake Kivu Gas Extraction, 2009) or alternatively extracted gas could be used as cooking

fuel. Such artificial gas extraction is not only beneficial for the surrounding countries, but also reduces the risk of a gas eruption because CH_4, due to its low solubility, accounts for ~80 % of total gas pressure in Lake Kivu.

Origin, transport and fate of gases in Lake Kivu

In contrast to the mostly geogenic origin of CO_2 in Lake Kivu, the analysis of ^{14}C-CH_4 by both Schoell et al. (1988) and Pasche et al. (2011) indicates that below 250 m, only ~66 % of the CH_4 is composed of old ^{14}C-dead carbon. Both authors suggest that the remaining ~33 % are produced by microbial degradation of settled organic matter at the sediment-water interface. Pasche et al. (2011) further argue that part of the substrate for CO_2 reduction consists of H_2, which is provided by the degradation of organic matter. As a consequence, the decomposition of organic matter can be indirectly responsible for an additional ~17 % of CH_4 production. So in total, Pasche et al. (2011) attribute ~50 % of CH_4 to the degradation of organic matter. The remaining 50 % could either be due to CO_2 reduction using geogenic CO_2 (and an unknown source of H_2), or the input of geogenic CH_4 by the hydrothermal groundwater sources. Above 250 m (i.e. above the main gradient), Pasche et al. (2011) found that the isotopic composition of CH_4 can be well explained by attributing all CH_4 production to the decomposition of organic matter. The different origin of CH_4 below and above 250 m is a result of the major groundwater source at ~250 m, which strongly dilutes the upwelling hydrothermal water

Due to the completely anoxic and sulphate-free deep water, there is no known process which could consume CH_4 below ~60 m. Thus, the only known sink of CH_4 in Lake Kivu is microbial oxidation at the oxycline, the depth of which varies seasonally between 20 and 60 m (Morana et al., 2015). As a result of microbial oxidation, only a small fraction of upward transported CH_4 can reach the atmosphere (Borges et al., 2011). In contrast, CO_2 has a possible deep water sink due to microbial reduction to CH_4 using H_2. However, this consumption of CO_2 would be small because CO_2 is around five times more abundant than CH_4 and only part of the CH_4 can be produced from geogenic CO_2 (Pasche et al., 2011).

While the origin and fate of CO_2 and CH_4 in Lake Kivu differ, they are affected by the same diffusive and advective transport processes. Diffusive mixing in Lake Kivu is a strong function of depth as only the top 30 – 60 m are usually affected by seasonal mixing (Figure 1.2). Below the seasonally mixed layer, the strong vertical density gradient suppresses wind induced turbulent mixing. Consequently, vertical mixing is much slower than horizontal mixing, and

Lake Kivu can be assumed to be horizontally mixed, as evidenced by well-matching temperature and salinity profiles in different parts of Lake Kivu (Ross et al., 2015a).

In the near absence of wind-induced mixing below ~60 m, two other mechanisms are mainly responsible for the vertical transport of gases, heat and salts in Lake Kivu. Firstly, there is a slow, depth-dependent upwelling of the whole water column due to the inflow of groundwater. In total, these groundwater inflows provide around 40 % (41 $m^3 s^{-1}$) of the total inflow into Lake Kivu (Schmid & Wüest, 2012) with the rest stemming from small surface tributaries (Muvundja et al., 2014). Around 90 % of the groundwater enters the lake as cool and fresh water at ~190 and ~250 m, while the hydrothermal groundwater contributes only 10 % to the total groundwater inflow (Schmid et al., 2005). The resulting magnitude of the upwelling is estimated to be between 0.15 and 0.8 m yr^{-1}, depending on lake depth (Pasche et al., 2009).

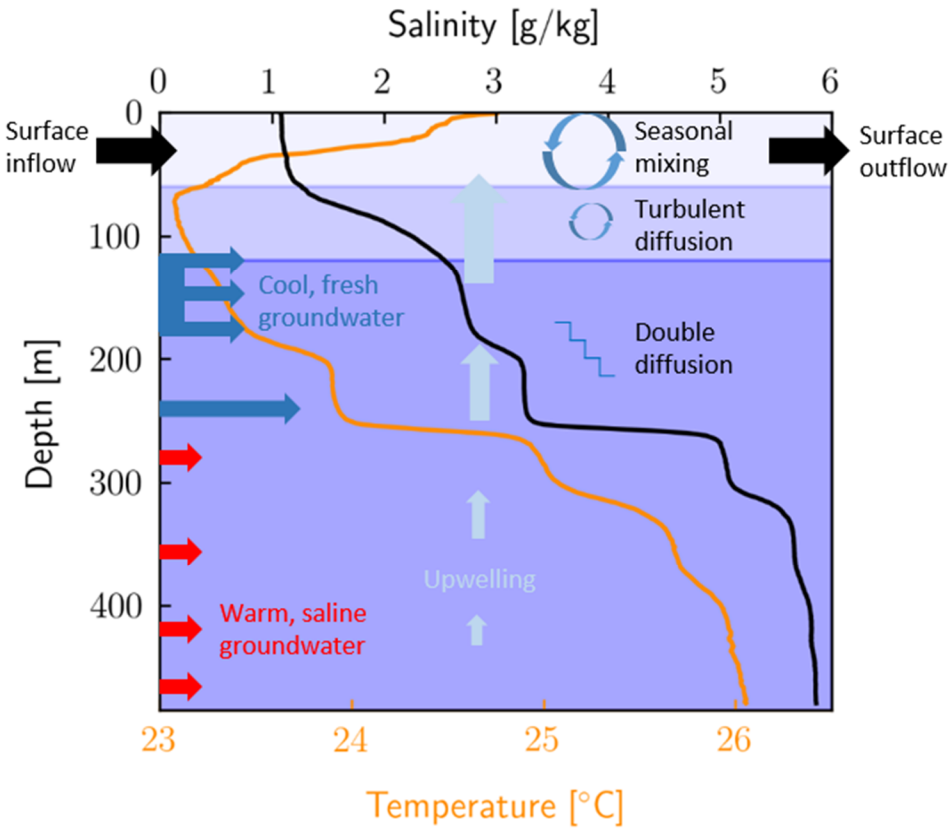

Figure 1.2. Schematic overview of advective and diffusive transport processes in Lake Kivu. The temperature and salinity profiles are the background profiles from Lake Kivu measured by Ross et al., 2015a.

Secondly, Lake Kivu exhibits a peculiar feature below 120 m down to its maximum depth of 485 m. More than 300 small mixed layers with an average thickness of ~70 cm and sharp, thin gradients in between form a staircase-like structure (Newman, 1976; Schmid et al., 2010;

Sommer et al., 2013). This phenomenon is commonly referred to as diffusive-type of double diffusive convection, and it is caused by the concurrent increase with depth of temperature on the one hand, and dissolved substances (salinity and gases) on the other hand. Temperature and dissolved substances have a contrary effect on density and a very different molecular diffusion coefficient, which is a prerequisite for the presence of the diffusive-type of double diffusion (see Kelley et al., 2003 or Wüest et al., 2012 for a review). Vertical transport through double diffusive staircases is governed by molecular diffusion across the thin interfaces (Sommer et al., 2013), and therefore, the transport of heat is much faster than the transport of salinity and gases, whose molecular diffusivities are around two orders of magnitude lower. In order to compare the effect of double diffusion on temperature, salinity and gases, we can introduce the concept of apparent diffusivity, which is the flux of an agent divided by its background gradient (i.e. smoothing out the staircases). For Lake Kivu, Sommer et al., 2019 calculated that the apparent vertical diffusivity of temperature is on average ~30 times larger than the apparent diffusivity of salinity. This results in a situation where the vertical transport of temperature is governed by both double diffusive convection and advection, while the transport of salinity, CO_2 and CH_4 is largely dominated by advection.

Between the seasonally mixed layer above 60 m and the double-diffusive region below 120 m, there is a depth region which is neither affected by seasonal mixing, nor by double-diffusive convection (Figure 1.2). In this depth region, diffusive transport is assumed to be weak as a result of the strong density gradient (Schmid et al. 2005). However, the analysis of stable water isotopes ^{2}H and ^{18}O by Ross et al. (2015a) indicated that mixing might be stronger than previously thought. In fact, the latter observed evaporative isotope signals penetrating deep into Lake Kivu, thereby exhibiting a seemingly smooth, mixing-induced decrease with depth. To date, there is no quantitative analysis of turbulent diffusion in this depth region.

Evolution of gas concentrations

The precise quantification of gas concentrations and gas saturation is an important measure to assess the risk of a potential gas eruption at Lake Kivu. Gas saturation is the ratio between dissolved gas pressure and local absolute pressure (hydrostatic and atmospheric pressure). It determines by how much a water parcel can be lifted without creating bubbles and potentially trigger a gas eruption. However, measuring gas concentrations in Lake Kivu is challenging

because the high dissolved gas pressure leads to the loss of most of the gas content from water samples at atmospheric pressure.

Several researchers have attempted to assess gas concentrations in Lake Kivu in the past with variable success. In 1935, Damas measured CO_2 and H_2S in samples after they degassed under atmospheric conditions. He therefore lost more than half of the CO_2 originally contained in the sample water (Damas, 1938). Between 1952 and 1954, Schmitz and Kufferath performed the first CH_4 measurements in Lake Kivu. However, they only quantified the fraction of CH_4 and CO_2, which outgassed under atmospheric conditions. While neglecting the gas fraction remaining in the sample water gave accurate results for the insoluble CH_4, the more soluble CO_2 was strongly underestimated (Schmitz and Kufferath, 1955). In 1974, K. Tietze used a sophisticated method to measure both CH_4 and CO_2 in the gas and the water phase of water samples and produced reliable and complete gas profiles (Tietze, 1978).

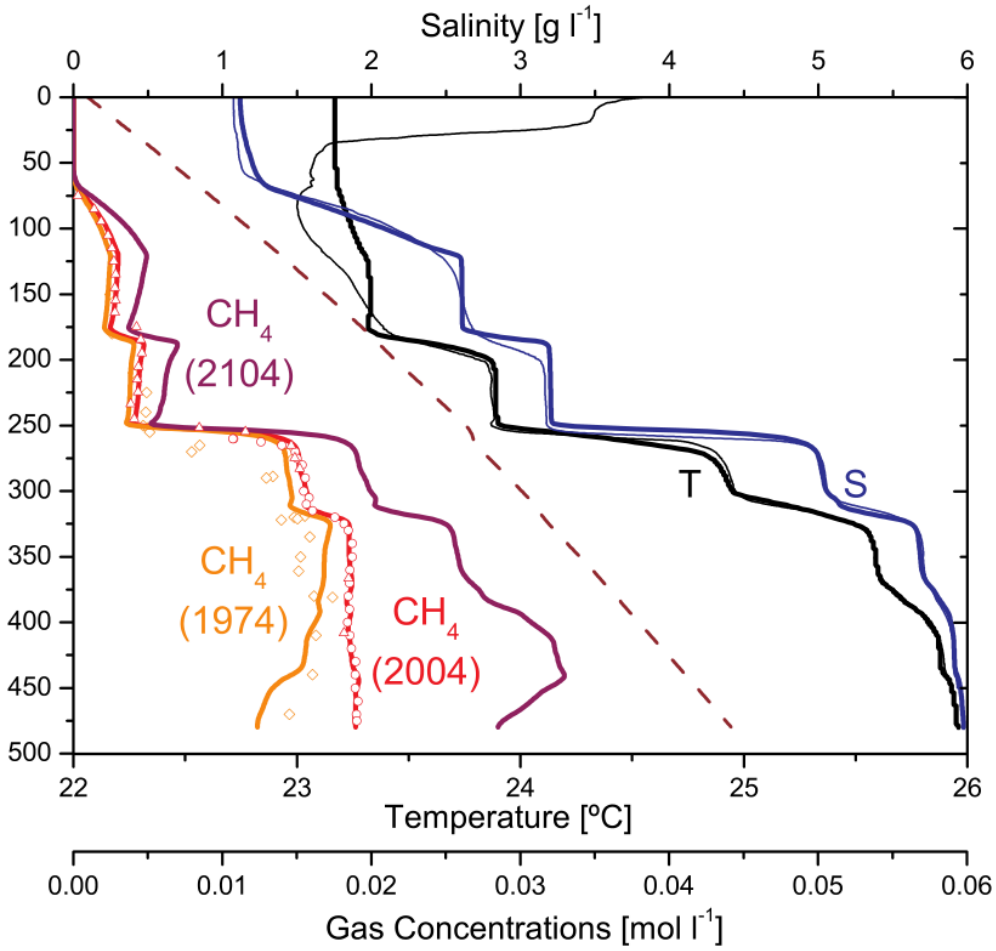

Figure 1.3. This Figure is reproduced from Schmid et al., 2005 and shows modelled CH_4 concentrations in 1974, 2004 and 2104 (thick lines) based on the trend calculated from the difference between the measurements by Tietze in 1974 (orange symbols, Tietze, 1978) and Halbwachs & Tochon in 2003/04 (red symbols, Schmid et al., 2005). Based on these measurements and modelling results, Schmid et al., 2005 suggested that CH_4 concentrations are increasing and that the inflow of hydrothermal groundwater is responsible for the warm and saline water below 250 m. (Schmid et al., 2005, Weak mixing in Lake Kivu: New insights indicate increasing risk of uncontrolled gas eruption, Geochemistry, Geophysics & Geosystems, Copyright 2005 by the American Geophysical Union).

From the first measurements in 1935 (Damas, 1938) to the data of Tietze in 1974 there was no clear temporal trend in observed gas concentrations. In 2003 however, the measurements of M. Halbwachs & J.-C. Tochon (published in Schmid et al., 2005) indicated that CH_4 concentrations had increased by ~15 % in the deep water within 30 years (i.e. since the measurements of Tietze in 1974, see Figure 1.3).

Numerical modelling

In view of increasing CH_4 concentrations (Schmid et al., 2005) and increasing temperature (summarized in Sommer et al., 2019), Schmid et al., 2005 developed a one-dimensional lake model for Lake Kivu using the software Aquasim (Reichert et al., 1994) to predict the future evolution of Lake Kivu's density stratification and gas concentrations. They found that if the observed trend from 1974 (Tietze, 1978) to 2003 continues, gas pressure could approach saturation at some depths within the 21st century (Schmid et al., 2005). The model was later extended and used to assess the future evolution of gas concentrations and nutrient availability as a function of different gas extraction scenarios (Wüest et al., 2009; Schmid et al., 2019). However, this model has several deficiencies, namely that i) turbulent mixing is fixed to constant values above 120 m and therefore does not adjust as a function of a changing density stratification in the lake, ii) vertical transport across the double diffusive staircases is parameterized based on data which underestimate the heat flux by a factor of 2 – 20 (Sommer et al., 2019), and iii) the groundwater inflows enter the lake at fixed depths instead of stratifying as a function of density.

Because of these simplifying assumptions, the model is not suitable for simulations with potentially large changes in lake stratification and gas concentrations over longer timescales. In view of a naturally changing lake and large-scale gas extraction projects, the need arises for a model which is able to simulate the future long-term evolution of Lake Kivu in potentially changing conditions. The most important requirements for such a model are that i) diffusive mixing is dynamically calculated over the whole depth range and ii) the stratification depth of inflowing groundwater is calculated as a function of density.

Outline and objectives of this dissertation

Since the measurements of Halbwachs & Tochon in 2003 (published in Schmid et al., 2005), which suggested a yearly increase of CH_4 concentrations of ~0.5 %, no reliable gas measurements have been performed. Therefore, one major objective of this dissertation was to produce a precise and reliable dataset of gas measurements in Lake Kivu (chapter 2). For this goal, we used the mobile mass spectrometer "MiniRuedi", which was recently developed at Eawag. The "MiniRuedi" allows the simultaneous quantification of several gases, and therefore, besides CH_4 and CO_2, we tried to quantify noble gas concentrations in Lake Kivu. Noble gases can shed light on gas and water transport processes, but existing noble gas data in Lake Kivu (Tassi et al., 2009) seems to be affected by sampling artefacts, e.g. the addition of air as indicated by the reported oversaturation of oxygen, nitrogen and argon, which appear highly unlikely for the anoxic deep water of Lake Kivu. To verify the noble gas data from the "MiniRuedi", we used an established noble gas measurement technique with copper tubes to store sample water for subsequent analysis in the noble gas laboratory at ETH (Beyerle et al. 2000). We adapted this measurement technique to the special, gas-rich conditions in Lake Kivu, where water samples need to be preserved under pressure to avoid gas loss during sampling. The results of this study are presented and discussed in chapter 3.

In the second part of this dissertation, we propose a new modelling approach using the one-dimensional k-ε model Simstrat (Goudsmit et al., 2002). In a k-ε model, the turbulent energy k and its dissipation rate ε are modelled explicitly as state variables, which allows the dynamic calculation of turbulent mixing, based on the current physical lake properties. As a part of this dissertation, Simstrat was coupled to the biogeochemical library AED2 in order to enable the simulation of dissolved gases and nutrients. The Simstrat-AED2 model has the following advantages over the model developed by Schmid et al., 2005: i) turbulent mixing is dynamically calculated above 120 m using meteorological data and Simstrat's k-ε turbulence closure; ii) vertical transport across the double diffusive staircases is parameterized using updated measurements (Sommer et al., 2013) and iii) the groundwater inflows are allowed to plunge/rise as a function of their density in relation to that of the surrounding lake water. In chapter 4, we present this model and we use it to shed light on the properties and origin of the groundwater sources. In addition, we perform long-term simulations to find out, whether the currently observed profiles can be reproduced starting with a completely homogeneous and degassed lake. This leads to the following structure of the thesis:

Chapter 2: No increasing risk of a limnic eruption at Lake Kivu: intercomparison study reveals gas concentrations close to steady state

In this chapter, we present our CO_2 and CH_4 measurements, along with the measurements of two other research teams (Helmholtz Centre for Environmental Research - UFZ and the Centre national de la recherche scientifique - CNRS). Eawag separated the gas and water phase of continuously flowing sample water in order to analyze the gas content of both phases using a mobile mass spectrometer. UFZ took in-situ water samples using gas-tight bags, filled by a small pump with a remote control. The bags were later analyzed using gas chromatography. In addition, UFZ also recorded in-situ gas pressure measurements. Finally, CNRS used a prototype in-situ laser spectrometer to measure CH_4 partial pressure in the top 150 m. To compare concentrations to partial pressure, we developed a conversion method, which is suitable to the gas-rich, high-pressure environment in Lake Kivu. Our results show a good agreement between the different measurement techniques (within 5 – 10 %). However, in contrast to the measurements of Halbwachs & Tochon (in Schmid et al., 2005) we did not observe an increase in CH_4 concentrations, and we conclude that the gas concentrations in Lake Kivu are currently close to a steady-state. This chapter has been published in PlosOne (Bärenbold et al., 2020a) and the results of this study have also been published in a technical report to the Rwandan government (Schmid et al., 2019).

Chapter 3: Missing atmospheric noble gases in a large, tropical lake: the case of Lake Kivu, East-Africa

Here, we present depth profiles of noble gases He, Ne, ^{36}Ar and Kr, as well as isotope ratios ^{3}He/^{4}He, ^{20}Ne/^{22}Ne and ^{40}Ar/^{36}Ar. This dataset was collected by adjusting an existing measurement technique to analyze water samples in copper tubes (Beyerle et al., 2000) to work under the challenging conditions in Lake Kivu. Our results show that the atmospheric noble gases Ne, ^{36}Ar and Kr are depleted by 50 – 70 % in Lake Kivu's deep water below 250 m. In addition, the elevated noble gas ratios ^{3}He/^{4}He and ^{40}Ar/^{36}Ar indicate the presence of magmatic gases. We developed three scenarios to explain the observed noble gas depletions in the lake. Among these, significant continuous outgassing is excluded based on the absence of a fractionation pattern in the ^{20}Ne/^{22}Ne depth profile. In contrast, the good correlation between the increase of salinity and He concentration with depth, and the simultaneous decrease of atmospheric noble gas concentrations suggest that these patterns are caused by the same mechanism. We concluded that noble gas concentrations in the hydrothermal groundwater sources feeding Lake

Kivu are likely depleted. This chapter has been published in Chemical Geology (Bärenbold et al., 2020b).

Chapter 4: Dynamic modelling gives new insights into development and maintenance of Lake Kivu's density structure

In this chapter, we present results from long-term simulations of Lake Kivu using a newly developed one-dimensional model. The model was calibrated using existing salinity and temperature data, and the vertical diffusive transport across double diffusive staircases was parameterized based on microscale measurements of temperature and salinity from Sommer et al. (2013). The properties (i.e. discharge, inflow depth, temperature, salinity and gas concentrations) of the groundwater inflows were calibrated manually with the goal of deriving a steady-state simulation which reproduces today's observations. The model was forced by meteorological data from the regional climate model MiroC5, which was adjusted to Lake Kivu using a time series of 7 years from a local weather station. We successfully produced a steady-state model, which agrees very well with currently observed salinity and gas concentrations and fairly well for temperature. Furthermore, using ^{3}H tracer data, we could show that the cooler groundwater sources, which enter the lake at ~190 and 250 m are probably a mixture of old, hydrothermal groundwater and recently infiltrated rainwater. Finally, our long-term simulations suggest that the current profiles can be reproduced starting from a homogeneous, degassed lake ~1500 – 2000 years ago. This chapter is in preparation for a submission in Journal of Geophysical Research Biogeosciences.

In **chapter 5**, we provide a short synthesis of the main findings of chapters 2 to 4. In addition, we suggest future applications of our model and further research directions.

Chapter 2

No increasing risk of a limnic eruption at Lake Kivu: intercomparison study reveals gas concentrations close to steady state

Fabian Bärenbold[1]*, Bertram Boehrer[2], Roberto Grilli[3], Ange Mugisha[4], Wolf von Tümpling[2], Augusta Umutoni[4], Martin Schmid[1]

[1]*Eawag, Swiss Federal Institute of Aquatic Science and Technology, Surface Waters - Research and Management, Kastanienbaum, Switzerland*

[2]*Helmholtz-Centre for Environmental Research – UFZ, Magdeburg, Germany*

[3]*CNRS, Université Grenoble Alpes, IRD, Grenoble INP, Institut des Géosciences de l'environnement, Grenoble, France*

[4]*Lake Kivu Monitoring Programme LKMP, Gisenyi, Rwanda*

**Corresponding author:*
Email: fabian.baerenbold@eawag.ch

This chapter has been published as:

Bärenbold, F., Boehrer, B., Grilli, R., Mugisha, A., von Tümpling, W., Umutoni, A., & Schmid, M. (2020). No increasing risk of a limnic eruption at Lake Kivu: Intercomparison study reveals gas concentrations close to steady state. *PloS one*, *15*(8), e0237836. https://doi.org/10.1371/journal.pone.0237836

Abstract

Lake Kivu, East Africa, is well known for its huge reservoir of dissolved methane (CH_4) and carbon dioxide (CO_2) in the stratified deep waters (below 250 m). The methane concentrations of up to ~ 20 mmol/l are sufficiently high for commercial gas extraction and power production. In view of the projected extraction capacity of up to several hundred MW in the next decades, reliable and accurate gas measurement techniques are required to closely monitor the evolution of gas concentrations. For this purpose, an intercomparison campaign for dissolved gas measurements was planned and conducted in March 2018. The applied measurement techniques included on-site mass spectrometry of continuously pumped sample water, gas chromatography of in-situ filled gas bags, an in-situ membrane inlet laser spectrometer sensor and a prototype sensor for total dissolved gas pressure (TDGP). We present the results of three datasets for CH_4, two for CO_2 and one for TDGP. The resulting methane profiles show a good agreement within a range of around 5 – 10% in the deep water. We also observe that TDGP measurements in the deep waters are systematically around 5 to 10 % lower than TDGP computed from gas concentrations. Part of this difference may be attributed to the non-trivial conversion of concentration to partial pressure in gas-rich Lake Kivu. When comparing our data to past measurements, we cannot verify the previously suggested increase in methane concentrations since 1974. We therefore conclude that the methane and carbon dioxide concentrations in Lake Kivu are currently close to a steady state.

Introduction

Lake Kivu, with a surface area of 2386 km^2 and a maximum depth of 485 m, is situated on the border between Rwanda and the Democratic Republic of the Congo (DRC). Along with other African great lakes Tanganyika and Malawi, Lake Kivu is part of the East African Rift System (EARS). To the north, Lake Kivu borders on the Virunga volcano chain, while to the South it drains into Lake Tanganyika via the Ruzizi River. Lake Kivu is fed by numerous small streams (Muvundja et al., 2014) and by subaquatic groundwater sources (Ross et al., 2015a) with the latter contributing about 45 % of the total inflow. The groundwater sources mainly enter the lake at the northern shore and can be divided into two categories: two cool and fresh sources above a depth of 260 m and several warm, saline and carbon dioxide (CO_2)-rich sources below 260 m. This has two main consequences, namely a very stable density stratification due to the salinity gradient, which prevents annual mixing below a depth of 50 to 60 m and the accumulation of dissolved CO_2 over long time scales. In addition to CO_2, biogenic methane (CH_4) is present in the deep waters in large amounts due to decomposition of organic matter at the lake bottom and CO_2 reduction (Schoell et al., 1988; Pasche et al., 2011).

Gas concentrations in Lake Kivu were first recorded by Damas in 1935 (Damas, 1938) who measured CO_2 and H_2S. However, Damas only analyzed the sample water after degassing, thus losing more than half of the CO_2 to the atmosphere. Between 1952 and 1954, Schmitz and Kufferath carried out the first CH_4 measurements and additionally determined CO_2 concentrations. However, they only analyzed the gas that outgassed under atmospheric conditions, neglecting the gas remaining dissolved in the water (Schmitz & Kufferath, 1955). In 1974, Tietze performed the first comprehensive survey of dissolved gas concentrations, including CH_4 and CO_2 from both the gas exsolved under atmospheric conditions and the remaining part in the sample water (Tietze, 1978). Tietze concluded that about 300 km^3 STP (gas volume at 0°C and 1 atm) of CO_2 and 60 km^3 STP of CH_4 were stored in the permanently stratified deep waters (below ~ 60 m) of Lake Kivu (Tietze, 1978). Subsequently, based on new measurements from M. Halbwachs and J.-C. Tochon in 2003 (published in Schmid et al., 2005), Schmid et al. (2005) suggested that CH_4 concentrations had increased by 15 % since 1974 and that they could possibly reach saturation within the 21st century. With the examples of deadly limnic eruptions due to high gas loads in Lakes Nyos (Kling et al., 1987) and Monoun (Sigurdsson et al., 1987), it was clear that the gas concentrations of Lake Kivu needed to be monitored. Besides the threat to the local population, the gas content in Lake Kivu also represents a valuable resource: In December 2015, a 26 MW gas power plant was connected to the Rwandan grid and several

hundred MW could follow according to projections (Expert Working Group on Lake Kivu Extraction, 2009).

In 2017, a gas intercomparison campaign was initiated by the Lake Kivu Monitoring Programme (LKMP) with the goal of 1) accurately determining CH_4 and CO_2 concentrations using different methodologies and 2) finding an appropriate technique to regularly monitor the gas concentrations in the future. However, gas sampling in highly outgassing environments is challenging and thus, the measurement methods had to be adapted accordingly. In this work, we describe the methodologies for three research teams involved in the campaign: The Swiss Federal Institute of Aquatic Science and Technology (Eawag), the Helmholtz Centre for Environmental Research (UFZ) and the National Center of Scientific Research in France (CNRS). Subsequently, we present the results of each group and compare them to the previous measurements of Tietze in 1974 (Tietze, 1978) and Halbwachs and Tochon in 2003 and Schmid in 2003 (both published in Schmid et al., 2005). Finally, we reevaluate the gas (CH_4 and CO_2) content in Lake Kivu and its potential change in time.

Materials and methods

The intercomparison campaign took place close to Gisenyi/Rubavu, Rwanda (1.74087°S / 29.22602°E) from 9 to 13 March 2018 and involved research teams from Eawag, UFZ, CNRS and from the power plant operator KivuWatt. Eawag prolonged its measurement period until 18 March and UFZ also included earlier measurements from 2017. The campaign was planned and organized by LKMP and therefore, no special permit was necessary to perform measurements on the lake. Further details on the results of the campaign can also be found in a report to LKMP (Schmid et al., 2019). Note that while the report includes the measurements of KivuWatt, the latter decided to not be part of this publication.

The measurements taken by each research team are summarized in Table 2.1. In this publication, only the approach of Eawag is explained more comprehensively, while further details on the methods of UFZ and CNRS can be found elsewhere (Boehrer et al., 2019; Grilli et al., 2018). In the following, we will first present the methodology of Eawag and then shortly summarize the approaches of UFZ and CNRS.

Table 2.1. Summary of gas measurements performed by the different research teams of Eawag, UFZ and CNRS.

	CH_4 0 – 150 m	CH_4 150 – 450 m	CO_2	TDGP
Eawag	-	+	+	-
UFZ	-	+	+	+
CNRS	+	-	-	-

The "+" indicates which measurements were performed by which groups.

Measurement method used by Eawag

The measurement setup was built around "MiniRuedi", a gas-equilibrium portable membrane-inlet mass spectrometric system (GE-MIMS) which allows on-site quantification of different dissolved gases in water (i.e. N_2, O_2, CO_2, CH_4, He, Ar, see Brennwald et al., 2016). The continuous sampling water flow (~ 1 L/min) required to maintain gas equilibrium at the MS inlet was provided by a submersible pump (0.75 kW, Lechner Pumpen) and 250 m long, 6 mm inner diameter polyamide (PA) tubing. The pump was used only above 250 m and yielded a flow of ~ 1.6 L/min. Below 250 m, TDGP increases drastically and, following initiation of the flow by a suction pump at the surface, the buoyancy due to bubble formation within the tube was sufficient to lift the water to the surface. 10 mm PA tubing was used in this case and the resulting flow was ~ 1 L/min (except between 270 and 310 m where it was ~ 0.5 L/min only). The water-gas mixture was subsequently dispersed through a nozzle into a custom-made cylindrical equilibration chamber (12.3 cm diameter, 38 cm height, see Figure A1 in Appendix A). While the degassed sample water accumulated and discharged at the bottom of the chamber, the gas phase stayed above and left the chamber through a tube at the top. The gas content in the gas phase and the water phase (via a headspace created by the membrane contactor Liqui-Cel G542, 260 cm^3 external volume) was analyzed by the "MiniRuedi". Finally, gas and water flow rates were recorded to compute in-situ gas concentrations in the lake as sketched in Figure A1 in Appendix A. The overall analytical accuracy (i.e. the maximum deviation from the true value) of the setup was deduced from the accuracies of its individual components and estimated to around ± 5 % for CO_2 and ± 10% for CH_4 in the deep water (see S1 Appendix for more details). Measurements were done at a resolution of 20 m starting from 10 m depth down to 450 m (430 m was omitted due to time constraints). Between 90 and 130 m, the gas flow was

too low to be quantified but still substantial enough to have an effect on gas results. Therefore, results for this depth range are not reported.

The mass spectrometer was calibrated using two gas standards (80 % CO_2 + 20 % CH_4 and 60 % CO_2 + 30 % CH_4 + 10 % air) with partial pressures similar to the average gas composition of water gassing out from Lake Kivu deep water. One of the gas standards additionally contained atmospheric air for potential calibration of N_2 and O_2. However, in the special setting of Lake Kivu, the determination of N_2 at mass/charge = 28 proved to be difficult because of the presence of a large peak of CO from the fragmentation of CO_2 during ionization in the mass spectrometer. The interference of the CO fragment accounted for more than 95 % of the intensity at mass 28. Therefore N_2 could not be determined reliably and hence was not included in this publication.

Measurement method used by UFZ

The measurement method used by UFZ had previously been used in highly gas charged mine pit lakes (for CO_2 see Boehrer et al., 2016, for CH_4 see Horn et al., 2017) and was modified for the conditions of Lake Kivu by Boehrer et al., 2019. Water was sampled using gas-tight bags, which were lowered to the appropriate depth together with a small pump and an automatic pump controller. The pump partially filled the bags while leaving enough space for the gas phase, which forms once the bags are retrieved. At the surface, the water and gas phases in the bags were equilibrated over night and the composition of the gas phase was analyzed using a gas chromatograph. Subsequently, the remaining amount of gas in the water phase was deduced by assuming equilibrium between gas and water phase. In order to compute in-situ gas concentrations, the gas and water volumes in the bag were determined using a syringe and a laboratory scale respectively. Total uncertainties for CH_4 (CO_2) concentrations were determined as ± 5 (± 6) % below and ± 7 (± 8) % above 250 m. Note again that these uncertainties should be interpreted as maximum deviation from the true value. The UFZ group also measured total dissolved gas pressure (TDGP) using a prototype probe from Pro Oceanus with an accuracy of ± 0.04 bar according to the manufacturer.

Measurement method used by CNRS

The measurement method applied by CNRS is fully described elsewhere (Grilli et al., 2018). In short, an in-situ membrane-inlet laser spectrometer (MILS), called SubOcean, was deployed

for continuous dissolved CH_4 measurements. The instrument is based on a patented membrane extraction system (Triest et al., 2017) coupled to an optical spectrometer for trace gas sensing based on an optical feedback cavity enhanced absorption spectroscopy (OFCEAS) technique (Morville et al., 2003; Morville et al., 2014). The extraction system does not rely on gas equilibration across the membrane, but the dry side of the membrane is maintained at low pressure while continuously flushing it with dry zero air. This allows achieving fast response times < 30 sec, making the technique adapted for fast 3D mapping of water masses (Jansson et al., 2019). The accuracy (standard deviation at the three sigma level) of the measurements was quantified to be ± 33 % from repeated measurements at the same depth. Note that the uncertainty is given at the three sigma level, which we judge roughly equivalent to the concept of "maximum deviation from the true value" used for the other two methods. In addition to the CH_4 signal, this method needs external TDGP and dissolved CO_2 measurements in order to compute CH_4 partial pressure in the lake water, which is finally converted to concentrations using the conversion method presented below.

Conversion from concentration to partial pressure

Eawag and UFZ measured gas concentrations while the MILS sensor used by CNRS provided partial gas pressure. In order to compare these results, conversion from concentration to partial pressure and vice-versa is required. However, this conversion is not straightforward as the gas-water partition coefficients (Henry coefficients) depend on temperature, salinity and hydrostatic pressure (Weiss, 1974). In addition, the fugacity effect cannot be calculated separately for each gas since it depends on the relative mixture of the involved gas species (Ziabakhsh-Ganji & Kooi, 2012). We thus express concentration C_i as a function of partial pressure p_i by the following equation:

$$C_i = K_i(T,S,P)p_i\varphi_i(T,P) \quad (1)$$

with φ_i the fugacity coefficient i.e. the ratio between the fugacity of a gas and its partial pressure at temperature T and pressure P, and K_i the solubility coefficient, i.e. the ratio between the dissolved concentration of a gas and its fugacity. The solubility coefficient $K_i(T,S)$ is computed as a function of temperature and salinity according to Weiss (1974) for CO_2, Wiesenburg & Guinasso (1979) for CH_4 and Weiss (1970) for N_2. The salinity terms of these equations were originally derived for sea salt and not for Lake Kivu, where salinity is dominated by bicarbonates. We accounted for this by assuming that the salinity effect mainly depends on the

ionic strength of the solution. More details about the salinity correction are provided in S2 Appendix.

According to Weiss (1974), the dependence of the solubility coefficient K_i on local total pressure (hydrostatic plus atmospheric pressure) can be written as

$$K_i(T,S,P) = K_i(T,S)e^{\left[\frac{(1-P)v_i}{RT}\right]}. \quad (2)$$

Here, R = 83.1446 cm^3 bar K^{-1} mol^{-1} is the gas constant, and v_i are the partial molar volumes. The partial molar volumes of CO_2 and N_2 were assumed constant at 32.3 cm^3 mol^{-1} (Weiss, 1974) and 35.7 cm^3 mol^{-1} (Moore et al., 1982) respectively, while for CH_4 it was calculated according to (Rettich et al., 1981).

The resulting pressure correction factors $K_i(T,S,P)/K_i(T,S)$ range between 1.00 at atmospheric pressure and 0.93 (CO_2) or 0.94 (CH_4) at 50 bar (485 m depth), i.e. the in-situ pressure reduces the solubility coefficient of the gases by 6 to 7 % in the lowest layers of Lake Kivu.

The fugacity coefficients $\varphi_i(T,P)$ of CO_2, CH_4 and N_2, including the interaction between the gases, are computed according to Ziabakhsh-Ganji & Kooi (2012). (Octave scripts available in S3 Appendix).

Results and discussion

Eawag results

The resulting CH_4 and CO_2 concentrations using the Eawag mass spectrometer setup are depicted in Figure 2.1, along with temperature and salinity profiles. We can identify the well-mixed epilimnion with constant salinity (above ~ 60 m) and the main chemocline at ~ 255 m. As expected, gas concentrations correlate well with salinity and temperature due to the common hydrothermal origin of CO_2, dissolved solids and heat (Schmid et al., 2005). The detailed CH_4 and CO_2 results can be found in Table A1 of the supporting information.

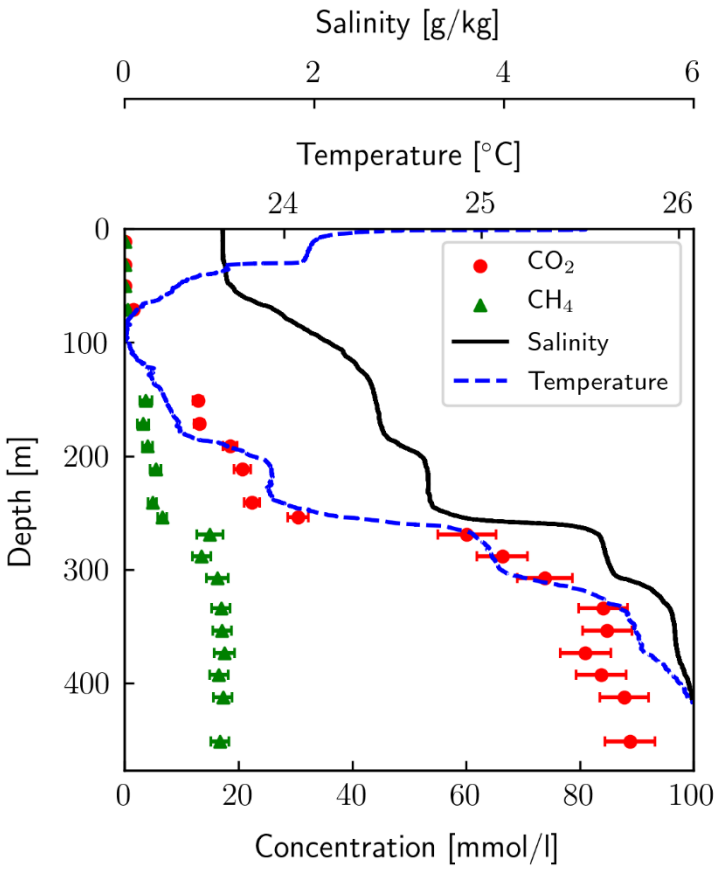

Figure 2.1. Dissolved CH_4 and CO_2 concentrations measured in Lake Kivu by Eawag in 2018; salinity and temperature were determined using a CTD from Sea and Sun in 2017 and 2018 respectively. The conversion from conductivity to salinity was done according to Wüest et al. (1996) using ionic composition. Gas concentrations between 90 and 130 m could not be measured due to too high gas load for using a membrane contactor only, but not high enough for the use of our equilibration chamber.

Contamination with atmospheric air is a major source of measurement errors in gas content analysis. Thus, we use our O_2 results to estimate the maximum atmospheric contamination affecting our measurements in the completely anoxic deep waters of Lake Kivu. We find that the mixing ratio of O_2 in the sampled gas phase is always less than 1 % (maximum between 270 and 310 m due to lower water flow at these depths). Most likely, this O_2 signal indicates a small contamination with atmospheric air. However, it could stem from gas fragmentation during ionization in the mass spectrometer. Independently of its origin, the signal is small enough to not significantly affect the CH_4 and CO_2 results.

Intercomparison of CH_4 and CO_2 using past and new measurements

The results of the dissolved gas measurements (CH_4 and CO_2) of Eawag, UFZ (Boehrer et al., 2019) and CNRS (Grilli et al., 2020) are shown in Figure 2.2. For both CH_4 and CO_2, the measurements agree well within the uncertainties of the different approaches. The profile from

Eawag shows higher CH_4 concentrations (up to 10 %) than UFZ between 250 and 350 m depth, whereas UFZ measured higher CH_4 and CO_2 concentrations (up to 5 %) below 400 m. In particular, the UFZ profile indicates further increasing CH_4 and CO_2 concentrations with depth below 400 m, while the Eawag profile levels off or even decreases. However, note that the comparison below 400 m is based on very few measurement points. The results of Eawag, UFZ and CNRS show a good agreement at their junction at 150 m, thus validating the conversion method under moderate hydrostatic pressure.

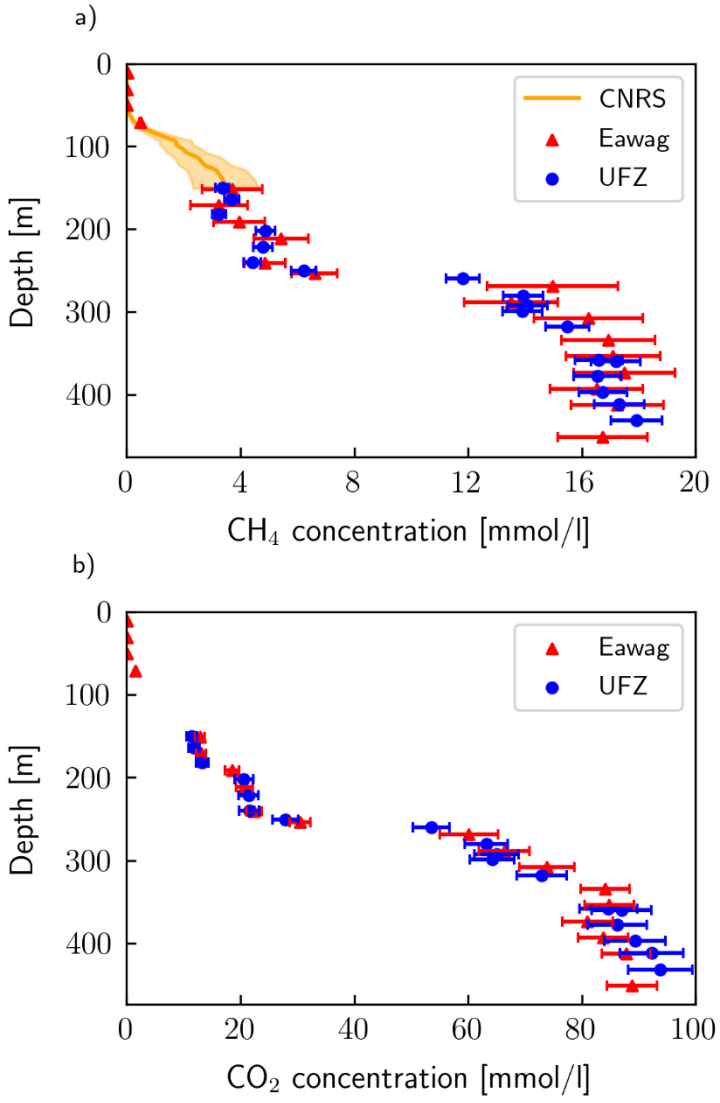

Figure 2.2. Comparison of CH_4 and CO_2 results from CNRS, Eawag and UFZ in 2018. Eawag and UFZ directly determined gas concentration while CNRS measured quasi-continuous partial CH_4 pressure, which was converted to concentration using the conversion method presented above.

In order to estimate the total gas content in the lake, we need to derive quasi-continuous depth profiles for CH_4 and CO_2 from the measurements depicted in Figure 2.2. We chose to interpolate the discrete profiles by fitting them to an electric conductivity profile (corrected to 25°C), because i) conductivity is most probably closely related to gas concentrations due to the long residence time in the lake and because similar transport processes affect both dissolved solids and gases (Schmid & Wüest, 2012) and ii) it can be easily measured at a high resolution.

The following procedure was applied to derive high-resolution curves for the CH_4 and CO_2 concentrations measured by UFZ and Eawag: The conductivity profile from Figure 2.1 was extended down to 480 m depth using the background conductivity profile published by Ross et al. (2015a). The latter was corrected with the mean difference between both profiles in their lowest common 20 m. From this profile, we then extracted the conductivity values at the depths of the gas measurements of UFZ and Eawag. Then, a 6^{th} order polynomial function was fitted ($R^2 > 0.995$ for all four profiles) with conductivity as the independent and gas concentrations as the dependent variables. The regression was used to compute the gas concentration as a function of conductivity and to relate it to depth. The resulting curves are shown in Figure 2.3 (at 0.5 m resolution), along with previous CH_4 and CO_2 measurements. The uncertainties of the previous measurements were assumed to be ± 5 % for Tietze (Tietze, 1978), ± 4 % for Halbwachs and Tochon (Schmid et al., 2005), and ± 10% for Schmid (Schmid et al., 2005 and pers. comm. M. Schmid).

In general, previous and current measurements are in good agreement. For both CH_4 and CO_2, the measurements of 1974 are at the lower end of the spectrum, and those of 2003 at the higher end. From this fact, Schmid et al. (2005) concluded that CH_4 concentrations had increased by 15 % from 1974 to 2003 and that they could possibly reach saturation within the 21^{st} century. Pasche et al. (2011) later determined an upper bound for the CH_4 increase of around half this value based on carbon cycle analysis. However, our new measurements show no measurable increase of CH_4 (and CO_2) concentrations within the last 45 years. This implies that the measured differences were largely due to measurement uncertainty and that the CH_4 and CO_2 concentrations in the lake are currently close to a steady state.

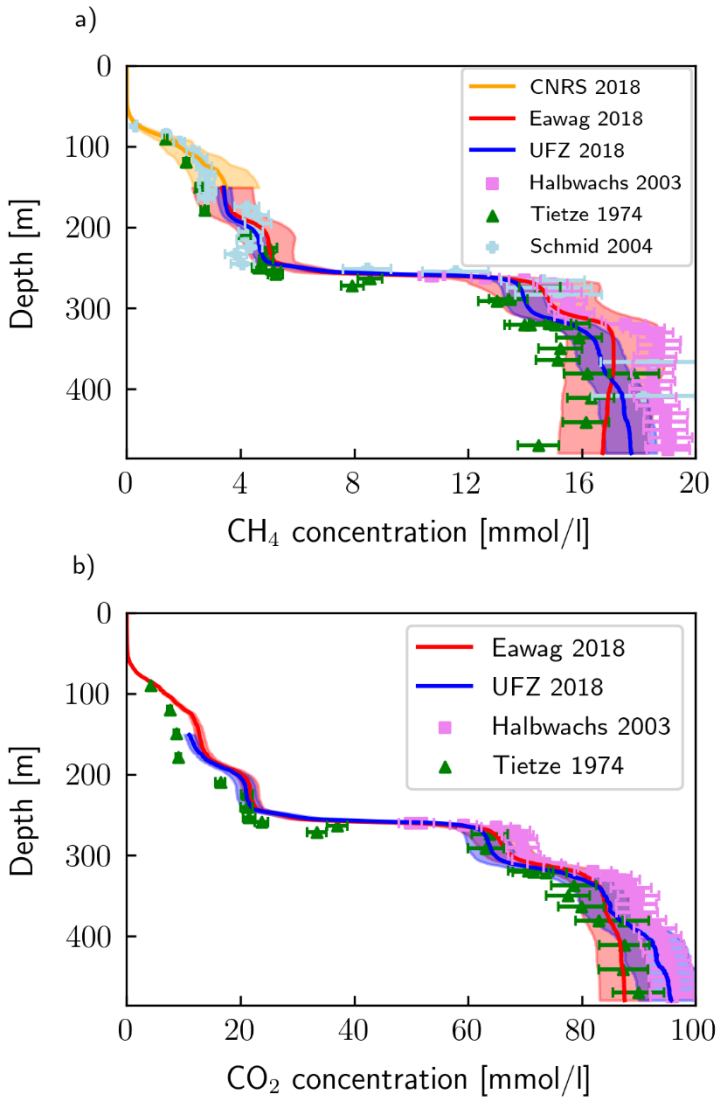

Figure 2.3. Interpolated CH_4 and CO_2 concentrations from this work compared to previous measurements. CH_4 and CO_2 concentrations of Eawag and UFZ are interpolated by fitting the profiles to a conductivity profile; shaded areas represent the uncertainties. Selected previous gas measurements are shown for comparison (Tietze, 1978; Schmid et al., 2005).

Risk assessment using total dissolved gas pressure (TDGP)

In order to assess the danger of a potential gas eruption associated with the high gas concentrations in Lake Kivu, it is helpful to look at gas pressure saturation within the lake. CH_4 and CO_2 concentrations thus need to be converted to partial pressure using the conversion method presented in the previous section. Besides CH_4 and CO_2, dissolved nitrogen (N_2) is the only gas present in sufficient amounts to influence gas pressure. As no N_2 data is available for Lake Kivu, we estimated its contribution assuming that it mimics the profile of atmospheric noble gases which show concentrations close to air saturated water (ASW) at the lake surface and a

decrease of ~50 % in the deep water (Bärenbold et al., 2020b). The derived N_2 profile was subsequently included in the conversion algorithm, which includes the effect of gas mixture between CH_4, CO_2 and N_2 on the fugacity coefficients.

The accuracy of the calculated TDGP is estimated from the accuracies of the gas/water flow measurements and the CH_4 concentration in the gas phase. The contributions to the accuracy from CO_2 and N_2 are negligible in comparison to CH_4 because of the high solubility of CO_2 and low concentration of N_2.

Figure 2.4 shows that calculated TDGP of Eawag and UFZ and direct TDGP measurements using the Pro Oceanus sensor are in good agreement, usually well within the uncertainties of the respective methods. Still, below 250m depth, TDGP calculated from Eawag and UFZ data is slightly higher than the measured TDGP. The mean difference between calculated and measured TDGP is 5.9 % (maximum of 8.7 % at 290 m) and 4.4 % (maximum of 8.8 % at 417 m) for Eawag and UFZ respectively. This discrepancy could be due to a bias in the conversion of concentrations to partial pressures, to an overestimation of concentrations by both Eawag and UFZ or to a problem of calibration of the TDGP sensor at high pressure.

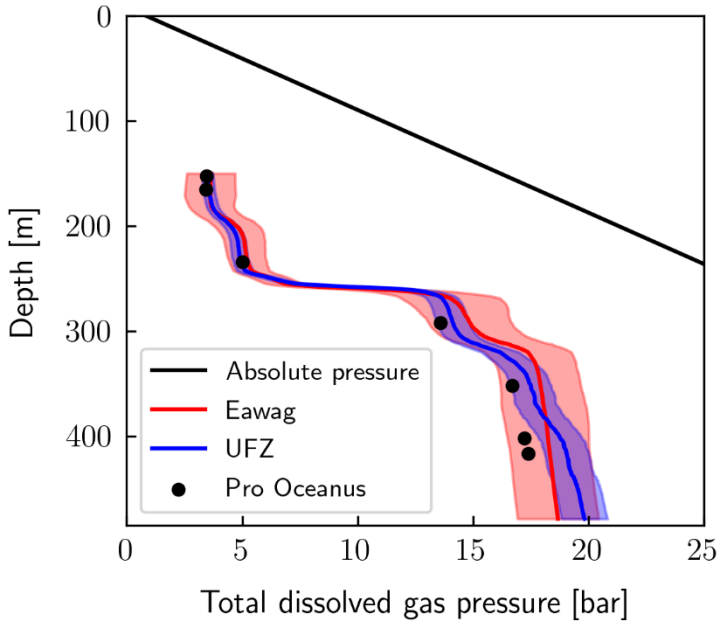

Figure 2.4. Comparison of measured TDGP with TDGP calculated from gas concentrations. TDGP is calculated from individual gas components (CH_4, CO_2 and N_2) using the conversion algorithm presented in this work. The concentration profile of N_2 was derived assuming a similar depth profile as Neon (Bärenbold et al., 2020b) thus not accounting for possible biological effects on N_2.

Gas concentrations are very high in the deep water of Lake Kivu. If this gas was released to the atmosphere, it would cause a large catastrophe by suffocating humans and animals in the surrounding area, qualitatively similar to the events at Lake Nyos in 1986 (Kling et al., 1987). Currently, total dissolved gas pressure (TDGP) is well below absolute pressure (hydrostatic plus atmospheric pressure) at all depths in Lake Kivu. The maximum gas saturation in terms of pressure is reached at 320 m and amounts to ~ 50 % (or a maximum of 57 % if we take the upper limit of the uncertainty range of the Eawag data). This means that the gas concentrations are still far away from the point of spontaneous ebullition (i.e. close to 100% saturation). Nevertheless, volcanic structures on the lake floor indicate frequent volcanic activity within the lake in the geologically recent past (Ross et al., 2015b). We cannot exclude that similar volcanic activity could trigger a gas eruption from the lake in the future, even though TDGP is far away from saturation. Therefore, in spite of no measurable increase of gas concentrations during the last 45 years, artificial degassing is still beneficial to reduce the danger of a potential natural disaster.

Update of Lake Kivu gas reserves

We estimated the gas content of Lake Kivu by multiplying our interpolated gas profiles (Figure 2.3) by the lake area at each depth and subsequent integration over the lake depth at a resolution of 0.5 m. The lake areas were deduced from the bathymetry of Lake Kivu by K.A. Ross from the blended bathymethric data of Ross et al. (2015b) and Lahmeyer & Osae (1998). Tables 2.2 and 2.3 show the gas content in different depth ranges for CH_4 and CO_2 respectively. The average CH_4 estimate from the 2018 campaign shows slightly lower values in the resource zone (7 %) and in the entire lake (4.5 %) than calculated from the data of Halbwachs and Tochon 2003 (published in Schmid et al., 2005). Similarly, the CO_2 content measured in 2018 is 6.5 % lower in the resource zone and 3 % lower for the entire lake. We do not think that this apparent decrease in gas concentrations since 2003 reflects the real gas dynamics in Lake Kivu because i) the total CH_4 extracted by the existing power plant was less than 0.2 km^3 until March 2018 (Schmid et al., 2019) and therefore not measurable by current methods, ii) the residence time of gases in the deep water is on the order of 1000 years (Wüest et al., 2012) and iii) to our knowledge, there is no process that would consume either CO_2 or CH_4 under the conditions present in the deep water of Lake Kivu (i.e. below 70 m, see Morana et al., 2015).

Table 2.2. CH_4 content in Lake Kivu in km^3 STP for different depth ranges.

Depth range [m]	Eawag 2018	UFZ 2018	CNRS 2018	Average	Halbwachs 2003
0 - 70	-	-	0.1 ± 0.3	0.1	
70 - 150	-	-	6.5 ± 2.1	6.5	
150 - 200	5.8 ± 1.6	5.7 ± 0.4	-	5.7	
200 - 260	8.5 ± 1.3	8.2 ± 0.5	-	8.3	8.5
260 - 300	12.5 ± 1.7	12.1 ± 0.6	-	12.3	
300 - 350	14.7 ± 1.6	13.8 ± 0.7	-	14.2	
350 - 400	9.5 ± 0.9	9.4 ± 0.5	-	9.5	
400 - 480	5.5 ± 0.5	5.7 ± 0.3	-	5.6	
Resource zone (260 - 480)	42.2 ± 4.8	40.9 ± 2.0	-	41.5	44.7
Upper resource zone (260 - 310)	15.6 ± 2.1	15.0 ± 0.7	-	15.3	
Lower resource zone (310 - 480)	26.6 ± 2.6	26.0 ± 1.3	-	26.3	
Entire lake				62.2	65.1

The reference values (Halbwachs 2003) were calculated in Wüest et al. (2012) based on the data of M. Halbwachs and J.-C. Tochon in Schmid et al. (2005). The resource zones are defined as in (Expert Working Group on Lake Kivu Gas Extraction, 2009), but including half of the bordering gradients.

Table 2.3. CO_2 content in Lake Kivu in km^3 STP for different depth ranges.

Depth range [m]	Eawag 2018	UFZ 2018	Average	Halbwachs 2003
0 - 150	24.7 ± 2.1	-	24.7	
150 - 200	23.4 ± 1.5	21.7 ± 1.5	22.5	
200 - 260	37.0 ± 2.3	37.0 ± 2.4	37.0	38
260 - 300	56.2 ± 4.2	55.2 ± 2.8	55.7	
300 - 350	68.7 ± 4.0	66.8 ± 3.4	67.7	
350 - 400	47.2 ± 2.4	48.2 ± 2.4	47.7	
400 - 480	28.1 ± 1.4	30.1 ± 1.5	29.1	
Resource zone (260 - 480)	200.2 ± 12.1	200.3 ± 10.0	200.2	214
Upper resource zone (260 - 310)	69.9 ± 5.1	68.2 ± 3.4	69.1	
Lower resource zone (310 - 480)	130.3 ± 6.9	132.1 ± 6.6	131.2	
Entire lake	285.3 ± 18.0		284.5	294

The reference values (Halbwachs 2003) were calculated in Wüest et al. (2012) based on the data of M. Halbwachs and J.-C. Tochon in Schmid et al. (2005). The resource zones are defined as in (Expert Working Group on Lake Kivu Gas Extraction, 2009), but including half of the bordering gradients.

Schmid et al. (2005) suggested a CH_4 production rate of 120 g C/m^2/year (grams of carbon in CH_4 per sediment area pear year) in order to explain the difference between the CH_4 profiles of K. Tietze in 1974 and M. Halbwachs and J.-C. Tochon in 2003. This rate would lead to a CH_4 increase of about 5 – 10 % since 2003 (i.e. 3 – 6 km^3) and thus can be excluded based on our data. Similarly, we can rule out a production rate of 93 g C/m^2/year in the deep water as proposed by Pasche et al (2011). Based on our data from 2018, we suggest that the actual

production rate of CH_4 is probably close to the steady state rates of 32 and 35 g C/m^2/year calculated by Schmid et al. (2005) and Pasche et al. (2011), respectively.

We conclude that the variability of gas concentrations measured in the last 45 years is due to the uncertainties of the applied methods. In contrast to previous work (Schmid et al., 2005), our data suggests that the lake gas content is currently close to a steady state with no or small net recharge rate. Consequently, the risk of a gas eruption does not seem to be increasing over time. Additionally, our findings question whether the methane in Lake Kivu is replenished fast enough to be used as a long-term energy source, once the current methane storage has been exploited.

The CH_4 content amounts to around 41.5 km^3 STP in the resource zone (between 260 and 480 m) and 62.2 km^3 in the whole lake. Furthermore, the results of the two methodologies suitable for deep water gas analysis (Eawag and UFZ) agree within the expected accuracy of 5 – 10 % for both CH_4 and CO_2. For regular gas monitoring in view of increased industrial gas extraction, the method of UFZ is easier to apply due to the use of relatively simple equipment. The prototype MILS sensor used by CNRS was able to record gas concentrations down to a depth of 150 m and provides the advantage of in-situ, fast and high-resolution data. However, the technique was not yet adapted to the high CH_4 concentration below 150 m in Lake Kivu. In addition, the sensor requires total dissolved gas pressure (TDGP) and dissolved CO_2 profiles to determine CH_4 partial pressure. The direct measurement of TDGP may be the most appropriate measurable quantity to monitor the risk of a spontaneous ebullition in the lake in the future. It also has the advantage of offering simple, reproducible and high-precision measurements for further monitoring purposes (see for example Sànchez-España et al., 2020).

Acknowledgements

Michael Plüss and Reto Britt for help with the development of sampling equipment and fieldwork. Ivo Beck, Maximilian Schmidt (Heidelberg University) and the team of LKMP (Lake Kivu Monitoring Programme), especially Epaphrodite Havugimana and Pierre Simbizi for help with fieldwork. Matthias Brennwald for assistance with the “MiniRuedi” mass spectrometer. Serge Robert and Patrick Kathriner for helpful discussions about gas measurements. Nic Spycher (Lawrence Berkeley National Laboratory) for discussing and reviewing the pressure-concentration conversion method and Zaman Ziabakhsh-Ganji (TU Delft) for providing maple scripts for computing fugacity coefficients.

Supporting information in Appendix A

Table A1. Detailed results of Eawag measurement method.

Table A2. Temperature data from a Sea and Sun CTD.

Table A3. Salinity data computed using conductivity data.

Appendix A1. Detailed description of Eawag measurement method and calculations.

Appendix A2. Calculation of salinity effect of Lake Kivu dissolved solids.

Appendix A3. Octave scripts for conversion of concentration to partial pressure.

Chapter 3

Missing atmospheric noble gases in a large, tropical lake: The case of Lake Kivu, East Africa

Fabian Bärenbold[1]*, Martin Schmid[1], Matthias S. Brennwald[2] and Rolf Kipfer[2,3]

[1] *Eawag, Swiss Federal Institute of Aquatic Science and Technology, Surface Waters - Research and Management, Kastanienbaum, Switzerland*

[2] *Eawag, Swiss Federal Institute of Aquatic Science and Technology, Water Resources and Drinking Water, Dübendorf, Switzerland*

[3] *ETH Zurich, Inst. of Biogeochemistry and Pollution Dynamics & Inst. of Geochemistry and Petrology, Zürich, Switzerland*

**Corresponding author, e-mail: fabian.baerenbold@eawag.ch*

This chapter has been published as:

Bärenbold, F., Schmid, M., Brennwald, M. S., & Kipfer, R. (2020). Missing atmospheric noble gases in a large, tropical lake: The case of Lake Kivu, East-Africa. Chemical Geology, 532, 119374. https://doi.org/10.1016/j.chemgeo.2019.119374

Abstract

Lake Kivu is a 485 m deep tropical rift lake in East-Africa and well-known for its very high concentrations of dissolved carbon dioxide and methane in the stratified deep waters. In view of future large-scale methane extraction for power production, there is a need for predicting the evolution of gas concentrations and lake stability using numerical modelling. However, knowledge about the geochemical origin and transport processes affecting dissolved gases in the lake is still partially missing. Due to their inert nature, the analysis of dissolved noble gases can help to shed light on such questions. To learn more about transport processes in Lake Kivu, we extended a well-established sampling method for dissolved noble gases to work in the lake's high gas pressure waters. The results of our analysis show a distinct non-atmospheric isotopic signal in the deep waters (below 250 m) with $^{3}He/^{4}He$ and $^{40}Ar/^{36}Ar$ ratios ~250% and ~20% higher than air saturated water (ASW). Moreover, the gas concentration profiles reveal a striking lack of atmospheric noble gases in the deep waters with respect to ASW. While Ne is depleted by ~45%, the more soluble ^{36}Ar and Kr even decrease by ~70%. In contrast, ^{4}He concentrations increase with depth by a factor of up to ~600. We attribute this excess He and the increases in $^{3}He/^{4}He$ and $^{40}Ar/^{36}Ar$ to the inflow of magmatic gases into Lake Kivu, along with a significant contribution of radiogenic ^{4}He. To explain the depletion of atmospheric noble gases, we present and discuss three different scenarios, namely continuous outgassing, the inflow of depleted groundwater and a large past outgassing event. Due to the best agreement with our observations, we conclude that the inflow of depleted groundwater is likely responsible for the observed atmospheric noble gas depletions.

Keywords: noble gases; Lake Kivu; depletion; groundwater; volcanic region

Introduction

Meromictic Lake Kivu is part of the East African rift system and is located on the border between Rwanda and the Democratic Republic of the Congo. It has a surface area of 2386 km^2 and a maximum depth of 485 m. The rather small catchment area of around 5100 km^2 (excluding lake area) includes part of the Virunga volcano chain to the North of the lake. In this northernmost part of the catchment, there is no surface runoff (Figure 3.1), but the rainfall feeds several subaquatic groundwater sources, which provide around 45 % of the total inflow into the lake (Muvundja et al., 2014). Due to high salinity and carbon dioxide (CO_2) content, some of these sources stratify close to the lake bottom, while two large, less dense sources remain at ~180 and ~250 m (Schmid et al., 2005; Ross et al., 2015a). Consequently, steep physical and chemical gradients can be observed at these depths due to the dilution of upwelling deep water rich in nutrients, gases and salts (Pasche et al., 2009). This situation leads to a strong density stratification, which suppresses turbulent mixing and therefore attenuates the upward transport of gases and nutrients (Schmid et al., 2005). In fact, the stratification effectively prevents annual mixing below a depth of around 50 – 65 m and thus enables the accumulation of CO_2 and biologically produced methane (CH_4) (Schoell et al., 1988; Pasche et al., 2011) over hundreds of years in the vertically stratified and horizontally mixed deep waters.

On one hand, the high CH_4 concentrations of up to 20 mmol/L (Schmid et al., 2005) represent a valuable resource, which is commercially exploited for electricity production by a 26 MW power plant since December 2015. On the other hand, the high total dissolved gas pressure (TDGP) in Lake Kivu is also a looming danger with a possible gas eruption endangering the life of around 2 million people around the lake. Indeed, the analysis of sediment cores in Lake Kivu indicates that mixing events have taken place in the past (Haberyan & Hecky, 1987) and that the most recent (partial) mixing event may have happened about 1000 years ago (Ross et al., 2015b).

In view of future large-scale gas extraction and changing lake temperatures (Katsev et al., 2014), it is important to predict the lake's response to such changes. A one-dimensional model has been used in the past to understand gas and nutrient dynamics (Schmid et al., 2005) and to predict the effect of gas extraction on stratification stability, nutrients and gas concentrations (Wüest et al., 2012). Since the development of this model, detailed investigations allowed better constraining the nutrient and methane cycles in the lake (Pasche et al., 2009; Pasche et al., 2011). Furthermore, some of the subaquatic groundwater sources were located in the lake by

Ross et al. (2015a). Nevertheless, there still persists a gap of knowledge regarding transport processes within Lake Kivu as well as the origin and gas content of the groundwater inflows.

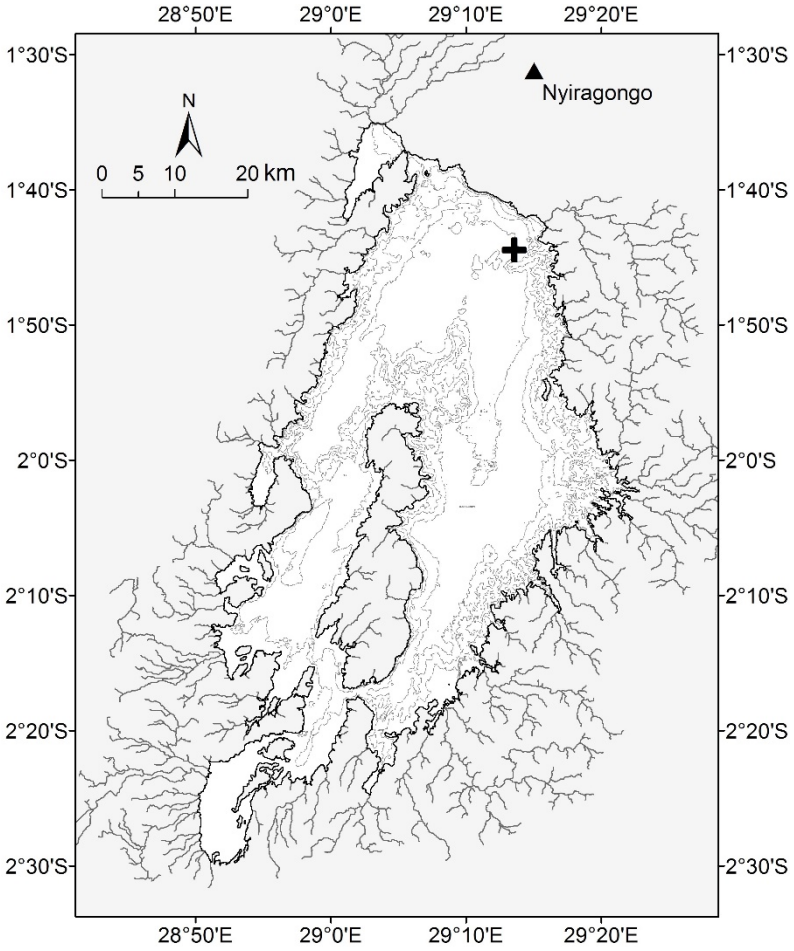

Figure 3.1. Lake Kivu bathymetry with contour lines every 100 m and surface tributaries. The cross indicates the sampling site (1.74087°S/29.22602°E) with a depth of 413 m. The triangle represents the active Nyiragongo volcano. Note the absence of surface run-offs in the northernmost region due to infiltration into the porous volcanic rock.

The chemically and biologically inert noble gases can provide valuable insight into gas and water dynamics of water bodies (see review by Kipfer et al., 2002). In particular, noble gas profiles could help constraining turbulent mixing in Lake Kivu or reveal potential outgassing processes (Kipfer et al., 2002; Holzner et al., 2008). In addition, noble gas isotopic ratios can give hints about the origin of inflowing magmatic gases or fluids (Tedesco et al., 2010).

In this work, we present an extensive dataset of noble gas concentrations from two field campaigns which took place at the northern shore of the Rwandan part of Lake Kivu. We start by describing the specially designed sampling equipment for the high gas pressure conditions in Lake Kivu. Thereafter, we present and discuss the recorded noble gas concentrations and

isotope ratios in detail. In particular, we evaluate three different scenarios to explain the observed depletion of atmospheric noble gases in the deep waters.

Materials and Methods

Sampling site and time

Water sampling was performed on the research platform of the LKMP (Lake Kivu Monitoring Programme) 5 km off-shore in the northern part of the lake (Figure 3.1). From there, a maximum sampling depth of around 410 m could be reached. An additional sample was taken from a boat 7 km further off-shore at a depth of 440 m. We took 6 samples in January 2017 between 0 and 200 m and 11 samples in March 2018 between 100 and 440 m.

Horizontal mixing dominates vertical mixing in Lake Kivu due to negligible vertical turbulent diffusion (Schmid et al., 2005) and a very slow upwelling (< 1 m/year, Pasche et al., 2009) and thus, the lake can be assumed to be horizontally mixed below 65 m. The high horizontal homogeneity is documented by well-matching vertical conductivity and temperature profiles in different parts of the lake (Ross et al., 2015a). Therefore, we can group together the samples from different locations and years and merge them into one depth profile.

Description of sampling method and analysis

Dissolved gas sampling is challenging in water bodies where TDGP exceeds atmospheric pressure (in Lake Kivu TDGP > 15 bar in the stratified deep waters). When the oversaturated water is lifted to the surface, the lack of hydrostatic pressure typically leads to severe loss of dissolved gases. To overcome this degassing of samples, we modified an existing in-situ sampling technique. As a starting point, we used the standard noble gas sampling technique described in Beyerle et al. (2000): copper tubes are flushed and filled with ~45 g of sampling water, sealed gas-tight using the clamps of a metal rack and later degassed and analyzed in the laboratory using mass spectrometry. In lakes without excessive gas content, the water is usually sampled using a standard Niskin sampling bottle, retrieved and filled into the copper tube at atmospheric pressure. The absence of atmospheric contamination is ensured by continuous flushing of the copper tube prior to closing it.

This sampling method was first extended to outgassing lakes by Winckler et al. (2000). They developed a special in-situ sealing mechanism (see Figure 2 in Winckler et al., 2000), using tapered metal plugs, which are pressed on the copper tube ends by the force of large springs. To keep the copper tube open, the springs are compressed by tripping levers which are attached to the triggering mechanism of a standard Niskin bottle by a thin steel cable. In the field, the whole setup is lowered to the required depth and a falling weight is used to release the springs and therefore close the copper tube. Back at the surface, the sample is permanently sealed using the metal clamps. We applied this method in January 2017, but observed gas loss in the samples below 200 m, and thus concluded that the springs were not strong enough to prevent gas loss above a certain TDGP.

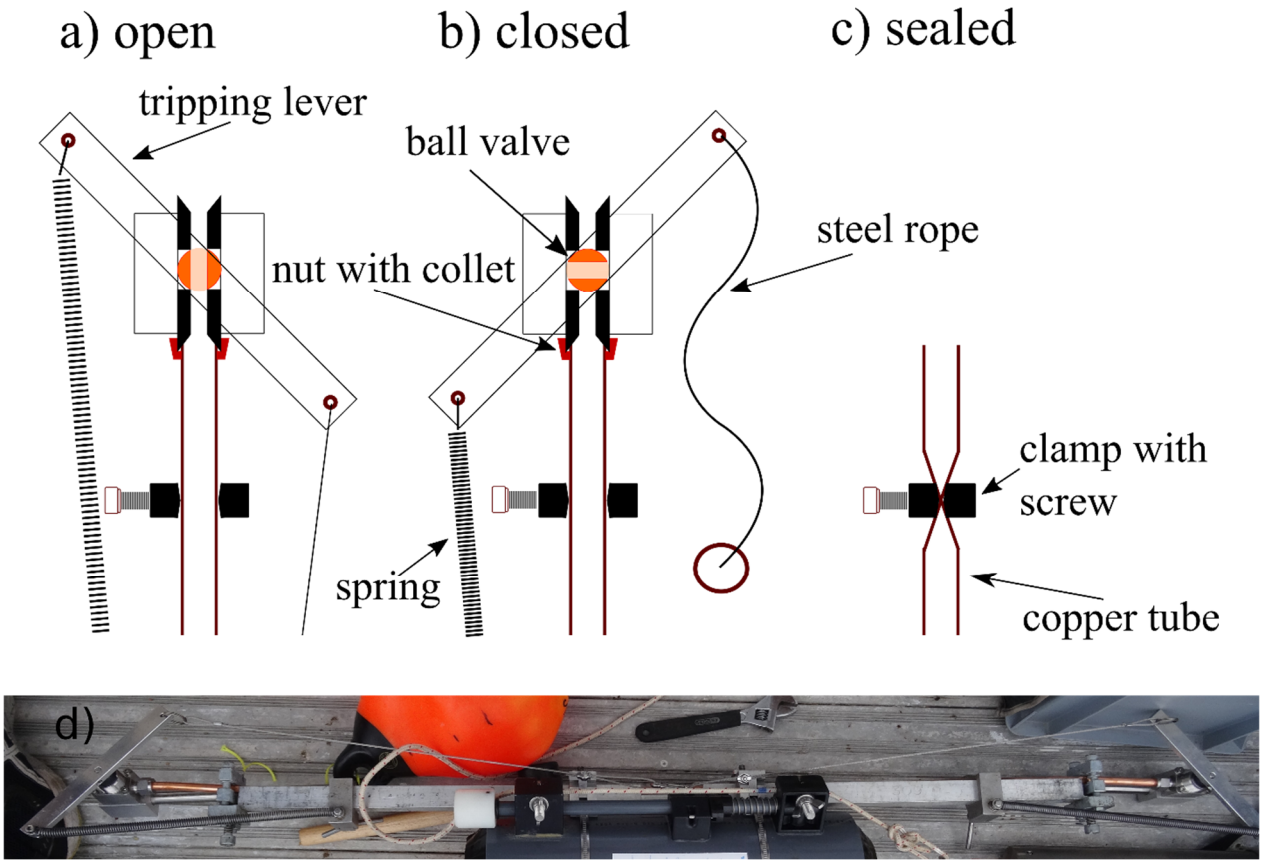

Figure 3.2. Schematic view and photo of the novel in-situ sealing mechanism using spring-loaded ball valves (Swagelok, pressure-proof to 172 bar). a) the tensioned steel rope keeps the ball valve open; b) the steel rope is detached (by a falling weight) and the spring closes the ball valve; c) the sample is permanently sealed using a metal clamp; d) photo of deployed sampling mechanism including a Niskin bottle (to use its trigger mechanism) and a buoy to keep the device upright in the water.

Therefore, we developed a new in-situ sealing-mechanism using pressure-proof Swagelok ball valves (gastight up to 172 bar according to the manufacturer) instead of plugs (Figure 3.2). The valves are attached on each side of the copper tube using vacuum seals and preloaded using

metal springs (Figure 3.2a). At the required sampling depth, the ball valves are triggered by a falling weight which closes the ball valves by detaching the steel ropes (Figure 3.2b). Once retrieved, the samples are sealed permanently using the clamps of the metal rack (Figure 3.2c). Finally, the samples are analyzed for noble gases ^{4}He, ^{20}Ne, ^{40}Ar, ^{86}Kr and ^{136}Xe as well as isotope ratios $^{3}He/^{4}He$, $^{20}Ne/^{22}Ne$ and $^{40}Ar/^{36}Ar$ at the Noble Gas Laboratory at ETH Zurich, Switzerland (Beyerle et al., 2000). Note that in the following sections, we usually give the total elemental concentrations (computed from the isotopes) if not mentioned otherwise. The analytical uncertainty (1σ) for gas concentrations and $^{3}He/^{4}He$ was determined to be between 0.5 and 1%, whereas for $^{20}Ne/^{22}Ne$ and $^{40}Ar/^{36}Ar$ it was found to be around 0.2% (Beyerle et al., 2000). For this work, we chose to specify the uncertainty at the 3σ level (i.e. a 99.7% probability that the true value lies within the error margins). However, due to the special gas composition in Lake Kivu samples with high amounts of CH_4 and CO_2, these uncertainties are estimated slightly higher at 5% (instead of 3%) for gas concentrations as well as $^{3}He/^{4}He$, and 1 % (instead of 0.6%) for $^{20}Ne/^{22}Ne$ and $^{40}Ar/^{36}Ar$.

Results

Noble gas concentrations

The elemental noble gases Ne, Kr and Xe, as well as the isotope ^{36}Ar are called atmospheric noble gases in the following because these elements/isotopes are predominantly of atmospheric origin in the environment (Kipfer et al., 2002). The observed concentrations of these gases are presented in Tables 3.1 and 3.2, and Figure 3.3 shows the depth profiles of Ne, ^{36}Ar and Kr, normalized to the concentration of air saturated water (ASW) at 25 °C and salinity of 0‰ (ASW calculated according to Weiss (1970), Weiss (1971) and Weiss & Kyser (1978).

In the top 100 m, the concentrations of Ne, ^{36}Ar and Kr are approximately constant and close to ASW at 25 °C and 0 ‰ S (~5 % lower). Below, the concentrations consistently decrease with depth. This decrease is probably linked to the inflows of subaquatic groundwater sources which were previously postulated and observed by Schmid et al. (2005) and Ross et al. (2015a), as summarized in Table 3.3. Between ~100 and 200 m, a gradual decrease is observed, in line with a diffuse groundwater source between 135 and 180 m (Ross et al., 2015a). The largest concentration gradient is observed at ~250 m where a strong, fresh groundwater point source enters the lake and dilutes the upwelling deep water, which is rich in nutrients and dissolved gases (Schmid et al., 2005; Pasche et al., 2009). Below ~265 m, we observe a depletion of ~45%

of Ne and even ~70% of the more soluble ^{36}Ar and Kr with respect to ASW. Note that although the salinity in Lake Kivu is rather high, this only results in a change in noble gas solubility (i.e. the Henry coefficient) of around 3 – 4% and therefore, cannot explain the observed noble gas depletions of ~45 and ~70% respectively.

Table 3.1. Measured noble gas concentrations (in ccSTP/g) and isotope ratios. Air saturated water (ASW) concentrations are calculated according to Weiss (1970), Weiss (1971) and Weiss & Kyser (1978) assuming a temperature of 25 °C and a salinity of 0‰. Note that we cannot explain the Xe concentrations and that they are not further discussed in this work.

Depth [m]	^{3}He/^{4}He	He	^{20}Ne/^{22}Ne	Ne	^{40}Ar/^{36}Ar	Ar	Kr	Xe
40	3.23E-06	7.19E-08	9.78	1.47E-07	296.1	2.34E-04	5.10E-08	6.89E-09
78	3.06E-06	1.90E-06	9.78	1.47E-07	297.4	2.40E-04	5.24E-08	7.07E-09
86	3.11E-06	2.61E-06	9.78	1.47E-07	298.3			
98	2.99E-06	3.92E-06	9.80	1.43E-07	298.8	2.36E-04	5.08E-08	7.29E-09
137	3.05E-06	6.20E-06	9.78					
167	3.31E-06	7.05E-06	9.78	1.36E-07	302.8	2.19E-04	4.71E-08	7.78E-09
196	3.13E-06	8.60E-06	9.79	1.34E-07	303.9	2.03E-04	4.34E-08	7.53E-09
213	3.29E-06	1.04E-05	9.78	1.28E-07	307.4	1.96E-04	4.19E-08	8.87E-09
254	3.68E-06	1.13E-05	9.78	1.20E-07	313.9	1.81E-04	3.92E-08	7.81E-09
273	4.41E-06	1.91E-05	9.79	1.03E-07	327.6	1.22E-04	2.29E-08	5.12E-09
294	4.16E-06	1.97E-05	9.80	9.69E-08	330.5	1.11E-04	2.13E-08	5.59E-09
337	4.33E-06	2.14E-05	9.81	9.47E-08	344.0	1.11E-04	2.29E-08	7.64E-09
348	4.72E-06	2.48E-05	9.80	9.18E-08	348.7			
368	4.79E-06	2.35E-05	9.77	8.92E-08	347.4	1.18E-04	2.18E-08	8.61E-09
390	4.57E-06		9.78	8.90E-08	352.9			
408	5.03E-06	2.38E-05	9.83	8.78E-08	350.6	9.41E-05	1.62E-08	8.05E-09
440	4.80E-06		9.81	8.43E-08	363.6			
Uncertainty	5 %	5 %	1 %	5 %	1 %	5 %	5 %	5 %
ASW	1.36E-06	3.83E-08	9.78	1.55E-07	295.5	2.46E-04	5.37E-08	7.41E-09

Conversely, the Xe profile (not plotted in Figure 3.3) is devoid of any significant vertical structure, but exhibits a large variability. This is surprising as we are not aware of any process which would influence Xe fundamentally differently from Ne, ^{36}Ar and Kr in Lake Kivu. We thoroughly checked the data, but we found that samples from different lakes measured in the same measurement batch did not show any unusual behavior of Xe. In addition, the Lake Kivu Xe measurements are consistent over two different sampling campaigns and measurement batches in two different years. As we don't find any reason to discard the data, but cannot offer any explanation for this peculiar behavior of Xe in Lake Kivu we report the data in Table 3.1, but we do not further discuss it.

Table 3.2. Noble gas concentrations (in ccSTP/g) and isotope ratios calculated from Table 3.1 (CO_2 and CH_4 data from M. Halbwachs and J.-C. Tochon in Schmid et al., 2005)

Depth [m]	^{3}He	R/R$_{air}$	^{36}Ar	^{40}Ar*	^{3}He/^{40}Ar*	^{4}He/^{40}Ar*	$CO_2/^3$He [x10^9]	$CH_4/^3$He [x10^9]
40	2.32E-13	2.38	7.91E-07					
78	5.83E-12	2.25	8.05E-07					
86	8.11E-12	2.29						
98	1.17E-11	2.20	7.91E-07					
137	1.89E-11	2.24						
167	2.33E-11	2.43	7.23E-07					
196	2.69E-11	2.30	6.69E-07					
213	3.43E-11	2.42	6.39E-07					
254	4.15E-11	2.70	5.75E-07	1.06E-05	3.92E-06	1.07		
273	8.44E-11	3.24	3.71E-07	1.19E-05	7.08E-06	1.60	18.0	4.0
294	8.20E-11	3.06	3.35E-07	1.17E-05	6.99E-06	1.68	19.1	4.2
337	9.27E-11	3.18	3.22E-07	1.56E-05	5.93E-06	1.37	21.4	4.5
348	1.17E-10	3.47					17.2	3.6
368	1.12E-10	3.52	3.40E-07	1.77E-05	6.37E-06	1.33	17.9	3.7
390		3.36						
408	1.20E-10	3.69	2.69E-07	1.48E-05	8.09E-06	1.61	17.6	3.5
440		3.53						

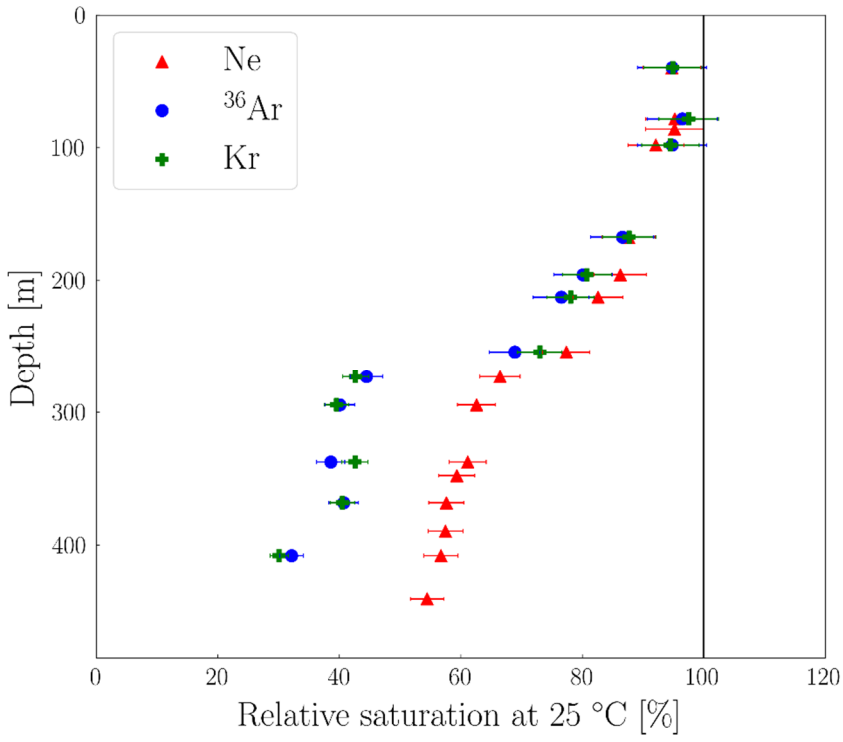

Figure 3.3. Depth profiles of noble gas concentrations Ne, ^{36}Ar and Kr measured in January 2017 and March 2018. Concentrations are normalized to the respective concentration of air saturated water at 25 °C and 0‰ S. ASW would be 3 to 4% smaller if S = 6‰ was used instead (maximum value in Lake Kivu, see Figure 3.4). ^{36}Ar is calculated from ^{40}Ar concentration and ^{40}Ar/^{36}Ar ratio measurements.

Table 3.3. Depths, discharges, temperature and salinity of groundwater sources according to Schmid et al. (2005) and Ross et al. (2015a), who used a 1D lake model to estimate the sources and their properties. The groundwater sources 1 and 2 are called "fresh", while the warmer, saltier sources 3-6 are called "hydrothermal" in this work. For the latter, the noble gas saturation depends on which scenario is chosen to explain the atmospheric noble gas depletion patterns (see discussion section).

No.	Depth [m]	Discharge [m³/s]	Temp. [°C]	Salinity [g/L]	Atm. noble gas conc.
1	135 - 180	22	22.7 – 23.2	2.1 – 2.5	Close to ASW
2	250 - 255	15	23.3	2.7 – 3.1	Close to ASW
Total fresh		37			
3	315	1	25.2	3.4	Depleted?
4	365	1.5	24.5	5.5	Depleted?
5	425	0.8	25.3	5.8	Depleted?
6	465	1.25	26.0	6.0	Depleted?
Total hydrothermal		4.55			

In contrast to the atmospheric noble gases, He concentrations show a strong increase with depth by a factor of up to ~600 compared to ASW in Lake Kivu (Table 3.1 and Figure 3.4). Such high He concentrations are commonly observed in lakes in volcanic environments and, according to Kipfer et al., (2002) can be ascribed to input of gases originating from the earth's mantle and/or radiogenic production within the crust. Figure 3.4 also shows that the He concentrations correlate very well with salinity.

Depleted noble gas concentrations have already been observed in crater lakes Nyos and Monoun in Cameroon, but with much higher variability (Nagao et al., 2010). These lakes are much smaller than Lake Kivu but both also have a history of gas eruptions (Kling et al., 1987; Sigurdsson et al., 1987) and are also located close to a volcanically active region. The ^{20}Ne, ^{36}Ar and ^{84}Kr concentrations measured in these lakes are similar to our results in Lake Kivu (60 – 70% depletion in Nyos and 70 – 80% depletion in Monoun). However, unfortunately Nagao et al. (2010) did not further discuss this unusual depletion of atmospheric noble gases.

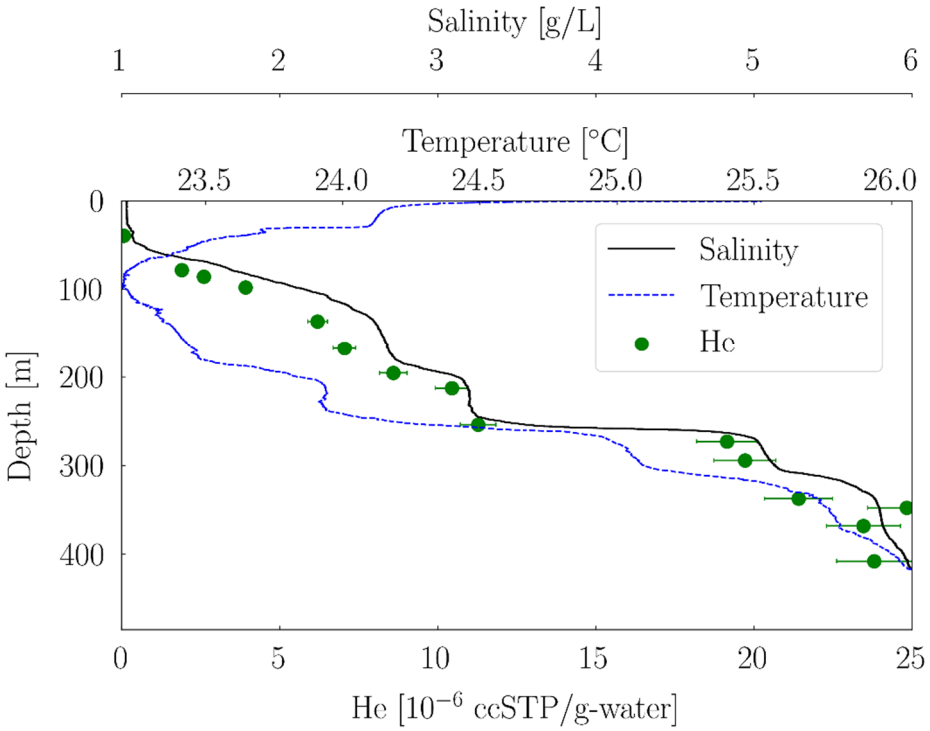

Figure 3.4. The depth profile of Helium is shown along with salinity and temperature. ASW for He at 25 °C and 0‰ S is 0.038 x 10^{-6} ccSTP/g. Conductivity and temperature were recorded using a conductivity-temperature-depth profiler (CTD) from Sea & Sun in 2017 and 2018 (Bärenbold et al., 2020a). Salinity is derived from conductivity using ionic composition according to Wüest et al. (1996). In Lake Kivu, salinity is mainly responsible for the density stratification.

Noble gas ratios

The noble gas ratios $^{3}He/^{4}He$ and $^{40}Ar/^{36}Ar$ increase by around 60 and 20 % respectively from the lake surface to the bottom layer (Figures 3.5a and c; Table 3.1). At the surface, the $^{40}Ar/^{36}Ar$ ratio is close to air saturated water (ASW) and starts to slightly increase below 100 m. Between 200 and 300 m, the increase is more marked, but not as steep as the salinity and He gradients in Figure 3.4. In contrast to $^{40}Ar/^{36}Ar$, the $^{3}He/^{4}He$ ratio is still around 2.5 times above ASW at the lake surface, but exhibits a similar increase below ~200 m. A very different behavior can be seen for the $^{20}Ne/^{22}Ne$ ratio (Figure 3.5b) which remains perfectly constant from 0 to 440 m. The maximum $^{40}Ar/^{36}Ar$ ratio of ~ 365 found in the Lake Kivu deep waters is roughly similar to the maximum value of 350 observed for fumaroles of the nearby Nyiragongo volcano, whereas it is around half for $^{3}He/^{4}He$ (~5 x 10^{-6} in Lake Kivu, ~11 x 10^{-6} in the fumaroles, Tedesco et al., 2010).

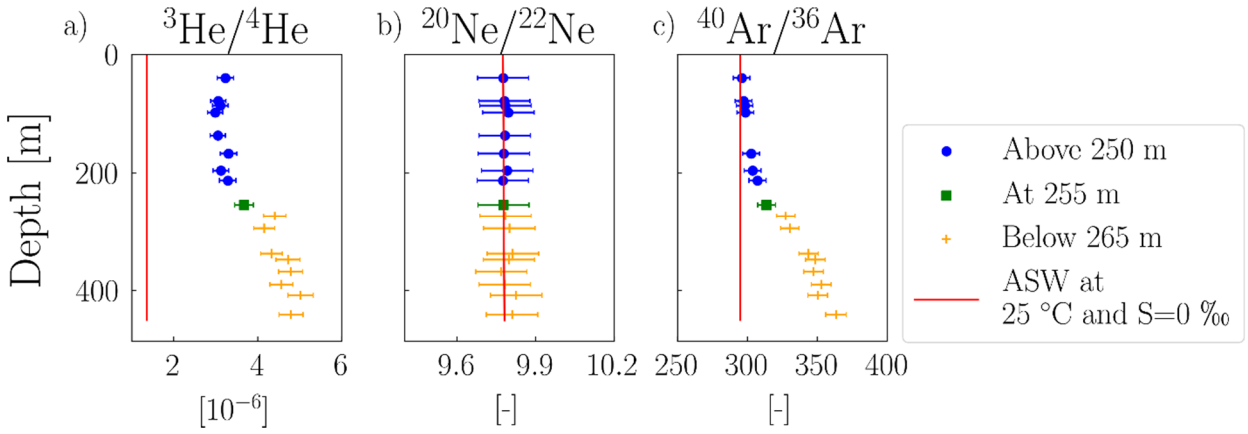

Figure 3.5. Depth profiles of measured isotopic ratios $^3He/^4He$, $^{20}Ne/^{22}Ne$ and $^{40}Ar/^{36}Ar$. The ratios in air saturated water (ASW) are shown for comparison.

Discussion

Why are the atmospheric noble gases depleted?

As noble gases are inert, only physical gas processes can be responsible for any deviation of the measured concentrations from ASW at the respective temperature and salinity. In Lake Kivu (but also in Lakes Nyos and Monoun), the depletion could be caused by 1) continuous outgassing either due to bubbles released from the sediment or from a point source, 2) the inflow of hydrothermal water which is itself depleted with respect to ASW or 3) a relic from a past, large outgassing event. In the following, we will evaluate the consistency of each of the three scenarios with regard to our observations.

Scenario 1: Continuous deep water outgassing

Scenario 1 implies stripping of noble gases out of the deep water by gas bubbles containing mostly CH_4 and CO_2. Such bubbles could either originate from point sources (e.g. bubble seeps at the bottom, see for example Holzner et al., 2008) or from homogeneous ebullition at the sediment interface (Walter et al., 2006). However, Lake Kivu is very deep and although its total dissolved gas pressure (TDGP) is very high, it is still significantly below hydrostatic pressure (a maximum of around 50% is reached at 320 m, Bärenbold et al., 2020a). Therefore, bubbles tend to redissolve at any depth. If the bubbles were produced by point sources, they would have to travel all the way up to the mixed zone (above 50 m). Otherwise, we would observe an accumulation of noble gases at some depths due to redissolution of bubbles. The existence of

such accumulations is not supported by our data, which show a monotonous decrease with depth.

The bubble dissolution model used in McGinnis et al. (2006) predicts that bubbles would need to have a diameter larger than around 20 mm in order to reach the mixed layer from the deepest point of Lake Kivu. This diameter is much larger than bubble sizes observed for deep seeps (Leifer & Culling, 2010; Greinert et al., 2010). It therefore seems unlikely that gas bubbles generated in the deep water can reach the lake surface. Conversely, if the gas bubbles were created homogeneously at the lake-sediment interface, they would not necessarily need to reach the surface to generate a net upwards transport of noble gases. In fact, bubbles could simply be generated at the sediment interface, migrate upwards a certain distance and redissolve. Due to the fact that there is a continuous lake-sediment interface at all depths, the result of such homogenous outgassing would be a depletion of noble gases in the deep waters.

Although there are no observations of major continuous outgassing in Lake Kivu, there is some indication of a free gas phase in the sediment (Figure 6 in Ross et al., 2015b) and even a possible gas emanating structure (Figure 4a in Degens et al., 1973). Potentially, larger noble gas stripping gas bubbles could originate from such free gas phases or gas emanating structures.

In addition to a depletion of atmospheric noble gas concentrations, continuous outgassing should also alter noble gas isotope ratios in the deep water by means of isotope fractionation at the bubble interface. The reason for this is the difference in molecular diffusion between the isotopes. This process is explained in detail in Brennwald et al. (2005), and we can use Equation (1) therein to check whether our measured $^{20}Ne/^{22}Ne$ and $^{40}Ar/^{36}Ar$ ratios agree with a Rayleigh fractionation pattern. For this purpose, we use the Ne and Ar diffusion coefficients found by Tyroller et al. (2014) and our Ne and ^{36}Ar concentrations at the deepest sampling depth. The results of this calculation indicate a $^{40}Ar/^{36}Ar$ ratio of ~315 for an Ar depletion of ~70% for the deepest sample of this work. This means that only around 30 % of the observed increase of $^{40}Ar/^{36}Ar$ (up to ~365, Figure 3.5c) compared to ASW can be explained by bubble stripping. Furthermore, a $^{20}Ne/^{22}Ne$ ratio of around 9.72 is predicted for the deepest sample if bubble stripping were responsible for the Ne depletion of ~45% in Lake Kivu. However, we observe a constant $^{20}Ne/^{22}Ne$ ratio of ~9.78 through all depths in Lake Kivu (Figure 3.5b). Based on the uncertainty of 1% attributed to the $^{20}Ne/^{22}Ne$ ratio, a systematic depletion of $^{20}Ne/^{22}Ne$ down to 9.72 cannot be excluded, but seems very unlikely. And, even if outgassing was responsible for the observed atmospheric noble gas depletion, we need a second process to explain the observed enrichment of ^{40}Ar compared to ^{36}Ar.

Scenario 2: Inflow of noble gas depleted groundwater

In scenario 2, the atmospheric noble gas concentrations of inflowing deep hydrothermal groundwater (Table 3.3) are assumed to be significantly below ASW. One mechanism which can lead to inflow of noble gas depleted water is described in Winckler et al. (2000) for the Red Sea and in Ma et al. (2009) for the Michigan basin. Adapted for Lake Kivu, the mechanism works as follows: i) groundwater is heated up in the volcanically active subsoil thus leading to a free gas/steam phase, ii) the noble gases preferentially partition into the gas/steam phase and iii) gas and water phases are separated, and only the water phase, now depleted in noble gases, reaches the lake. In Lake Kivu, the water temperature close to supposed hydrothermal groundwater inflows exceeds that of the lake water by a few degrees (Table 1 in Ross et al., 2015a), which suggests that indeed the groundwater had been heated up before entering the lake. Other possible causes for noble gas depletion in groundwater are sketched in Ma et al. (2009) including gas exchange between groundwater and an initially noble gas free oil phase. As heavier noble gases are more soluble in oil, this would explain why ^{36}Ar and Kr are more depleted in Lake Kivu compared to Ne. Incidentally, oil prospection is indeed going on in the Lake Kivu region (Mugisha, 2018).

Scenario 3: Large past outgassing event

Scenario 3 assumes at least one large outgassing event to have happened in the past, which is supported by observations in sediment cores (Zhang et al., 2014; Ross et al., 2015b; Votava et al., 2017). During such an event, not only large parts of the main gases CO_2 and CH_4 would leave the lake, but also most of the atmospheric noble gases would be stripped. Subsequently, groundwater inflow and exchange with the atmosphere would slowly increase the noble gas concentrations until they reach values close to ASW again after hundreds of years. Note that in this scenario, in contrast to scenario 2, the hydrothermal groundwater sources are assumed to have noble gas concentrations close to ASW.

We can do a plausibility check for this scenario by comparing the residence time of the deep water (i.e. below ~265 m) to the time elapsed since the last supposed lake overturn. If one of these times is much larger than the other, we can exclude scenario 3 because of either too slow or too fast flushing of the water since the last overturn. However, both times are comparable and estimated to around 1000 years (see Schmid et al., 2005 for residence time and Ross et al., 2015b for time elapsed since lake overturn). Based on this, we can expect the deep water to be

completely replaced by hydrothermal groundwater within 1000 years. This means that there was enough inflow of noble gas saturated groundwater to bring the deep lake water close to saturation again. The reason why our observations differ from saturation could be explained by the absence of mixing processes in this assessment. Mixing may retain an unknown fraction of the depleted lake water in the deep layers, thus keeping this scenario within the realms of possibility.

Yet, due to their high density (as suggested by Ross et al., 2015a), the deep groundwater sources 4 - 6 (Table 3.3) should stratify at the lake bottom. And since in scenario 3 (and also 1), we assume that these sources are close to saturation in atmospheric noble gases, we would expect increasing atmospheric noble gas concentrations with depth towards the lake bottom for these scenarios. This seems to be in contradiction to our data, as we recorded constant or rather monotonously decreasing atmospheric noble gas concentrations with depth below 265 m (Figure 3.3). Therefore, our data does not support the concept of the deep waters being refilled with atmospheric noble gases from the deep groundwater sources as suggested in scenarios 1 and 3.

Most realistic scenario

Scenario 1, the large-scale continuous outgassing is not very likely to happen in Lake Kivu due to i) the tendency of bubbles to redissolve at any depth and ii) the constant $^{20}Ne/^{22}Ne$ ratio, which suggests that isotope fractionation is not taking place. Similarly, we can reject scenario 3 by the lack of increasing noble gas concentrations towards the lake bottom. Therefore, we retain scenario 2, the inflow of atmospheric noble gas depleted groundwater, as the most promising scenario for the observed depletions in the lake. Furthermore, the almost perfect correlation between Ne, ^{36}Ar and Kr (Figure 3.6b and c) supports the view that this one mechanism can explain the depletion of all the atmospheric noble gas species.

As explained, in scenario 2 a fraction of the atmospheric noble gases is lost to a gas/steam phase in the subsoil. In principle, we would expect that a larger fraction of Ne is lost compared to the more soluble ^{36}Ar and Kr, which would lead to a larger depletion of Ne in the lake. However, we actually observe a larger depletion for ^{36}Ar and Kr and less depletion for Ne. Possible explanations for this observation include the contact of the hydrothermal groundwater sources with a (noble gas free) oil phase rather than steam (Ma et al., 2009) or the presence of large amounts of excess air (Kipfer et al., 2002).

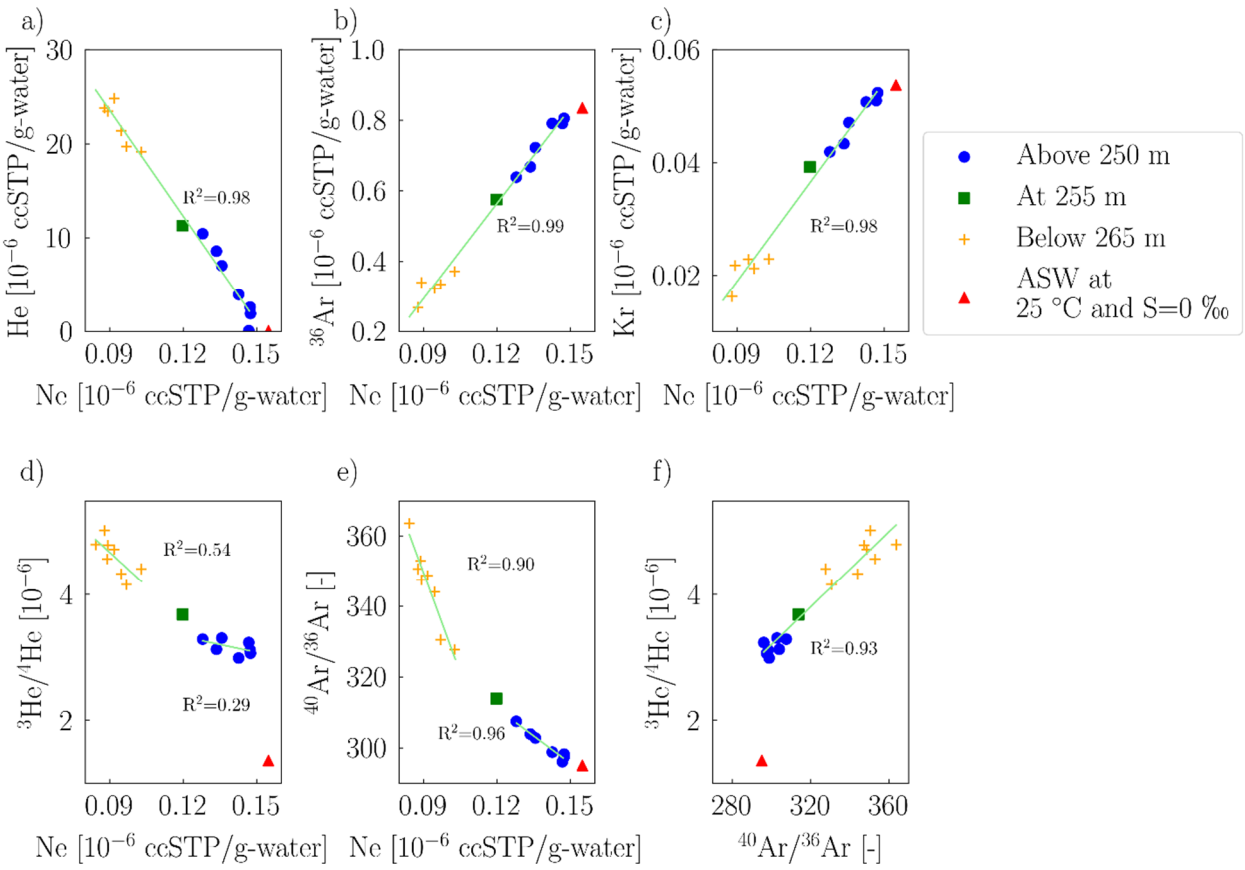

Figure 3.6. a) – c) Noble gas concentrations are plotted against Ne, along with a linear fit. We have $R^2 > 0.98$ for the correlation between He, ^{36}Ar, Kr and Ne. d)-e) The relationship between noble gas ratios $^{3}He/^{4}He$ and $^{40}Ar/^{36}Ar$ against Ne is explained using two linear fits with different slopes. f) $^{3}He/^{4}He$ is plotted against $^{40}Ar/^{36}Ar$. The red triangle shows air saturated water at T = 25 °C and S = 0‰.

Inflow of magmatic ^{3}He, ^{40}Ar and CO_2

The increasing $^{3}He/^{4}He$ and $^{40}Ar/^{36}Ar$ ratios with depth (Figure 3.5a and c) confirm the presence of magmatic gases and/or fluids in Lake Kivu, as suggested by Tedesco et al. (2010). These results are similar to reported observations from Lakes Nyos and Monoun (Nagao et al., 2010). Furthermore, the monotonous increase with depth of these isotope ratios indicate that the main source has to be located close to the lake bottom (i.e. below the maximum sampling depth of 440 m). For scenario 2, this suggests that ascending magmatic gases mix with groundwater in the subsoil, subsequently enter the lake and stratify at the lake bottom. The linear relationship between Ne, $^{3}He/^{4}He$ and $^{40}Ar/^{36}Ar$ on Figures 3.6d) and e) below 265 m confirms this link between atmospheric noble gas depletion and magmatic gases. However, the slope of this relationship changes above 250 m. There, the inflow of a different kind of groundwater is supposed at ~250 – 255 m and 135 – 180 m (Schmid et al., 2005; Ross et al., 2015a and Table 3.3). The hypothesis of inflow of groundwater admixed with magmatic gases is also in line with

the explanation of Nagao et al. (2010) for enriched $^{3}He/^{4}He$ and $^{40}Ar/^{36}Ar$ ratios in volcanic lakes Nyos and Monoun in Cameroon. The comparatively higher $^{3}He/^{4}He$ and $^{40}Ar/^{36}Ar$ values found in these lakes (up to ~8 x 10^{-6} and ~550 respectively, compared to ~5 x 10^{-6} and ~365 in Lake Kivu) can be readily explained by a higher fraction of magmatic gases in the respective mixture.

We can further use our isotope data to compute the $^{3}He/^{40}Ar^{*}$ ratio, where $^{40}Ar^{*}$ is the excess, non-atmospheric ^{40}Ar, computed as $^{40}Ar^{*} = {}^{36}Ar\ [(^{40}Ar/^{36}Ar)_{measured} - (^{40}Ar/^{36}Ar)_{air}]$. The $^{3}He/^{40}Ar^{*}$ values in the deep water of Lake Kivu of 0.6 - 0.8 x 10^{-5} (Table 3.2) are somewhat smaller than maximum values found for the Nyiragongo crater fumaroles of around 1.1 x 10^{-5} (calculated from the data in Tedesco et al., 2010). In addition, we can use the CO_2 measurements of M. Halbwachs and J.-C. Tochon (published in Schmid et al., 2005) together with our ^{3}He measurements to derive the $CO_2/^{3}He$ ratio (Table 3.2). We find values of 17 – 21 x 10^{9} in the Lake Kivu deep waters which agree very well with the Nyiragongo crater gas values of ~20 x 10^{9} found by Tedesco et al. (2010). The $CO_2/^{3}He$ ratios therefore confirm that the CO_2 in Lake Kivu is mostly of volcanic origin.

Input of radiogenic ^{4}He and its link with atmospheric noble gas depletion

Figures 3.4 and 3.6a show that the He concentrations correlate very well with salinity and Ne concentrations (and thus the concentrations of the other atmospheric noble gases ^{36}Ar and Kr). These correlations strongly suggest that the He excess in Lake Kivu is governed by the same mechanism as these quantities, i.e. by the hydrothermal groundwater inflows. However, the admixture of magmatic gases (previous section) and the dilution by fresh water sources (Table 3.3) alone are not sufficient to explain the observed He concentration and $^{3}He/^{4}He$ ratio profiles. Specifically, the He concentration in the (supposedly) ASW saturated fresh groundwater sources is >2 orders of magnitude lower than in the deep water and therefore, there is simply not enough ^{4}He to generate the observed $^{3}He/^{4}He$ profile. To show this, we use the total hydrothermal and fresh discharges given in Table 3.3. In this situation, ~4.55 m^3/s of deep water with 2.4 x 10^{-6} ccSTP/g He and a $^{3}He/^{4}He$ ratio of 5.03 x 10^{-6} (Table 3.1) are diluted by ~37 m^3/s with He = 3.8 x 10^{-8} ccSTP/g and $^{3}He/^{4}He$ = 1.36 x 10^{-6} (i.e. ASW, see Table 3.1). The resulting $^{3}He/^{4}He$ ratio at ~100 m depth is only ~1% lower than at 410 m due to the large difference in total He concentration between the two components. However, in our data we observe a change of the $^{3}He/^{4}He$ ratio from ~5 x 10^{-6} to ~3 x 10^{-6}, i.e. a decrease of 40%. To explain this large difference, we suggest the contribution of radiogenic ^{4}He (with $^{3}He/^{4}He=10^{-8}$), produced in the

rocks (Kipfer et al., 2002). We calculate that we need ~50 times more ^{4}He from radiogenic production than from the ASW saturated groundwater sources to obtain the observed change with depth of He concentration and $^{3}He/^{4}He$ ratio in Lake Kivu.

Moreover, the measured $^{3}He/^{4}He$ ratios in the deep waters of Lake Kivu are only around half of that in its supposed source, i.e. the magmatic gases of the Nyiragongo volcano. The mixture of these magmatic gases with ASW saturated groundwater cannot produce water with high He and $^{3}He/^{4}He$ values at the same time. If the mixture involves enough groundwater to lower the $^{3}He/^{4}He$ ratio to around 50% of its original value, the corresponding decrease in He concentration would be 98 %. Once again, the contribution of both radiogenic and magmatic He is required to explain the observed He concentrations and $^{3}He/^{4}He$ ratios.

Overall, we suggest that the observed He concentration and $^{3}He/^{4}He$ ratio profiles can be explained by a combination of hydrothermal He inflow with ~50% He derived from magmatic gases and ~50% of radiogenic ^{4}He (the effect of ASW saturation is negligible) and fresh groundwater inflow with ~98% He from radiogenic ^{4}He and ~2% from ASW saturation.

Conclusion

We successfully analyzed noble gas concentrations in highly gas-rich Lake Kivu. The in-situ noble gas sampling showed a remarkable depletion of atmospheric noble gases Ne, ^{36}Ar and Kr by about 45 to 70% compared to ASW. In addition, magmatic noble gas isotopes ^{40}Ar and ^{3}He, as well as radiogenic ^{4}He are enriched in the deep waters. The $^{3}He/CO_2$ ratio observed in the deep water is very similar to values found for the Nyiragongo crater gas, supporting the idea that the CO_2 in Lake Kivu is indeed mostly of magmatic origin.

We presented three possible mechanisms which could lead to the observed noble gas depletion. Scenario 1, the continuous stripping of noble gases in the lake by bubbles, is not supported by our $^{20}Ne/^{22}Ne$ and $^{40}Ar/^{36}Ar$ profiles. There is no fractionation in the $^{20}Ne/^{22}Ne$ profile, which indicates that kinetic fractionation during bubble formation did not occur. Scenario 3 consists of an initially atmospheric noble gas free lake (after an overturn) and the gases are resupplied by hydrothermal sources. This scenario is largely compatible with reported residence time and groundwater discharges. However, the salinity profile suggests that the groundwater sources stratify at the lake bottom and thus we should observe the largest concentrations of atmospheric

noble gases close to the bottom. In contrast, our observations show the lowest concentrations at the largest depths.

Scenario 2, the inflow of noble gas depleted groundwater, is best supported by our data. The arguments in favor include positive temperature spikes (as observed by Ross et al., 2015a) at supposed locations of groundwater inflows and a very good correlation between atmospheric noble gases and He, indicating that the depletion of atmospheric gases and the enrichment of He have a common origin. We also observe that Ne is less depleted than the more soluble ^{36}Ar and Kr. To explain this, a considerable amount of excess air needed to be trapped during original infiltration of the water, which later formed the hydrothermal sources (Kipfer et al., 2002).

Acknowledgements

We would like to thank Reto Britt, Michael Plüss, Ivo Beck, Maximilian Schmidt and the whole team from LKMP (Lake Kivu Monitoring Programme) for help with field work. Augusta Umutoni and Ange Mugisha from LKMP for help with the organization of the field campaigns. Andreas Raffainer and the Eawag workshop for the development of the in-situ sampling mechanism. Edith Horstmann and Alexandra Lightfoot for help with sample analysis.

Funding: This project was supported by the Swiss National Science Foundation (grant 200021_160114).

Chapter 4

Dynamic modelling provides new insights into development and maintenance of Lake Kivu's density stratification

Fabian Bärenbold[1], Rolf Kipfer[2,3], and Martin Schmid[1]

[1]*Eawag, Swiss Federal Institute of Aquatic Science and Technology, Surface Waters – Research and Management, Kastanienbaum, Switzerland.*
[2]*Eawag, Swiss Federal Institute of Aquatic Science and Technology, Water Resources and Drinking Water, Dübendorf, Switzerland.*
[3]*ETH Zurich, Institute of Biogeochemistry and Pollution Dynamics & Institute of Geochemistry and Petrology, Zürich, Switzerland.*

Corresponding author: Fabian Bärenbold (fabian.baerenbold@eawag.ch)

This chapter is in preparation for submission in Journal of Geophysical Research Biogeosciences.

Abstract

Lake Kivu is a 485 m deep, tropical rift lake with huge amounts of carbon dioxide and methane dissolved in its stably stratified deep waters. In view of future large-scale methane extraction and a general warming trend in the lake, one-dimensional numerical modelling is an important and computationally inexpensive tool to analyze the evolution of stratification and gas content in Lake Kivu. In this work, we use the physical lake model Simstrat to resolve the hydro-dynamic processes in Lake Kivu. Compared to an earlier modelling approach, Simstrat offers several key improvements, most importantly the dynamic evaluation of mixing over the whole water column and density-stratified groundwater inflows. As the k-ε turbulence closure of Simstrat is not able to correctly reproduce double diffusive mixing below 120 m, a parameterization using the background profiles of model state variables was derived. In order to simulate CO_2 and CH_4, we coupled Simstrat to the biogeochemical library AED2. The model successfully reproduced today's near steady-state, and we used the model to assess two main questions: 1) could the current lake state be reproduced if the model is initiated with a completely mixed and degassed lake, 2) are the atmospheric noble gas depletions in the deep water a consequence of a past lake overturn? Our results demonstrate that a complete mixing event ~2000 years ago is fully compatible with today's physical and biogeochemical state. In addition, our model confirms that an active process (i.e. groundwater inflow) is needed to reproduce the observed noble gas depletion patterns.

Introduction

Lake Kivu is a large (2386 km^2) and deep (485 m) tropical rift lake, situated on the boundary between Rwanda and the Democratic Republic of the Congo (DRC), directly south of the Virunga volcano chain. It is fed by numerous small streams, and discharges, via the Ruzizi River, into Lake Tanganyika (Figure 4.1). In addition to surface streams, ~45 % of the inflow into Lake Kivu is provided by groundwater sources (Schmid & Wüest, 2012), some of which were identified in the northern part of the lake using temperature and salinity profiles (Ross et al., 2015a, see Figure 4.1). Part of this intruding groundwater is hydrothermal, meaning that it is warm, salty and rich in carbon dioxide (CO_2). Due to the high density, these hydrothermal sources have a tendency to plunge before eventually stratifying (Ross et al., 2015a). In addition to the hydrothermal groundwater, two cooler and less salty sources were proposed based on numerical modelling (Schmid et al., 2005) and subsequently identified by conductivity and temperature profiling (Ross et al., 2015a). The model of Schmid et al. (2005) suggested that the discharge of the cooler sources is one magnitude larger than the hydrothermal discharge, and that they explain the strong thermo- and chemoclines at around 190 and 250 m.

The groundwater intrusion into Lake Kivu has two major consequences for the whole water column: i) a continuous upwelling of up to 1 m y^{-1} (Pasche et al., 2009), and ii) a strong density stratification and therefore meromixis below 60 m. Below the main chemocline at 250 m, the lake water probably has not been in contact with the atmosphere for up to 1000 years and hence, the inflowing CO_2 accumulated to concentrations of up to almost 100 mmol L^{-1} (Tietze, 1978; Schmid et al., 2005; Bärenbold et al., 2020a). Furthermore, the decomposition of settling organic matter and the reduction of CO_2 (Pasche et al., 2011) also lead to the accumulation of methane (CH_4) in the deep water. The current total content of CO_2 and CH_4 is estimated to ~285 and ~62 km^3, respectively (Bärenbold et al., 2020a).

The CH_4 reservoir in Lake Kivu is a valuable resource for the neighboring countries Rwanda and DRC, but also a looming danger for the surrounding population. In fact, the smaller gas-rich lakes Nyos and Monoun have experienced limnic gas eruptions in the past (Kling et al., 1987; Sigurdsson et al., 1987), and 1746 and 37 people were killed by asphyxiation, respectively. In 2002, the volcano Nyiragongo erupted, and lava flowed into Lake Kivu. It was feared that the hot lava could sink to the deeper strata of Lake Kivu, and warm up water to an extent that it could rise to a level where the hydrostatic pressure is no longer sufficient to keep the gases trapped. However, Lorke et al. (2004) showed that the influence of the lava on the lake

was minimal, and they concluded that subaerial volcano eruptions are not likely to trigger a limnic eruption at Lake Kivu.

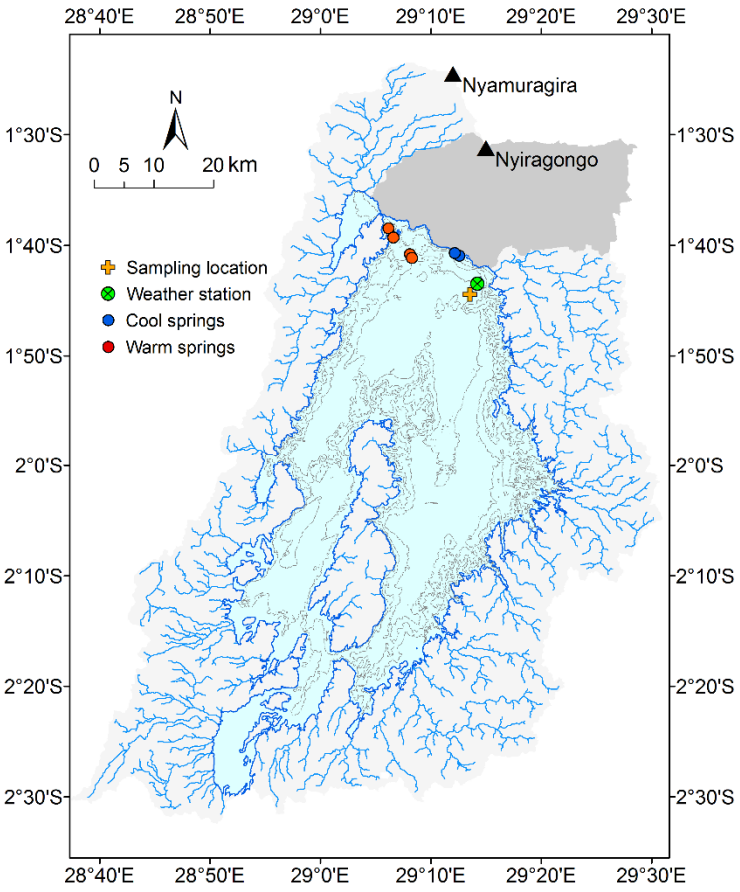

Figure 4.1. Map of Lake Kivu with bathymetry (contour lines every 100 m), surface tributaries and delimitation of the watershed. The part of the watershed, which is not drained by surface tributaries is colored in dark-grey and accounts for 13.5 % of the total watershed. The ^{3}H sampling site and the location of the Lake Kivu weather station are indicated, as well as locations, where temperature and salinity spikes indicate the intrusion of groundwater (according to Ross et al., 2015a). Warm and salty, and cooler and fresher groundwater are marked with red and blue dots, respectively.

In order to prevent further gas eruptions, Lakes Nyos and Monoun, as well as Kabuno Bay, which is a small, 150 m deep subbasin of Lake Kivu with only low CH_4 content, are degassed artificially today. Degassing is performed using long pipes which transfer gas-rich deep water by self-siphoning to the lake surface (Kusakabe, 2017; Halbwachs et al., 2020). In the main basin of Lake Kivu, an artificial decrease of gas concentrations is beneficial for two reasons: i) decreasing gas pressure increases the safety margin, i.e. the distance that a water parcel can rise without outgassing during a mixing event, and ii) the extracted CH_4 can provide energy for both Rwanda and the DRC.

In December 2015, the U.S. company ContourGlobal started the operation of the first large-scale CH_4 extraction facility "KivuWatt" with an electric capacity of 26 MW. KivuWatt extracts water from a depth of 350 m, removes most of the CH_4 and reinjects the partially degassed water at ~240 m, right above the main chemocline. The projected expansion of gas extraction at Lake Kivu (Expert Working Group on Lake Kivu Gas Extraction, 2009) would lead to a major redistribution of warm, salty and nutrient-rich deep water within the lake. If not managed carefully, such redistribution of water has the potential to change stratification, gas distribution and nutrient availability in Lake Kivu during the next decades. For example, if the deep water ends up too close to the lake surface it could provoke harmful events like outgassing or algal blooms. Regular monitoring of stratification and gas concentrations combined with numerical modelling for forecasting are key to prevent such negative consequences (see Schmid et al., 2019 for a detailed discussion on monitoring).

Due to the almost perfect horizontal homogeneity in the main basin (Schmid & Wüest, 2012), one-dimensional modelling is an adequate tool to assess the changes discussed above. Such modelling of Lake Kivu's water and gas dynamics was previously performed by Schmid et al. (2005) using Aquasim, a tool for simulating diverse aquatic systems (Reichert, 1994). This model was later improved, and used to predict changes in the lake's stratification, gas content and nutrient concentrations for different methane extraction scenarios (Wüest et al., 2009 and Schmid et al., 2019). However, the model by Schmid et al. (2005) included several simplifycations and assumptions that could lead to erroneous conclusions if applied to long-term transient simulations. Most importantly, the model could not reproduce feedbacks between changes in lake stratification and the intrusion depths of the subaquatic springs, which are likely to occur in long-term transient simulations.

Here, we propose a new modelling approach using the physical one-dimensional lake model Simstrat (Goudsmit et al., 2002), which we coupled to the biogeochemical library AED2. An uncalibrated version of Simstrat had already been used to model Lake Kivu's surface waters in a lake model intercomparison study and performed reasonably well (Thiery et al., 2014). In short, the new modelling approach has the following advantages: i) diffusive transport between 0 and 120 m is dynamically computed using a k-ε turbulence model, ii) the transport through double diffusive staircases below 120 m is parameterized based on recent field observations and iii) the groundwater inflows are free to plunge and rise as a function of their density compared to the density of the ambient lake water. Due to these advantages, our new model can replace the model developed by Schmid et al. (2005) for longer, transient simulations of Lake

Kivu, i.e. for modelling the evolution of gas concentrations and stratification due to large-scale gas extraction projects.

In this work, we do not focus on the changes induced by gas extraction. Instead, we use the model to address three specific scientific questions. Firstly, it was previously suggested (Ross et al., 2015a) that the cool and relatively fresh sources at ~190 m and ~250 m might mainly consist of recently infiltrated rainwater at the northern shore of the lake. There, rainwater probably quickly percolates through the porous volcanic rock. We can test this hypothesis using our model and recently acquired tritium (^{3}H) measurements. Secondly, based on observations in the sedimentary record, several authors (Ross et al., 2015b; Votava et al., 2017; Uveges et al., 2020) suggest that Lake Kivu experienced a large-scale mixing event ~1000 ka with nutrient- and gas-rich water reaching the surface layers and creating algae blooms. To assess whether a complete mixing event could have happened at that time, we use our model to determine whether and within which time period today's stratification and gas concentrations could have developed from a homogeneous (i.e. completely mixed) and degassed lake. Finally, we previously observed large depletions of atmospheric noble gases in the deep water of Lake Kivu (Bärenbold et al., 2020b). Using our model, we test our hypothesis that the inflow of depleted groundwater is the most probable cause of these depletions.

This publication is organized as follows: First, the new model and the key adaptations for its application for Lake Kivu are explained in detail in the Methods section. We then proceed to present and discuss our simulation results, as well as a new set of ^{3}H measurements. We start with the calibration of a few important parameters to reproduce seasonal mixing and turbulent mixing at intermediate depths. Subsequently, we will discuss in detail the three scientific question listed above.

Materials and Methods

Basic model description

The lake model Simstrat was originally developed at Eawag by Goudsmit et al. (2002) and it is available on github (https://github.com/Eawag-AppliedSystemAnalysis/Simstrat). Simstrat solves the one-dimensional hydrodynamic equations on a staggered grid, using an implicit Euler numerical scheme. Turbulent diffusion is resolved by a k-ε closure, which means that the turbulent kinetic energy k and its dissipation ε are explicitly modelled as state variables. The

main sources of turbulent kinetic energy are direct wind forcing and buoyant instability of the water column. However, Simstrat also allows for turbulent energy production by indirect wind forcing, i.e. the dissipation of internal waves (see Goudsmit et al., 2002 for more details).

The original version of Simstrat has been updated several times in the past. The most important upgrades were the use of a different heat flux parameterization (Schmid and Koester, 2016), the implementation of density-driven plunging of inflows (Gaudard et al., 2017), and the possibility to simulate lake ice cover (Gaudard et al., 2019). In order to explicitly simulate the formation of CH_4 in Lake Kivu, we coupled Simstrat v2.2 with the biogeochemical model library AED2 v1.3.5 (https://github.com/AquaticEcoDynamics/libaed2), which is developed by the University of Western Australia. AED2 consists of a set of biogeochemical modules (carbon, nitrogen, phosphorus, phytoplankton etc.), which each can be switched on and off, or adjusted according to specific needs. In this work, we use the carbon and oxygen modules of AED2 to simulate the carbon cycle, including the formation and consumption of CH_4.

The calculation of the radiation budget in Simstrat requires some basic physical parameters. Water albedo is determined as a function of latitude and seasonality by using a linear interpolation of the modified values of Grishchenko in Cogley (1979), which are implemented in Simstrat v2.2. We use a standard value of 0.35 for the fraction of shortwave radiation absorbed as heat in the surface boundary layer. The remaining shortwave radiation is absorbed in each water layer with an extinction coefficient of 0.27 m^{-1} (Thiery et al., 2014). In addition, we need to define the geothermal heat flux, which is not well constrained in the Lake Kivu region. Degens et al. (1973) recorded a few measurements in the sediment which indicate a range of 0.016 – 0.18 W m^{-2}. For our simulations, we chose a value of 0.13 W m^{-2}, which is well within this range and leads to the best agreement between observed and simulated deep water temperatures. All Simstrat settings and parameters are summarized in the supporting information (Tables B1 and B2).

In the AED2 carbon module, the CH_4 sediment flux P_{CH_4} in mmol m^{-2} d^{-1} is modelled taking into account oxygen inhibition and temperature dependence:

$$P_{CH_4} = F_{sed,CH_4} * \frac{K_{sed,CH_4}}{K_{sed,CH_4}+[O_2]} * \theta_{sed,CH_4}^{T-20} \quad (4.1)$$

where $F_{sed,CH_4}$is the maximum sediment CH_4 flux at 20 °C, K_{sed,CH_4} is the half saturation constant for the inhibition of CH_4 production by oxygen, $[O_2]$ is the oxygen concentration and θ_{sed,CH_4} is the Arrhenius temperature multiplier for CH_4 production.

Similarly, CH_4 oxidation by methanotrophs Ox_{CH_4} in mmol m^{-3} d^{-1} is modelled as

$$Ox_{CH_4} = R_{ox,CH_4} * \frac{[O_2]}{K_{ox,CH_4}+[O_2]} * vT_{ox,CH_4}^{T-20} \quad (4.2)$$

where $R_{ox,CH_4}$is the maximum oxidation rate at 20 °C, K_{ox,CH_4} is the half saturation constant for CH_4 oxidation, $[O_2]$ and vT_{ox,CH_4} is the Arrhenius temperature multiplier for CH_4 oxidation.

Due to the narrow range of temperature in Lake Kivu, we neglect the temperature dependence in both equations, and equation (4.1) then reduces to a constant production rate F_{sed,CH_4} in the anoxic waters below ~65 m (see Table B3 for numerical values). CH_4 oxidation by methanotrophs (equation 4.2) on the other hand happens right at the oxycline and therefore is a function of oxycline depth. Note that for computational efficiency, we did not include the simulation of nutrients and phytoplankton, so oxygen consumption is underestimated and the oxycline depth is probably overestimated, which slightly affects the depth at which CH_4 disappears.

Modifications of the model for Lake Kivu

Due to exceptionally high CH_4 and CO_2 concentrations and the presence of double-diffusive staircases, the simulation of Lake Kivu requires some changes to the original Simstrat-AED2. This adjusted version is called Kivu-Simstrat (code will be published with this chapter), and it is used throughout this work. The respective changes are described in this section.

<u>Parameterization of double diffusive transport</u>

One of the unique features of Lake Kivu are the ~300 double diffusive staircases, which exist below a depth of 120 m and all the way down to the lake bottom at 485 m (Newman, 1976;

Sommer et al., 2013). These staircases consist of thin mixed layers with an average thickness of ~70 cm and sharp gradients in between (Sommer et al., 2013). Double diffusion is caused by the coexistence of two substances with a reciprocal effect on density and very different molecular diffusion coefficients. In Lake Kivu, the temperature increase with depth destabilizes the water column, while the increase with depth of salinity and CO_2 (somewhat weakened by the CH_4 increase) stabilizes it. Consequently, the strong stratification suppresses turbulent diffusion below 120 m, but molecular transport is enhanced by the step-wise profile compared to a smooth profile. By measuring the temperature and salinity gradients between double diffusive layers, Sommer et al., 2019 concluded that the apparent temperature diffusivity (calculated as the heat flux divided by the smoothed temperature gradient) is usually between 10^{-6} and 10^{-5} m^2 s^{-1}, while the molecular diffusivity of heat is only ~1.4 x 10^{-7} m^2 s^{-1}. Therefore, double diffusion in Lake Kivu enhances the heat flux by a factor of ~10 – 100 compared to a smooth profile. Conversely, the salinity flux, which has a molecular diffusion coefficient of 1.2 x 10^{-9} m^2 s^{-1}, is even increased by a factor of 30 – 300 due to the steeper interface gradients (Sommer et al., 2013).

Double diffusive convection is an inherently three-dimensional process and therefore not readily replicable in one-dimensional models. We initially chose a very high depth resolution (grid cells < 1 cm) in order to correctly represent the thin interfaces. However, the simulated interfaces were too steep and the mixed layers too large and thus, the resulting double diffusive heat flux was on the order of 0.3 W m^{-2} instead of 0.1 – 0.15 W m^{-2} (determined by Sommer et al., 2013). Because of this disagreement with data and because such a high spatial resolution is computationally very expensive, we decided to resort to a coarser resolution of 2 m, which produces a smoothed profile between 120 and 485 m without double diffusive staircases. The double diffusive transport of heat and salinity is expressed as apparent diffusion through this smoothed profile, and we parameterize it as a function of stability N^2 [s^{-2}], which is given by

$$N^2 = -\frac{g}{\rho_0}\frac{\partial \rho}{\partial z} \tag{4.3}$$

where g is gravitation, ρ is water density, ρ_0 is the density of freshwater (1 kg L^{-1}) and z is elevation. N^2 is thus proportional to the density gradient and positive values indicate a stably stratified water column, while negative values represent unstable conditions and thus convective instability. Figures 4.2a and b show that the relationships between the apparent

diffusivities of temperature $K_{T,app}$ and salinity $K_{S,app}$ (data from Sommer et al., 2019) and N^2 correlate well in the log-log domain.

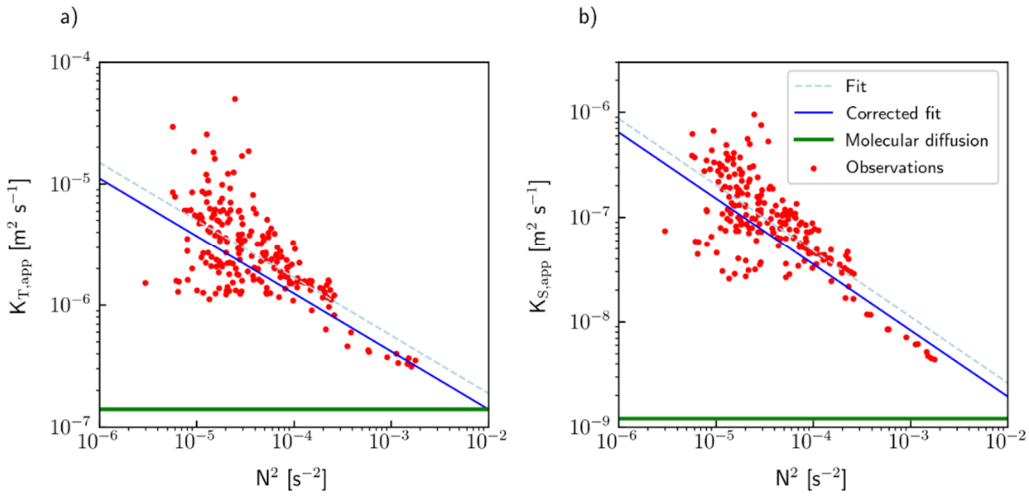

Figure 4.2. Regression between N^2 and apparent temperature and salinity diffusivities (data from Sommer et al., 2019). The corrected regression line includes a correction factor, but preserves the slope. Molecular diffusion is used as the lower boundary of apparent diffusivity. a) Apparent temperature diffusivity $K_{T,app}$, b) apparent salinity diffusivity $K_{S,app}$.

The diffusivities can therefore be expressed as power laws according to

$$K_{T,app} = 2.12 * 10^{-8} * N^{-0.95} * F \tag{4.4}$$

$$K_{S,app} = 1.44 * 10^{-10} * N^{-1.26} * F \tag{4.5}$$

where $F = 0.74$ is a dimensionless correction factor. This correction factor accounts for the fact that the parameterization tends to lead to steeper temperature and salinity gradients in the model compared to observations of Sommer et al. (2019) and thus slightly overestimates vertical transport. At the logarithmic scale, this correction factor consists of an offset of the y-axis, but preserves the slope of the regression line.

At high values of N^2, the lower limit for apparent diffusion is the respective molecular diffusion (Figure 4.2). Conversely, when N^2 is very close to zero (i.e. $< 10^{-6}$ s^{-2}), our parameterization simulates convective instability and can produce very high diffusivities. To avoid unphysically

high mixing rates, we use a threshold of 10^{-10} s^{-2} for N^2, which yields upper bounds of ~8 x 10^{-4} and ~2 x 10^{-4} m^2 s^{-1} for the diffusivities of temperature and salinity, respectively.

The molecular diffusion coefficients of CO_2, CH_4 (Sommer et al., 2013), noble gases (Wise & Houghton, 1968) and water isotopes ^3H and ^2H (Mills, 1973) are of similar order of magnitude compared to salinity, and therefore the double-diffusive transport of each of these variables is approximated as

$$K_{i,app} = K_{S,app} * \frac{D_{i,mol}}{D_{S,mol}} \tag{4.6}$$

where $D_{i,mol}$ and $D_{S,mol}$ are the molecular diffusion coefficients of variable i and salinity, respectively.

Influence of dissolved gases on density

Due to their high concentrations, salinity and the concentrations of dissolved gases need to be taken into account in water density calculations for Lake Kivu. In our model, we compute water density ρ as a function of temperature T and salinity S according to Chen & Millero (1986) and we add the effects of CO_2 and CH_4 similarly to Schmid et al. (2004):

$$\rho(T, S, CO_2, CH_4) = \rho(T) * (1 + \beta_S * S + \beta_{CO_2} * CO_2 + \beta_{CH_4} * CH_4) \tag{4.7}$$

where β_S, β_{CO_2} and β_{CH_4} are the contraction coefficients of salinity, CO_2 and CH_4 respectively (see Schmid et al., 2004 for numerical values). In equation 4.7 and throughout this work, S is computed from conductivity measurements by using ionic composition in Lake Kivu according to Wüest et al. (1996).

Total alkalinity

In the AED2 carbon module, total alkalinity (TA) is derived as a regression of dissolved inorganic carbon (DIC) and S with different built-in regression functions to choose from. For Lake Kivu, Wüest et al., 2009 showed that TA in mmol m^{-3} is a linear function of S in g kg^{-1} and suggested the following relation:

$$TA = 11960 * S \tag{4.8}$$

We implemented this option in AED2 and used it throughout our simulations.

Lake – atmosphere interactions of water isotopes (^{3}H and ^{2}H) and noble gases

In order to model the water isotopes ^{3}H and ^{2}H, we take into account their interaction with the atmosphere using the Craig-Gordon model (see for example Aeschbach-Hertig, 1994). The net flux F_C of the isotope concentration C out of the water column is given by the combined effect of evaporation and precipitation:

$$\mathbf{F_C = E * \alpha \frac{C_P - h_w C_L}{1 - h + \Delta\varepsilon} + R * C_P} \quad (4.9)$$

where C_P is the concentration in precipitation, C_L the surface concentration in the lake, E the evaporation rate, R the precipitation rate, h_w the relative humidity with respect to surface water temperature, α the equilibrium fractionation coefficient and Δε the kinetic enrichment. For ^{3}H, we assume an equilibrium fractionation factor α of 0.89 and negligible kinetic fractionation (Aeschbach-Hertig, 1994). For ^{2}H, α is computed according to Majoube, 1971 and the kinetic enrichment factor Δε is derived from relative humidity (Gonfiantini, 1986). Finally, we need to determine the precipitation isotope signals. For ^{3}H, we use the database of the Global Network of Isotopes in Precipitation (GNIP). Because data is scarce in Africa and there is no measurement station close to Lake Kivu, we use the average of surrounding stations to derive a time series with yearly data from 1953 – 2018 (IAEA/WMO, 2020). Note that there is no data available after 2000 and thus, we calculate the values from 2000 to 2018 using exponential extrapolation of the trend from 1990 to 2000 (see Figures B1 and B2 in Appendix B).

We express ^{2}H in δ notation, i.e. as excess with regard to its ratio with the Vienna Standard Mean Ocean Water (VSMOW), and we use a constant precipitation value of -4.5 ‰ because: i) the value is in the range of observed values (IAEA/WMO, 2020), ii) data is too scarce for deriving seasonal variation, and iii) the value leads to a good agreement between modelled δ^2H signals and observations at the lake surface. Note that we also use these ^{3}H and δ^2H precipitation values for the surface inflows (tributaries) into Lake Kivu, thus neglecting evaporation. The assumption of neglecting evaporation effects on the isotopic composition of the tributaries is motivated by the fact that the watershed is small and thus rainwater ends up in the lake quickly. In reality, there is substantial evaporation despite the small watershed and this in turn would lead to higher δ^2H values in tributaries compared to precipitation. We neglected this evaporation

effect in our study (i.e. assumed the same δ^2H in both tributaries and precipitation) because we do not simulate ^2H dynamics in the surface waters).

The exchange of noble gases across the lake-atmosphere interface was approximated by prescribing air saturated water at 25 °C at the lake surface due to virtually constant concentrations of noble gases in the atmosphere and because the surface water temperature of Lake Kivu is usually close to 25 °C,

Meteorological forcing

Simstrat requires air temperature (T_a), horizontal wind speed at 10 m above the water surface (UV_{10}), wind direction (φ), atmospheric vapor pressure (e_a), incoming short-wave radiation (SW_{in}), and incoming long wave radiation (LW_{in}). These meteorological variables are monitored continuously every 30 minutes by an automatic weather station on a platform on Lake Kivu (see Rooney et al., 2018 for details). W. Thiery from Vrije Universiteit Brussel kindly provided continuous data from October 2012 to September 2019 from this weather station. To allow for the simulation of longer time-scales, we use the output of a regional climate model, which is used for scenario simulations within the ISIMIP project (Inter-Sectoral Impact Model Intercomparison Project). The regional climate model outputs were made available by L. Raman Vinna, and they consist of daily modelled values of all important meteorological variables from the year 1660 to 2300 at Lake Kivu (grid cell 1.75°S/29.2°E). We chose MiroC5 from the four available regional models but the choice of climate model is not important, as long as interannual variability is well represented. The air pressure and air temperature of the climate model are corrected by adjusting their average to the measured average by the weather station, while wind speed and incoming radiation are adjusted using Simstrat's built-in correction factors (Table 4.1). Note that the difference in air pressure and temperature (Table 4.1) is because the climate model grid cell is located at a higher elevation than Lake Kivu. We also noticed that wind directions differ between observations and the regional climate model, probably due to local effects below the grid scale of the climate model. However, simulation results are only weakly sensitive to wind direction in the lake model. Finally, the difference in

wind speed could be shown to be caused by the different time resolutions of the weather station (half-hourly) and the climate model (daily averages).

Using the corrected climate modelling output of MiroC5, we created two forcing time series: i) the control dataset "piControl" from 1660 to 2300 which represents climate forcing with constant, pre-industrial greenhouse gas concentrations and ii) a combination of a historical dataset from 1860 to 2005 and a projection from 2006 to 2100, with a net radiative forcing of 6.0 W m^{-2} in 2100, which will be called "RCP6" (representative concentration pathway 6.0). The goal of the "piControl" time series is to provide a realistic, but stochastic distribution of seasonal mixing depth for the steady-state and long-term simulations (see Results section), while RCP6 is only used for the transient simulation of ^{3}H from 1953 – 2018.

Table 4.1. Averages of meteorological data from an automatic weather station on Lake Kivu (Rooney et al., 2018) and the output of the regional climate model MiroC5. All variables of the weather station are measured half-hourly and the daily averaged wind speed is shown for comparison (in parentheses). Wind speed is actually measured at a height of 7.2 m, and thus was corrected to 10 m assuming a logarithmic wind profile.

Period: 2012 – 2019	**Weather station**	**Climate model**	**Corrected**	**Calibrated in**
P [mbar]	852	812	Yes	No
T [°C]	21.75	18.51	Yes	No
h [%]	77.0	75.4	No	No
UV_{10} [m/s]	3.13 (1.38)	1.28	No	Yes
SWin [W/m^2]	206	197	No	Yes
LWin [W/m^2]	387	374	No	Yes

Water balance

The water balance of Lake Kivu can be written as

$$P + I + G = E + O \tag{4.10}$$

with precipitation P, surface inflow I, groundwater inflow G, evaporation E and outflow O. Precipitation and evaporation are almost equal in Lake Kivu (Schmid and Wüest, 2012; Muvundja et al., 2014), meaning that the discharge of inflowing tributaries and groundwater is mostly balanced by the outflowing Ruzizi River. In our model, we use the values by Schmid and Wüest, 2012, who suggest average values of 63 m^3 s^{-1} for surface inflow, 41 m^3 s^{-1} for

groundwater inflow and 95 m^3 s^{-1} for the outflow. We add the net difference between P and E to the outflow, which then amounts to 108 m^3 s^{-1}.

Tritium (^{3}H) measurements

^{3}H (or T) is a radioactive hydrogen isotope, which is transported in the environment as tritiated water (HTO). It is extremely rare in nature due to low natural production and a relatively fast decay with a half-life of ~12.3 years. However, the atomic bomb tests in the 1950s and 60s released large amounts of ^{3}H into the atmosphere (up to several hundred tritium units TU, where 1 TU is 1 ^{3}H atom per 10^{18} water atoms). Since then, ^{3}H has been widely used in lake and groundwater environments as a physical tracer (Kipfer et al., 2002).

We took water samples using the pressure-proof sampling equipment described in Bärenbold et al., 2020b and analyzed them for ^{3}H content by measuring its decay product ^{3}He according to Beyerle et al., 2000. In this procedure, samples are degassed under vacuum in order to evacuate the naturally present ^{3}He, then left on the shelf to allow for sufficient decay of ^{3}H to ^{3}He (typically 6 - 12 months), and subsequently analyzed for newly produced ^{3}He. Knowing the amount of ^{3}He produced in the sample and the elapsed time, one can back calculate the original amount of ^{3}H present in the sample. Due to the high helium content in Lake Kivu (Bärenbold et al., 2020b), some of our samples had to be degassed twice to remove all naturally present ^{3}He. The estimated standard deviation of our measurements due to calibration uncertainty and possible contamination with atmospheric air is in the range of 0.03 – 0.10 TU. In addition to this data, we added two unpublished ^{3}H measurements taken by our own group during an expedition in 2004.

Results and discussion

Seasonal mixing dynamics (0 – 60 m)

Seasonal mixing in Lake Kivu usually occurs during the dry season and affects the top ~30 – 60 m. It is strongest during July and August due to high wind speeds and lower air temperatures, which lead to convective instability and enhanced mixing (Schmid & Wüest, 2012). Interannual variability of seasonal mixing depth is therefore mainly driven by meteorological conditions. The extent of the surface layer (where conductivity is nearly constant) gives an impression of

varying mixing depth in different years (Figure 4.3a). The typical range of surface temperatures in Lake Kivu is ~23 – 26 °C (Thiery et al., 2014; Morana et al., 2015) with warmer temperatures in the stratified rainy season and cooler temperatures in the windier dry season.

In the model, average mixing depth and surface temperature are mainly determined by the calibration parameters of wind speed, short wave radiation and long wave radiation. By manually tuning these three parameters (Table B2 for numerical values), we can adequately reproduce mixing depth, which varies between ~20 and 60 m (Figure 4.3b). Modelled water temperatures exhibit a range of ~23 – 27 °C (Figure 4.3c), with peak water temperatures during stratified periods occasionally 1 – 2 °C higher than typical observations (Thiery et al., 2014; Morana et al., 2015). However, as long as the temporal distribution of the mixed layer extent is realistic, these higher surface temperatures will not influence our model results.

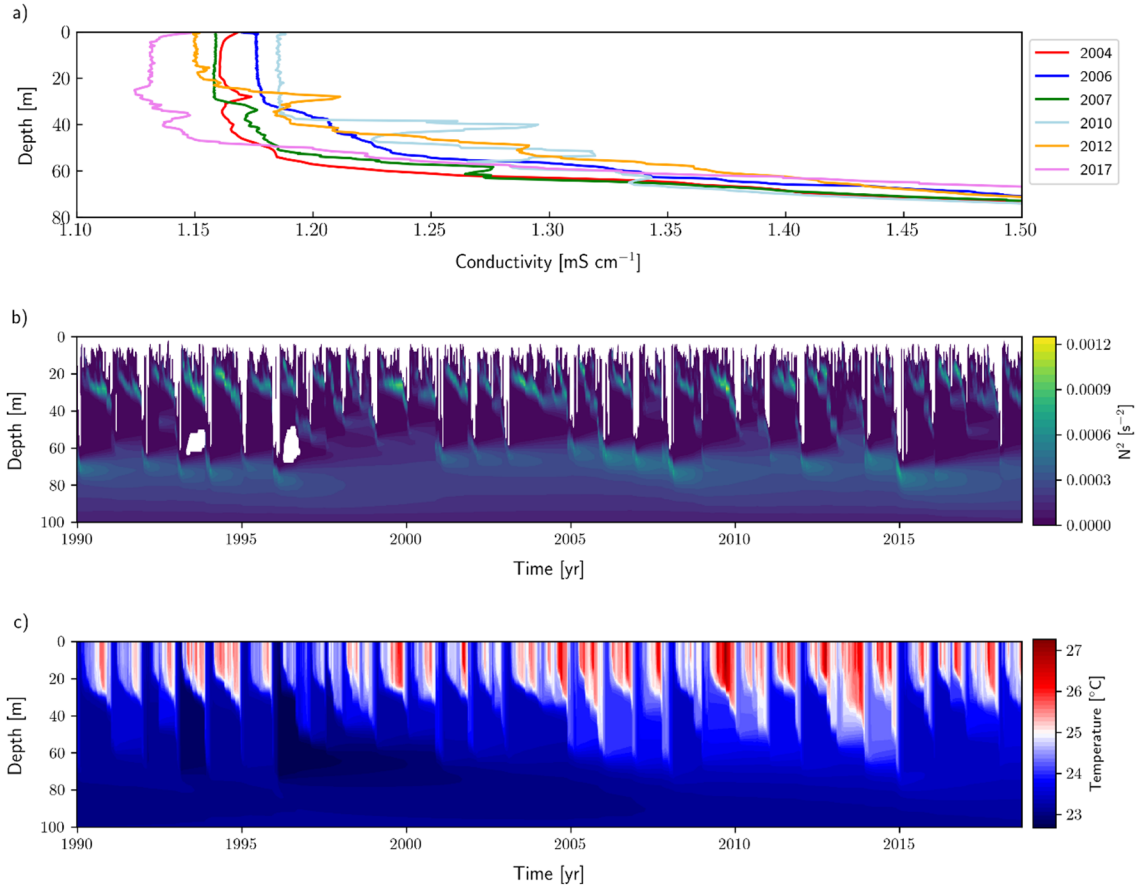

Figure 4.3. a) Conductivity profiles measured in the top 80 m in different years: February 2004 (Schmid et al., 2005), May 2006 and May 2007 (Pasche et al., 2009), January 2010 and January 2012 (Ross et al., 2015a), March 2017 (Bärenbold et al., 2020a), b) Simulated stability N^2 in the top 100 m during 18 years (forced by RCP6), where white is negative stability, i.e. represents convective mixing, c) Simulated temperature in the top 100 m during 18 years (forced by RCP6).

Turbulent mixing at intermediate depths (60 – 120 m)

Diffusive transport between ~60 – 120 m is governed neither by seasonal mixing nor by double diffusive convection. This depth region is characterized by a strong increase in salinity with depth and therefore a strong density gradient. It was therefore put forward by Schmid et al., 2005 that turbulent mixing in this region is weak. In contrast, the stable isotope measurements by Ross et al. (2015a) indicate that mixing might be stronger than previously thought. In fact, their measurements seems to show that the evaporative isotope signal at the lake surface seems to be mixed down against the groundwater-induced upwelling.

Our simulation results suggest that direct wind-induced turbulent mixing is indeed very weak in Lake Kivu below 60 m. The wind-induced currents are not able to penetrate below the surface layer, and without considering the energy transfer via internal seiches, the modelled salinity gradient below the surface mixed layer becomes much steeper than observed (Figure 4.4a). In Simstrat, the seiche energy parameter α_s represents the ratio of seiche energy to the amount of available wind energy. If it is tuned to 0.0027 (i.e. 0.27 % of wind energy is transformed to seiche energy), our model can reproduce the observed salinity gradient very well (Figure 4.4b), except for a small jump at ~120 m. This jump is an artefact caused by the transition from the k-ε mixing scheme to the parameterization of double diffusion. We were able to reduce the size of the jump by tuning the calibration parameter q^{NN} but not to eliminate it. The parameter q^{NN} determines how the mixing energy from internal seiching is distributed vertically as a function of stability N^2.

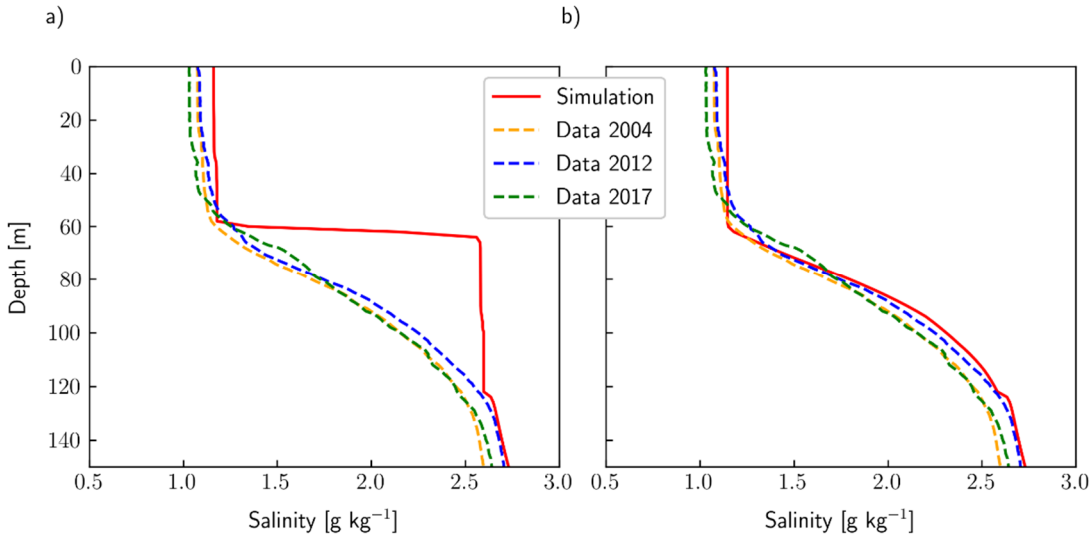

Figure 4.4. Simulated salinity profiles (after a 500 year steady-state simulation) compared to observations from 2004 (Schmid et al., 2005), 2012 (Ross et al., 2015a) and 2018 (Bärenbold et al., 2020a) in the top 150 m. a) Without seiche induced mixing (α_s = 0), b) including seiche induced mixing (α_s = 0.0027, i.e. 0.27 % of the available wind energy is transferred to seiching).

We conclude that internal seiching can explain why there is still a certain amount of turbulent mixing (10^{-7} – 10^{-6} m^2 s^{-1}) in a depth region where the density gradient is very strong.

Steady-state simulation

While diffusive transport is computed using the k-ε closure (0 – 120 m) and a parameterization of double diffusive convection (120 – 485 m), vertical advection is a function of the discharge, inflow depth and properties (T, S, CO_2, CH_4) of the different groundwater springs present in Lake Kivu. Unfortunately, the properties of the groundwater sources are inherently difficult to measure in the field. However, despite the lack of data, we can use indirect evidence to shed light on the influence of the groundwater sources on Lake Kivu.

Using the water balance of Lake Kivu, Schmid & Wüest (2012) suggest that the total groundwater input into Lake Kivu is between 32 and 48 m^3 s^{-1}. In addition, Ross et al. (2015a) were able to identify several warm and saline signals below 250 m, as well as a strong cool and less saline signal right at the chemocline (~250 m) and a more diffusive cool signal between ~90 and 195 m. Based on this information and the current vertical structure of the lake, we assume that: i) four hydrothermal point sources enter the lake below 250 m and plunge due to their high density, ii) two cooler point sources enter the lake at 253 and 190 m, and iii) one diffusive groundwater source, which has the same properties as the point source at 190 m, enters the lake between 90 and 195 m depth (Figure 2 in Ross et al., 2015a).

We summarized this information in Table 4.2. Throughout this work, we refer to the ground-water sources at 190 and 253 m as cool sources 1 and 2, respectively; and the sources below 250 m as hydrothermal sources.

Table 4.2. Summary of groundwater inflows into Lake Kivu used in this work. The inflow depths and discharges are calibrated in order to produce a steady-state close to today's profiles.

Name	Depth [m]	Properties	Type	Q [m^3 s^{-1}]	Ross et al., 2015
Cool source 1a	190	Cool / fresh	Point source	6.0	Identified
Cool source 1b	90 - 195	Cool / fresh	Diffusive source	23.6	Identified
Cool source 2	253	Cool / fresh	Point source	11.0	Identified
Hydrothermal 1	310	Warm / saline	Point source	1.5	-
Hydrothermal 2	330	Warm / saline	Point source	0.6	-
Hydrothermal 3	400	Warm / saline	Point source	1.0	-
Hydrothermal 4	430	Warm / saline	Point source	1.2	-

The water introduced as point sources is free to plunge or rise according to their density in Simstrat, thereby entraining ambient lake water. The final stratification depth of these groundwater inflows is not only influenced by their temperature, salinity and gas content, but also by the current lake density profile, which leads to a highly complex and interdependent calibration problem with many unknown variables.

In order to calibrate inflow depth and discharge, but also temperature, salinity and CO_2 content of the groundwater sources, we chose to tune our model with the goal of producing a steady-state with temperature, salinity and gas profiles close to today's observations. This approach is motivated by the findings of Bärenbold et al., 2020a who conclude that CH_4 and CO_2 concentrations did not show a clear temporal trend during the last ~45 years. Conversely, Sommer et al., 2019 found that Lake Kivu is showing a very slow warming trend in the stratified waters below 60 m, which is approximately 0.01 °C per year. We chose to neglect this warming rate in our simulations for two reasons: i) the observed warming trend seems variable in time and is comparably small, and ii) we focus on the present state and the past evolution of Lake Kivu in this work, not on its future evolution. Note however, that a warming rate could be introduced by slightly modifying the temperature of the hydrothermal groundwater inflows or the geothermal heat flux.

While most of the CO_2 stems from groundwater inflow this is not true for CH_4, which was shown to contain a mixture of modern and old, ^{14}C-dead carbon (Schoell et al., 1988; Pasche et al., 2011). Using ^{14}C analysis, Pasche et al. (2011) showed that the degradation of organic matter can only provide a maximum of ~50 % of CH_4 below 250 m. The remaining 50 % stem either from reduction of old, geogenic CO_2 or from the direct inflow of geogenic CH_4. The absolute CH_4 fluxes derived in Pasche et al. (2011) lead to an increase in CH_4 concentrations of around 7 – 8 % within 30 years. However, such an increase is clearly not validated by the most recent measurements (Bärenbold et al., 2020a), which indicate approximately constant concentrations since the measurements of Tietze in 1974 (Tietze, 1978). Therefore, we assume that the actual CH_4 production below 250 m is close to a steady-state production of ~30 gC m^{-2} y^{-1}. According to Pasche et al. (2011), ~50 % of this production is supplied by degradation of organic matter, and therefore we set $F_{sed,CH4}$ in AED2 to 3.2 mmol m^{-2} d^{-1} CH_4 (14.0 gC m^{-2} y^{-1}) for the whole lake depth. For the remaining 50 % below 250 m, we will explore two scenarios: i) the reduction of geogenic CO_2 to CH_4 within the lake (implemented analogously to CH_4 production from organic matter), and ii) the direct groundwater-mediated inflow of geogenic CH_4. In both cases, an additional ~3.2 mmol m^{-2} d^{-1} of CH_4 is added below 250 m, thus yielding a total CH_4 production of ~6.4 mmol m^{-2} d^{-1} (28 gC m^{-2} y^{-1}) below 250 m.

Figure 4.5 shows simulation results for temperature, salinity, CO_2 and CH_4 for a simulation duration of 500 years (exact groundwater properties used in the simulation are provided in Table B4). The initial conditions used in this simulation are the temperature and salinity background profile of Ross et al. (2015a) and the CH_4 and CO_2 concentrations measured in 2018 (Bärenbold et al., 2020a). Our model assumptions and tuned inflows lead to steady-state after 400 – 500 years for temperature, salinity and CO_2 concentrations, with CO_2 concentrations agreeing with observations well within measurement uncertainty. The agreement between data and simulation is also excellent for salinity, but not for temperature. While the general structure of the temperature profile is generally well reproduced, temperature is ~0.3 °C too low between 250 and 350 m and ~0.1 °C too high below 400 m. Despite a large calibration effort on the groundwater properties, these differences could not be eliminated. The main difference between temperature and the other main agents in Lake Kivu is that the transport of salinity and gases is dominated by vertical advection (i.e. the upwelling caused by groundwater inflow), while for temperature both advection and diffusive transport are important (Sommer et al., 2019). As a consequence, it seems that the properties of the groundwater sources are well calibrated, while the parameterization of heat transport through the double diffusive staircases only works satisfactorily. Indeed, Figure 4.2a shows that the proposed linear regression reflects well the general relationship between stability and apparent temperature diffusivity. However, the variability is rather large, thus indicating that the prediction capacity of stability to deduce double diffusive transport in Lake Kivu is limited.

For CH_4, we explored two scenarios with different origins for the ^{14}C-dead part of CH_4. Scenario 1 implies that the remaining 50 % of CH_4 are produced by CO_2 reduction within the lake (Figure 4.5d), while in scenario 2 the remaining 50 % stem from groundwater (Figure 4.5e). Scenario 1 indicates that CH_4 concentrations should reach a clear maximum between 300 and 400 m and decrease towards the lake bottom due to the inflow of CH_4-free groundwater there. This decrease is supported by the CH_4 data of Tietze in 1974 (Tietze, 1978) and the Eawag dataset in Bärenbold et al. (2020a), but not by the data of Halbwachs and & Tochon in 2003 (Schmid et al., 2005) and the UFZ dataset in Bärenbold et al. (2020a). Scenario 2 also shows slightly decreasing concentrations at the lake bottom, but this decrease is small, and could probably be eliminated by further tuning the CH_4 concentrations in the groundwater sources (see Table B4 for values used in scenario 2). Scenario 2 agrees better with observed CH_4 concentrations and thus, our results suggest that at least part of the remaining 50 % of CH_4 are introduced by the hydrothermal groundwater sources. In both scenarios, CH_4 production from the decomposition of organic matter is assumed constant with depth. In reality, sediment

focusing or the reduction of degradable organic matter at greater depths due to longer settling times could potentially lead to varying CH_4 production with depth.

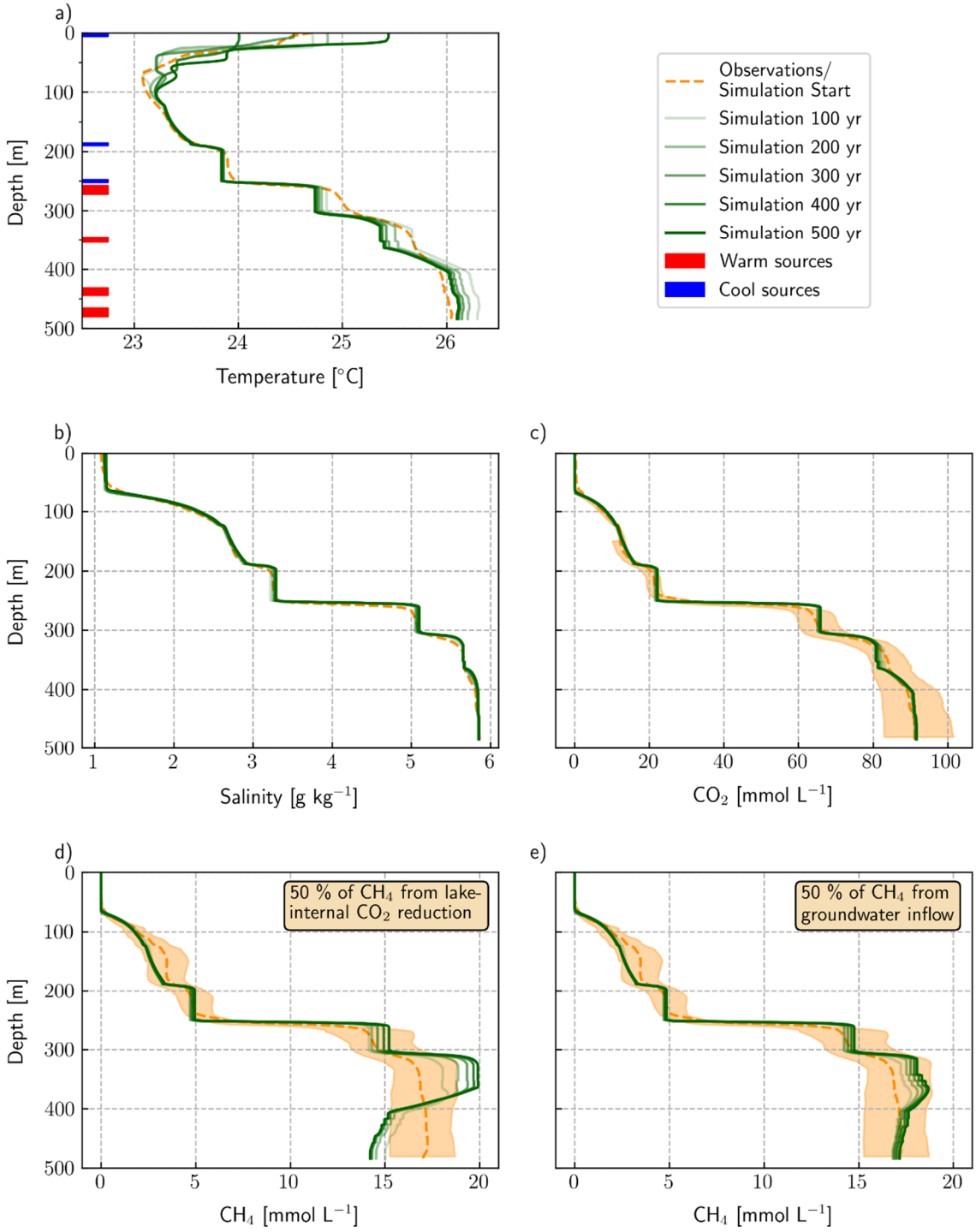

Figure 4.5. Depth profiles at different simulation times of a 500 year steady-state simulation compared to observations. The temperature and salinity simulations are compared to the background data by Ross et al. (2015a) and the CO_2 and CH_4 simulations to Bärenbold et al. (2020a) (average of Eawag and UFZ datasets therein, and the uncertainty is the maximum uncertainty of both datasets). The simulation is initialized with the observations, and forced by constant groundwater inflows (see Table B4) and meteorological input (piControl). a) Temperature profile; the horizontal bars represent the depths where groundwater inflows stratify, b) Salinity profile, c) CO_2 profile, d) CH_4 profile with 50 % of CH_4 produced by each degradation of organic matter and CO_2 reduction, e) CH_4 profile with 50 % of CH_4 produced by each degradation of organic matter and groundwater inflow.

Water tracer simulations

In this section, we use the calibrated steady-state model to reproduce the ^{3}H and $\delta^{2}H$ measurements from this work and by Ross et al. (2015a) respectively.

^{3}H simulations: water age and origin

There are no direct ^{3}H measurements available from the groundwater sources. In general, ^{3}H in groundwater can have two origins, namely a low, rather constant background signal due to interaction with rocks (Mamyrin & Tolstikhin, 1984), and a variable signal due to gas exchange with the atmosphere. Therefore, we make the following assumptions for our model runs: i) the old, hydrothermal groundwater in the Lake Kivu basin has a constant background ^{3}H signal of 0.5 TU due to interaction with rocks, ii) young groundwater stems from the recent infiltration of precipitation and has an atmospheric ^{3}H signal and, iii) all groundwater sources in Lake Kivu can be a mixture of old and young groundwater. Note that we assume that the time from infiltration of precipitation to groundwater recharge is short, i.e. there is no lag that would decrease the ^{3}H concentration due to radioactive decay. This assumption is justified by the fact that the northern shore, where the groundwater sources were found (Ross et al., 2015a) consists of permeable volcanic rock, which allows fast infiltration of rainwater.

Figure 4.6a shows simulation results under the assumption that every groundwater source is entirely composed of old hydrothermal groundwater, and field observations from 2004 and 2018. The observations show a decrease in time in the seasonal mixed layer from 2.2 TU in 2004 to 1.6 TU in 2018 and a decrease with depth from 1.6 TU to close to 0 at 200 m. The decrease in time can be explained by decreasing ^{3}H concentrations in the atmosphere due to radioactive decay of the remaining bomb ^{3}H, while the decrease with depth shows that the water below 60 m is predominantly old (i.e. no recent interaction with the atmosphere), and that vertical mixing is weak. The assumption that all groundwater sources are entirely composed of old groundwater agrees very well with the observations in the mixed layer, as well as with the observation below 300 m. However, between 100 and 200 m, the measured ^{3}H concentrations are higher than predicted by the simulation, thus indicating that the cool groundwater sources do also contain atmospheric ^{3}H. Indeed, if we adjust the fraction of young groundwater in the

cool sources 1 and 2 to 45 % and 20 %, respectively, we get a very good agreement with the observations in the corresponding depth region (Figure 4.6b).

The finding that the cool groundwater sources are partially young is supported by the absence of surface tributaries in the north of Lake Kivu where Ross et al. (2015a) identified the cool sources. This northern part of the catchment has a surface area of ~686 km^2, which accounts for ~14 % of the whole Lake Kivu catchment area of 4940 km^2. We can estimate a lower bound for the amount of water which infiltrates and feeds the groundwater sources by using the surface inflow of 63 $m^3\ s^{-1}$ (Schmid & Wüest, 2012). As 86 % of the catchment produce ~63 $m^3\ s^{-1}$ of run-off, the remaining 14 % would yield a potential groundwater recharge of ~10 $m^3\ s^{-1}$. However, precipitation is expected to infiltrate quickly through the porous volcanic rock in the north and thus, there is less water lost to evaporation than in the remaining watershed. An upper bound of the infiltrated water can be derived by using the average precipitation of 1470 mm yr^{-1} (Muvundja et al., 2014) which would give ~32 $m^3\ s^{-1}$ over volcanic part of the catchment. The amount of young water required by our calibrated model to fit the observed ^3H profile is ~15.5 $m^3\ s^{-1}$ with a range of ~11.5 – 18 $m^3\ s^{-1}$ (range estimated from uncertainty of ^3H) and is therefore well within the range of 10 – 32 $m^3\ s^{-1}$ given by precipitation and run-off data.

We conclude that the cooler groundwater sources are probably a mixture of old and more recent groundwater, with ~45 and ~20 % of recently infiltrated in cool sources 1 and 2, respectively. Conversely, our only observation below 300 m suggests that the deep groundwater sources predominantly consist of old, hydrothermal water.

δ^2H simulations contradict field observations

In contrast to ^3H, there are field observations available for δ^2H for at least some of the groundwater sources (Ross et al., 2015a). Below 200 m, Ross et al. (2015a) found very variable δ^2H groundwater signals ranging from -2.8 to 17.4 ‰. In our model, we cannot use these values because our implemented hydrothermal sources do not directly correspond to the hydrothermal sources found by Ross et al. (2015a). Therefore, the δ^2H concentrations of the hydrothermal sources are adjusted in order to fit the observations. In contrast, the cool sources 1 and 2 were clearly identified by Ross et al. (2015a) and thus, Figure 4.6c shows a simulation where the δ^2H concentration of cool sources 1 and 2 correspond to the values found by Ross et al. (2015a), while in 4.6d we adjust all sources to fit the observed background profile. For both simulations,

the δ^2H concentration in precipitation was fixed to -4.5 ‰ and therefore the model is not able to reproduce seasonal changes in δ^2H.

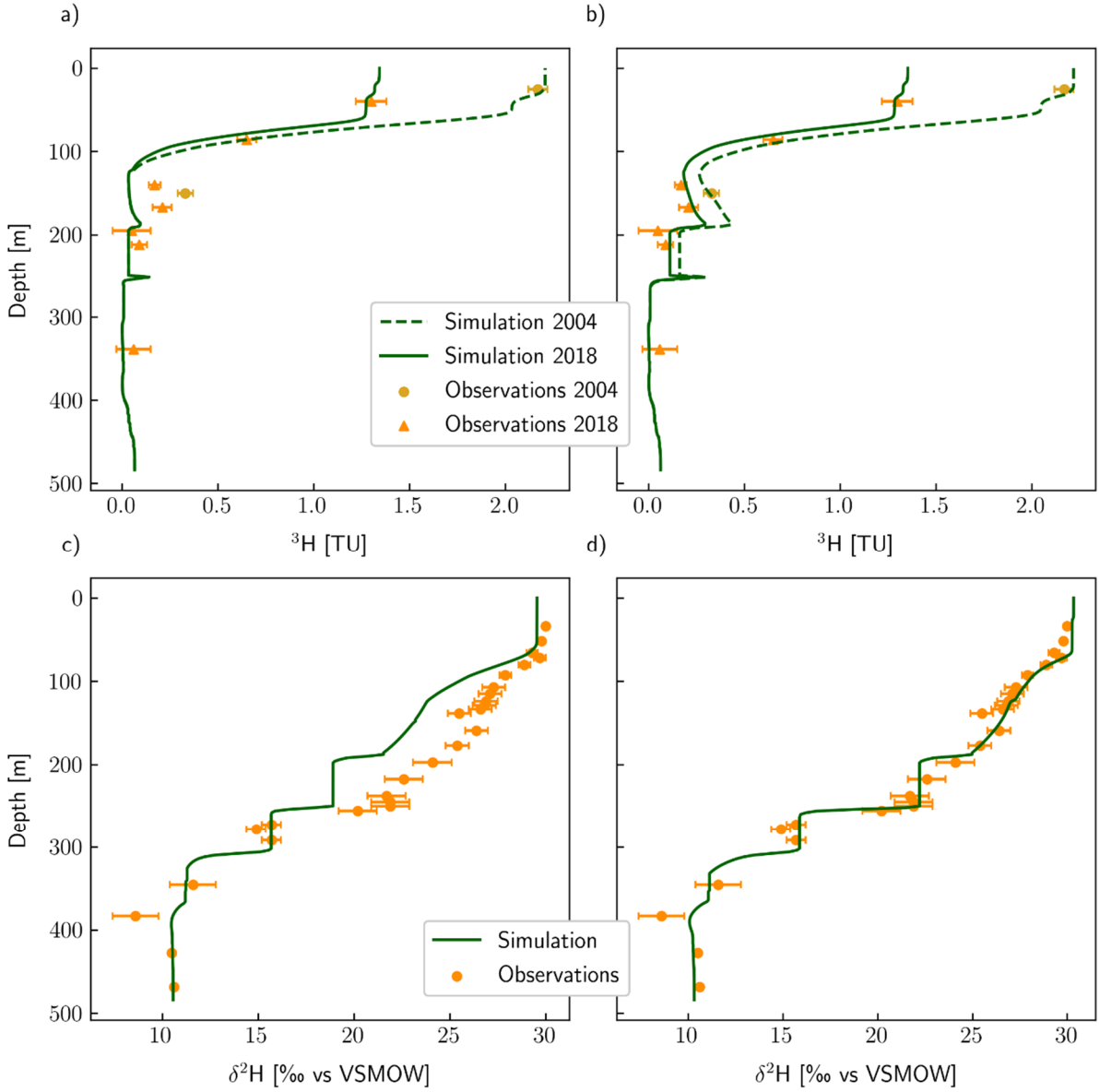

Figure 4.6. Water tracer simulations compared to field observations. Transient simulation for ^{3}H (1953 – 2018) with meteorological input from RCP6 compared to ^{3}H data from 2004 and 2018; steady-state simulation for δ^2H (100 years) with meteorological input from RCP6 compared to observations by Ross et al. (2015a). a) Simulation results with 0 % modern ^{3}H for all sources, b) Simulation results with 45 % modern ^{3}H at 190 m and 20 % modern ^{3}H at 250 m (see Table B5 for numerical values), c) Simulation results with δ^2H concentrations in cool sources 1 and 2 as measured by Ross et al. (2015a), d) Simulation results with δ^2H concentrations in cool sources 1 and 2 adjusted to fit the background observations of Ross et al. (2015a), (see Table B5 for numerical values).

The observed δ^2H groundwater concentrations above 250 m are considerably lower compared to simulated δ^2H (Figure 4.6c). The δ^2H concentrations necessary to provide a good agreement of observations and simulation are around 15 and 40 % higher for cool sources 1 and 2,

respectively (Figure 4.6d, see Table B5 for numerical values). These differences are well beyond measurement uncertainty and in addition, both δ^2H groundwater observations consist of several measurements with rather low variability (pers. comm. K. A. Ross). The results of the δ^2H simulations are further corroborated by ^{18}O simulations (not shown in this work), which exhibit the same systematic deviation from observations.

We conclude that our model is able to perfectly reproduce the observed δ^2H profiles if the inflow concentrations are freely adjustable and allowed to have an evaporative δ^2H signal. Therefore, the observed stable isotope profiles are not in contradiction with low turbulent mixing in Lake Kivu. However, the observed δ^2H concentrations close to cool sources 1 and 2 are not high enough to explain the observed lake profiles. Potentially, a certain discrepancy could be because δ^2H in the groundwater inflows (or the groundwater inflows themselves) are variable in time. However, it is unlikely that this could explain a difference of 15 and 40 % in inflow concentrations.

Origin and maintenance of the density stratification

It is generally assumed that Lake Kivu has experienced several (partial) degassing events in the past (Haberyan & Hecky, 1987; Zhang et al., 2014; Ross et al., 2015; Votava et al., 2017; Uveges et al., 2020). This may have happened by spontaneous ebullition due to gas over-saturation in the deep waters. Another possibility is the creation of instability within the water column due to either subaquatic volcanism (Ross et al., 2015b) or hyperpycnal flows due to exceptional rain events (Zhang et al., 2014). Ross et al. (2015b) and Uveges et al. (2020) both estimate that the last large mixing event may have occurred ~800 – 1000 years ago, with several smaller events between 800 years BP and the present. In this context, we can use our model to evaluate how long it takes Lake Kivu to reach its current state. Because we don't know when and to what extent Lake Kivu has mixed in the past, we assume that i) the lake is completely mixed and gas-free at the start of the simulation, ii) the groundwater discharge and properties (i.e. temperature, salinity and gas concentrations) are constant in time and the same as today, and iii) the average seasonal mixing depth is constant and the same as today.

Our simulated salinity and gas concentrations agree well with today's state after roughly 1500 years (Figure 4.7), thus confirming that the density-driven inflow of several groundwater sources can explain today's vertical lake structure. This result is in contrast to arguments by Hirslund (2020) who suggests that the inflow of groundwater sources cannot be responsible for

Lake Kivu's density stratification. For temperature, it takes more time to reach a steady-state. The reason is that double-diffusive transport is much faster for temperature compared to salinity and gases due to the much higher molecular diffusion coefficient. While the vertical transport of salinity and gas concentrations is dominated by advection, double diffusion contributes around half of the vertical heat flux. The double-diffusive heat flux is parameterized as a function of N^2 and therefore, a stable temperature profile will only develop once the density stratification (mainly determined by salinity and CO_2) is fairly stable after ~1500 years. At this point, the overshooting temperature below 350 m decreases again and converges to ~26 °C.

Our model results suggest that we should see slightly decreasing deep water temperatures if the lake is close to a steady-state. In contrast, recent temperature observations indicate an increase of ~0.01 °C y^{-1} (Sommer et al., 2019). There are several possible answers to this problem: i) the lake is not at a steady-state and thus, temperature, salinity and gas concentrations are still slightly increasing, ii) the lake was close to a steady-state, but there was an increased discharge of hydrothermal water during the last decades which counteracts the temperature decrease, and iii) our parameterization of double-diffusive heat flux is not suitable for the simulation of a near-homogeneous lake at the start of the simulation and thus the simulated overshooting is a model artefact. Note that answer ii) would also imply a slight steepening of the main chemocline at 250 m due to increased upwelling as it was observed recently (Hirslund et al., 2012). However, this steepening stopped again after 2012 (pers. comm. M. Schmid).

Assuming constant groundwater inflows throughout the simulation duration, our simulations show that it is improbable that today's lake structure has developed within only 1000 years from an initially homogeneous and degassed lake. The time which is necessary to reach a steady-state close to today's observed temperature, salinity and gas concentrations rather seems to be around 2000 years. Therefore, a potential mixing event ~1000 years ago, as suggested by Ross et al. (2015b) and Uveges et al. (2020), could not have mixed the entire lake. However, a partial mixing event ~1000 years ago or even smaller mixing events during the last few centuries are well compatible with our simulations.

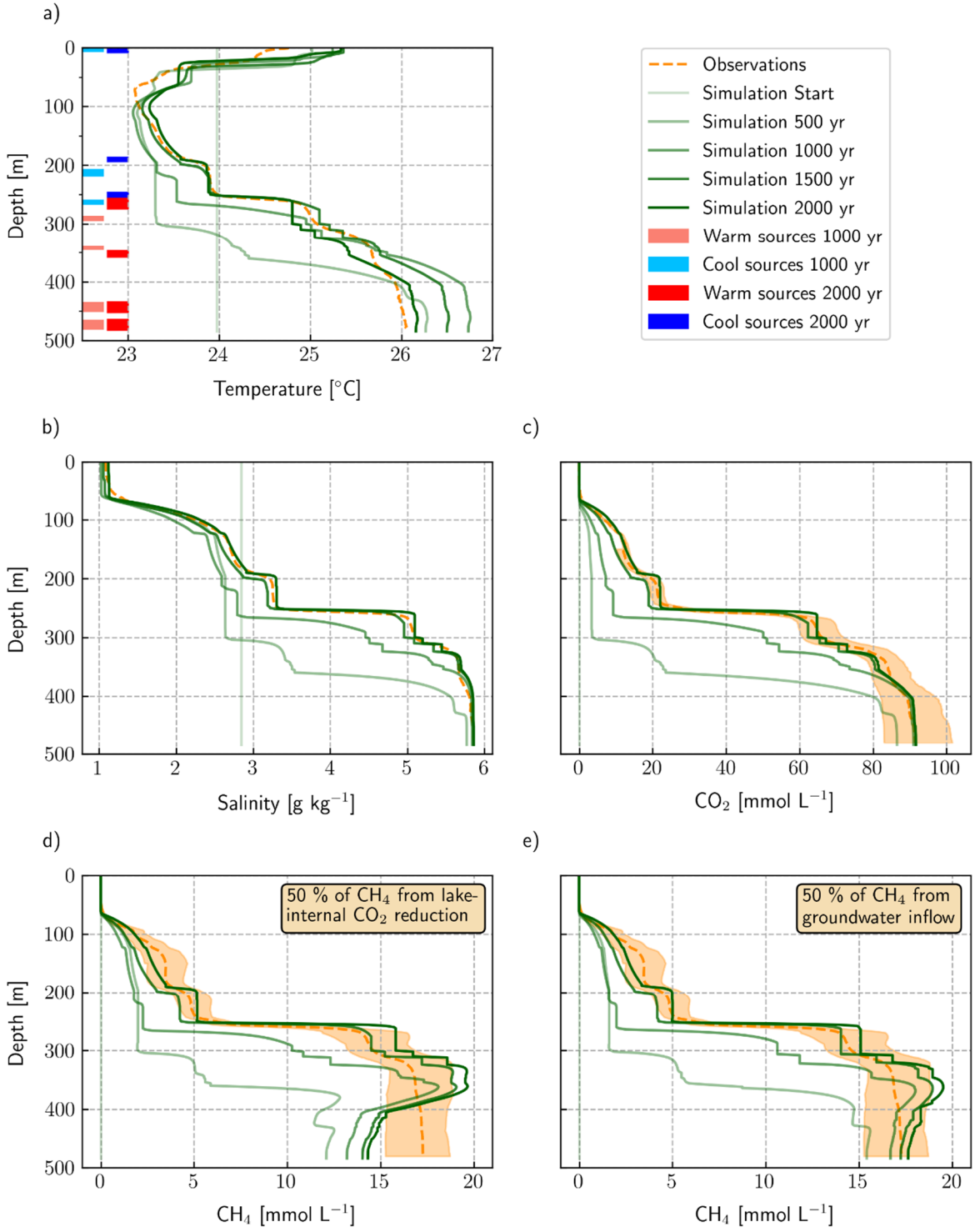

Figure 4.7. Depth profiles at different simulation times for a long-term transient simulation compared to observations. The temperature and salinity simulations are compared to the background data by Ross et al. (2015a) and the CO_2 and CH_4 simulations to Bärenbold et al. (2020a) (average of Eawag and UFZ datasets therein, and the uncertainty is the maximum uncertainty of both datasets). The simulation is initialized with a completely homogeneous and gas-free lake, and is forced by constant groundwater inflow (see Table B4 for groundwater properties) and meteorological input (piControl). a) Temperature profile; the horizontal bars represent the depths where groundwater inflows stratify at 1000 and 2000 years respectively, b) Salinity profile, c) CO_2 profile, d) CH_4 profile with 50 % of CH_4 produced by each degradation of organic matter and CO_2 reduction, e) CH_4 profile with 50 % of CH_4 produced by each degradation of organic matter and groundwater inflow.

Atmospheric noble gas depletions in the deep water

In an earlier publication, we described that the atmospheric noble gases (i.e. the noble gases whose main source is the atmosphere) Ne, ^{36}Ar and Kr are depleted by 55 – 70 % in the deep water of Lake Kivu (Bärenbold et al., 2020b). Therein, we discussed three different mechanisms to explain the observed noble gas depletions, namely i) continuous outgassing, ii) the inflow of noble gas depleted groundwater, and iii) a relic of a past large outgassing event. Mechanism i) was subsequently excluded because the isotope ratios ^{20}Ne/^{22}Ne and ^{40}Ar/^{36}Ar did not show the expected depletion patterns (Bärenbold et al., 2020b). We further argued that mechanism ii), the inflow of depleted groundwater is the most probable reason for the observed profiles.

In this section, we use the model setup of the previous section to test and evaluate hypotheses ii) and iii). For hypothesis ii), we adjusted the concentrations in the groundwater sources to fit the observed noble gas profiles in Bärenbold et al. (2020a). Conversely, in hypothesis iii) the noble gas concentrations in the groundwater are fixed to those of air saturated water (ASW) at 25 °C. The resulting Ne profiles indicate that we can exclude that the currently observed profiles are a result of a past outgassing event only (Figure 4.8b). In contrast, the observed concentrations can be perfectly reproduced by the inflow of noble gas depleted groundwater (Figure 4.8a). The best agreement with observations is reached if the hydrothermal sources are depleted by 40 – 50 % (Table B5) and the cool sources 1 and 2 by 5 % and 10 %, respectively. The depth profiles of the other atmospheric noble gases measured in Bärenbold et al. (2020b) can be successfully reproduced as well, but are not shown here.

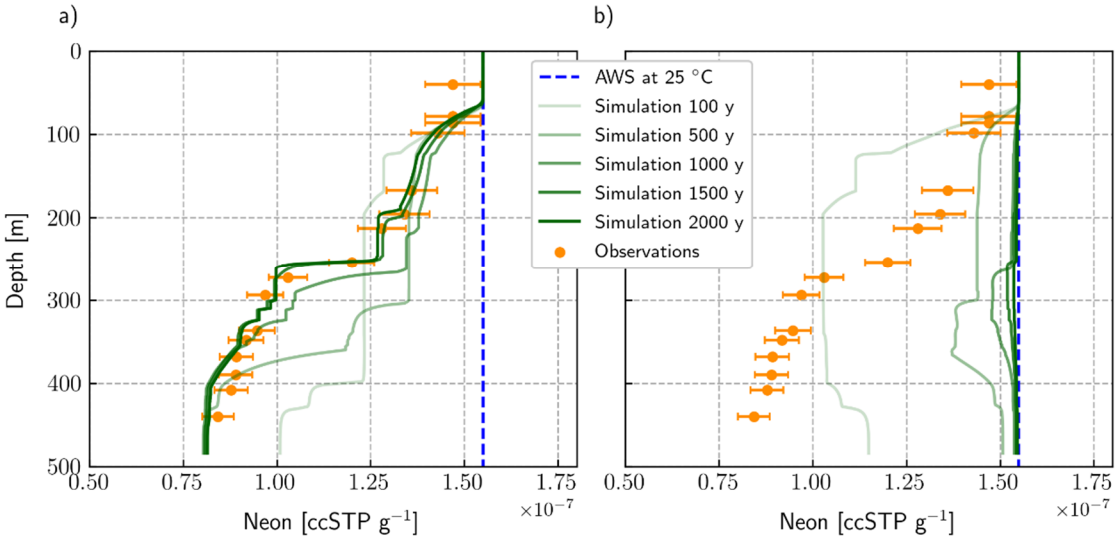

Figure 4.8. Simulated Neon depth profiles over 2000 years, starting with a homogeneous, degassed lake, compared to observations from Bärenbold et al., 2020b: a) depletion of hydrothermal inflows is 40 – 50 % and depletion of cool sources 1 and 2 is 5 and 10 % compared to air saturated water (ASW), respectively (see Table B5 for numerical values), b) all inflows contain air saturated water at 25 °C.

Model limitations

Compared to past one-dimensional modelling attempts on Lake Kivu (Schmid et al., 2005), one of the main advantages of our model is the fact that turbulent transport is dynamically calculated throughout the whole water column. From 0 to 120 m, we use Simstrat's built-in k-ε turbulence closure, and below, we apply a newly derived parameterization, which is based on measurements by Sommer et al. (2013). This situation creates an artificial transition point at 120 m. However, while both the transition at 120 m and the parameterization are valid for today's lake structure back to at least 1976 (Newman, 1976), we have no information about the presence and extent of double diffusive staircases during the past centuries. Particularly, during periods with a weaker density stratification, we do not know how well our parameterization performs. Nevertheless, it can be assumed that an initially weak density stratification quickly becomes stronger due to the constant deep inflow of salts and CO_2. As a consequence, although turbulent transport might initially be underestimated by our parameterization, this probably does not significantly alter the simulations results.

Another important simplifying assumption of our modelling exercise is the fact that the discharges and properties of all groundwater sources are constant in time. Part of the cooler groundwater sources seems to have an atmospheric ^3H signature, and thus we expect the discharge and properties of these sources to vary with climate conditions (i.e. higher discharge in a wet climate, lower discharge during droughts). Furthermore, volcanic activity can greatly influence hydrological parameters like evaporation and rock permeability and thus lead to variable infiltration and groundwater properties over time. For example, Votava et al. (2017) suggest that the intermittent deposition of $CaCO_3$ found in lake sediments indicate a corresponding intermittency of deep groundwater inflow into Lake Kivu. However, for our long-term simulations it is not crucial to know whether the inflow does vary over shorter timescales as long as the average discharges over longer timescales remain stable.

Conclusions

We developed and calibrated a one-dimensional model for Lake Kivu, exploiting the fact that the lake is well mixed horizontally. In order to simulate the effect of dissolved gases CO_2 and CH_4 on lake physics, we first coupled the physical lake model Simstrat with the biogeochemical model library AED2. We then developed a parameterization of vertical transport of heat, salts

and gases across the double-diffusive staircases of Lake Kivu (below 120 m) as a function of lake stability N^2. After manually calibrating temperature, salinity and gas content of the inflowing groundwater sources, we were able to reproduce today's lake profile by a steady-state simulation. Using this steady-state model and our ^3H dataset allowed to show that the cooler groundwater sources, which enter the lake between 100 and 250 m, are probably a mixture of modern and old, hydrothermal water.

Most importantly, we showed that the evolution of Lake Kivu from a completely homogeneous and gas-free state to today's density stratification within 2000 years is successfully reproduced using a 1-dimensional lake model with constant groundwater inflows. Our results demonstrate that the stratification depth of groundwater inflows markedly shifts a function of the evolving density structure of the lake. As the duration of 2000 years is an upper bound, which is valid for an initially completely mixed lake, our model indicates that a partial mixing event ~1000 years BP (Zhang et al., 2014; Ross et al., 2015b; Uveges et al. 2020) is in good agreement with the currently observed state of the lake. Furthermore, our simulation results suggest that the depletion of atmospheric noble gases in the deep water of Lake Kivu (Bärenbold et al., 2020b) are not a relic from a past outgassing event, but have to be sustained by an active process (i.e. inflow of noble gas depleted groundwater).

In this work, we used our model to focus on finding a steady-state solution for today's lake structure, and on reproducing the past evolution of Lake Kivu. In the future, our model can be a valuable tool to simulate the effect of a changing climate on lake temperature, stratification and nutrient availability. In addition, it can facilitate the decision-making concerning the construction and operation of ongoing and future methane harvesting projects in Lake Kivu. In order to better constrain the discharge and properties of the groundwater inflows in future model applications, more research on the hydrogeological setting in the Lake Kivu region would be beneficial. Moreover, the sampling of inflowing groundwater sources using a remotely operated underwater vehicle (ROV) could allow the determination of temperature, salinity and gas concentrations of groundwater sources without contamination with lake water.

Acknowledgements

We would like to thank Reto Britt, Michael Plüss, Maximilian Schmidt and the whole team from LKMP (Lake Kivu Monitoring Programme) for help with tritium sampling in Lake Kivu.

We also want to thank Alexandra Lightfoot and Matthias Brennwald from the noble gas laboratory at ETH Zurich for help with tritium sample analysis. Adrien Gaudard and Davide Vanzo provided helpful insights into modelling and the implementation of new Simstrat features. Particularly, Adrien's manual was of great help. We also would like to acknowledge Wim Thiery from Vrije Universiteit Brussel who made the data of the Lake Kivu weather station available for us and Love Raman Vinna for providing the regional climate model input files for Simstrat.

Supporting information in Appendix B

Figure B1. ^{3}H atmospheric input function.

Figure B1. Extrapolation of ^{3}H input function to 2018.

Table B1. Simstrat-AED2 configuration parameters.

Table B2. Simstrat model parameters.

Table B3. AED2 model parameters.

Table B4. Inflow depth, discharge and properties of groundwater inflows.

Table B5. ^{3}H, $\delta^{2}H$ and Ne concentrations of groundwater inflow.

Chapter 5

General conclusion

Summary of results

The research conducted as part of this dissertation yielded three main results, each covering a different aspect of what makes Lake Kivu unique. In the second chapter, we presented updated methane (CH_4) and carbon dioxide (CO_2) concentrations, including the results of two other research teams. Contrary to previous measurements (Halbwachs & Tochon in Schmid et al., 2005), our results indicate that there has been no clear temporal trend in CH_4 and CO_2 concentrations in Lake Kivu during the last ~45 years, i.e. since the measurements of Tietze in 1974 (Tietze, 1978). In addition, calculated and observed total dissolved gas pressure (TDGP) show that gas pressure in Lake Kivu is below 55 % saturation at any depth, and therefore far away from a state where spontaneous ebullition could occur.

In chapter 3, we presented a complete dataset of noble gas concentrations and isotope ratios. Prior to our campaign, noble gas data for Lake Kivu was scarce or of bad quality (Tassi et al., 2009). The most striking feature of our dataset is a depletion of atmospheric noble gases Ne, ^{36}Ar and Kr of 50 to 70 % compared to air saturated water (ASW) in the deep waters of Lake Kivu. We discussed three hypotheses to explain the observed depletions, of which we excluded continuous, slow outgassing because there is no corresponding fractionation signal in the isotope ratio profiles. In contrast, the good correlation between salinity and atmospheric noble gas concentrations suggests that both the salinity increase and the depletion of noble gas concentrations are caused by the intrusion of hydrothermal groundwater into Lake Kivu. The hypothesis of noble gas depleted groundwater is confirmed by temperature spikes close to the shore, which indicate that the groundwater could have been much warmer before entering the lake, thus potentially losing large parts of dissolved gases. Moreover, increasing $^{3}He/^{4}He$ and $^{40}Ar/^{36}Ar$ profiles with depth suggest a magmatic origin of the gases present in Lake Kivu.

In the fourth chapter, we used one-dimensional modelling of Lake Kivu to conclude that the cool and fresh groundwater sources at ~190 and ~250 m are probably a mixture of old hydrothermal groundwater and recently infiltrated rainwater. Furthermore, we confirmed that the observed noble gas depletions (chapter 3) could be the result of the inflow of noble gas depleted groundwater. The most significant result of our simulation study is the fact that the currently observed stratification and gas profiles can be reproduced, starting from a completely homogeneous and degassed lake. The use of a homogeneous, degassed lake as initial conditions is relevant because it may represent the result of an earlier extreme lake overturn event suggested to have happened ~1000 BP by Ross et al (2015b) and Votava et al. (2017). Our simulations indicate that the time to reach a steady-state after such an extreme mixing event is

on the order of ~2000 years, and that therefore, the suggested mixing event ~1000 years ago did probably not completely mix and degas the lake.

Our modelling approach has two main advantages compared to a previous one-dimensional model (Schmid et al., 2005; Wüest et al., 2009), namely the dynamic calculation of mixing throughout the water column, and the stratification of inflowing groundwater according to density. While diffusive mixing (i.e. double diffusive convection) is important for the vertical transport of heat, the transport of dissolved solids and gases is dominated by vertical advection below 120 m. Hence, we show that salinity and gas profiles in Lake Kivu are mainly driven by the discharges and properties of plunging subaquatic groundwater inputs.

Implications for the management of Lake Kivu

Our findings have consequences on two important aspects of the management of Lake Kivu. Firstly, our measurements suggest that there is no clear temporal trend in CH_4 concentrations, and therefore that the risk of a spontaneous limnic gas eruption does not seem to be further increasing at the moment. Therefore, there is no need of immediate action to artificially decrease gas concentrations in Lake Kivu. However, Lake Kivu has a long history of lake overturns (Ross et al., 2015b; Votava et al., 2017; Uveges et al., 2020; R. Hecky pers. comm.), of which some could have caused catastrophic degassing. Today's near steady-state is strongly linked to the properties and the discharge of hydrothermal groundwater sources in an unstable volcanic region. A subaqueous volcanic eruption could potentially trigger a dangerous lake overturn, or, a gradual change of groundwater properties could alter the lake's steady-state. Both of these scenarios could lead to the uncontrolled release of gases and therefore, it is still of paramount importance to artificially decrease gas concentrations in Lake Kivu using gas extraction systems.

Secondly, our results suggest that there is no significant net recharge of CH_4 and that thus, CH_4 inflow and production are balanced by vertical transport and oxidation at the oxycline. Therefore, our measurements question the idea of permanently using Lake Kivu's CH_4 gas for electricity production (Expert Working Group on Lake Kivu Gas Extraction, 2009), as apparently the CH_4 is replenished much slower than previously thought. Based on the observed CH_4 increase between 1974 and 2003, Schmid et al. (2005) suggested a CH_4 recharge rate of 120 g C m^{-2} y^{-1} (including both production and inflow), while the steady-state production rate determined in this thesis is only around 28 g C m^{-2} y^{-1}. Still, the recharge rate could potentially

increase in the future because the extraction-induced CH_4 decrease may increase the concentration gradient across the lake's water-sediment interface, and thus lead to higher CH_4 fluxes out of the sediment. However, it is impossible to quantify the duration and extent of such an increase in the CH_4 recharge rate and therefore, it should not be relied upon when managing Lake Kivu's CH_4 resources.

Although gas concentrations are currently close to a steady-state, they need to be closely monitored in the future for several reasons: i) the uncertainty of gas measurements in Lake Kivu is relatively high, and it is still possible that gas concentrations are currently increasing to some extent, ii) groundwater discharge or/and internal methane production could vary in time and therefore, the observed steady-state may not hold in the future, and iii) large-scale CH_4 extraction will modify gas concentrations in the future. The goal of monitoring Lake Kivu is to detect such changes at an early stage to adjust management strategies accordingly, and thus to prevent undesired consequences like weakening of the stratification or gas accumulation at certain depths, which could eventually lead to outgassing.

Gas monitoring in Lake Kivu can be done with two different approaches, either by individually measuring the concentrations of CH_4 and CO_2, or by using an in-situ probe to determine total dissolved gas pressure (TDGP). The former is rather challenging due to sample outgassing, but it has the advantage of directly providing CH_4 concentrations, which are useful for gas extraction management. In contrast, the latter is relatively straightforward and offers a direct estimation of gas saturation (i.e. TDGP divided by the sum of hydrostatic and atmospheric pressure), which is a good proxy for risk evaluation. The ideal monitoring strategy involves both approaches with i) frequent (i.e. monthly) conductivity and temperature profiling to detect changes in stratification, ii) regular (i.e. yearly) assessment of gas pressure using a gas pressure probe, and iii) regular monitoring of gas concentrations using for example one of the methods presented in chapter 3. A much more detailed discussion of gas monitoring can be found in the technical report, which is based on the data of chapter 3 (Schmid et al., 2019).

Outlook

The dynamic model developed in this dissertation was applied to long-term scenarios of the past evolution of Lake Kivu and to a steady-state simulation of the present state. In the future, it could be used to study the short- and long-term evolution of the lake's temperature, stability and gas concentrations as a function of gas extraction projects and a changing climate. In

addition, our coupled physical-biogeochemical model would allow assessing the danger linked to potential algae blooms due to the redistribution of nutrient-rich deep water close to the surface by gas extraction facilities. Another possible application is exploring the meteorological conditions which could lead to deep mixing by producing dense surface water and thus buoyant instability. Such events include for example a volcanic winter (i.e. dimming of sunlight by volcanic particles) or large turbidity currents due to flooding.

One caveat of the use of the new model is the long duration that the simulated temperature needs to reach a steady-state (~500 years). If the model is started with initial conditions that are not equal to the model steady-state, it will converge towards this steady-state. In such a situation, it could be difficult to differentiate the converging trend from the trend caused by the investigated changes (i.e. warming rate or gas extraction). The evolution of the model during this initial time is not reflecting reality, but a transition from observations to their best representation as a simulation. In order to investigate real changes (i.e. devoid of model artefacts) the model probably needs to be initiated with steady-state conditions rather than observations.

Besides the parameterization of temperature diffusivity, the most significant uncertainty of the model are the subaquatic groundwater sources, i.e. their discharge, inflow depth and properties (temperature, salinity and gas concentrations). In chapter 4, we determined a set of inflow parameters, which enable the simulations to closely match the observed profiles. However, the system is strongly overparameterized and therefore, there may well be different sets of inflow parameters which give similar simulation results. Accurate field observations of these inflow parameters would help identifying the right set of parameters, but they are difficult to obtain. Ross et al. (2015a) used a conductivity-temperature-pressure (CTD) probe and water samples to determine temperature, salinity and other properties close to supposed groundwater inflows. Unfortunately, it is difficult to know to what extent the sampled water was already mixed with surrounding lake water. Such problems could be circumvented by using a remote operated underwater vehicle (ROV) to identify and sample groundwater sources. This approach is probably most promising for the cool groundwater sources at ~190 and ~250 m, which have a large discharge and whose inflow depths are well-known (Ross et al., 2015a).

Finally, the Simstrat-AED2 model can be readily adjusted to accommodate any number of additional physical state variables (e.g. gases, gas isotopes and water isotopes). It is therefore a useful tool to interpret new observations of physical tracers in Lake Kivu. One such application is already in progress with the collaboration with a research team of the Kirchhoff Institute of

Physics (KIP) in Heidelberg, who collected a ^{39}Ar dataset in Lake Kivu. ^{39}Ar is an extremely rare, radioactive isotope with a half-life of ~269 years, and thus it is a potentially useful tracer to further constrain water age and transport processes in Lake Kivu.

Acknowledgments

On the day I defend this thesis, it will be 5 years (minus 1 day!) ago that I joined Eawag in Kastanienbaum. And due to Covid19, it will also be 8 months ago that I have last worked in my office (except for 2 days) just in front of the beautiful (and always pleasantly warm) Vierwald-stättersee. It has been great 5 years with great people and I am already looking forward to 3 more!

I would like to thank my supervisor Martin Schmid for the possibility to work on this fascinating project about Lake Kivu, and especially for accepting my 70 % employment. His reliability and availability for questions, reviews and discussions was always of great help.

I am equally grateful to my supervisor RoKi (Rolf Kipfer). His enthusiasm about science was infectious, and I especially benefitted from his seemingly naïve questions and ideas, which sometimes opened new angles in scientific discussions.

Prof. Bernhard Wehrli and Prof. Werner Aeschbach accepted to be part of my PhD-committee and to review my work. Thank you!

During my field work at Lake Kivu, I always had great help and I would like to thank all of them, who made this thesis possible: Ivo Beck who was able to repair a dearly needed generator, Reto Britt who also handcrafted part of the sampling equipment, Michi Plüss for persistence in cutting fishing nets off the CTD, and Max Schmidt for guiding us out of the storm.

Special thanks to the local team of LKMP (Lake Kivu Monitoring Programme): Augusta Umutoni and Ange Mugisha for the local organization of the field campaigns, Pierre Simbizi for the daily boat commutes to the lake platform, Epa Havugimana for his strong arms during km's of pulling up samples, our car drivers John and Jean and many more…

I also would like to acknowledge my fellow gas researchers at Lake Kivu Bertram Boehrer, Wolf von Tuempling and Roberto Grilli with whom we had a great time at Lake Kivu.

I am very grateful to Andi Raffainer and his crew from the Eawag workshop for building the noble gas sampler, and to Matthias Brennwald for his assistance with the building and running the "MiniRuedi" mass spectrometer.

The people from the ETH noble gas lab, Matthias Brennwald, Alex Lightfoot and Edith Horstmann sometimes had to deal with my very awkward samples from Lake Kivu. Thanks for that!

At Eawag, Serge Robert always had an open ear for my issues with gas samples. Merci! Thanks also to Patrick Kathriner who helped me out on a lot of smaller problems.

The start of my project was a bit shaky due to the uniqueness of Lake Kivu, where standard approaches would just not fit. I would like to thank Matthias Zimmermann and Andi Brand for their discussions about what is physically possible (and what not). Special thanks to Chregu Dinkel for going on Lake Vierwaldstättersee with me to test what is physically not possible (i.e. water sampling using the tiny CTD circulation pump).

Special thanks to Adrien and his great Simstrat manual, which made the start with this software much easier (although he always complained that I never read it).

I am very grateful for the great administrative support of Eliane Scharmin and Patricia Achleitner during my PhD!

I would like to thank my small but great working group at Eawag: Philipp Meier and later Davide Vanzo for all the help with my software issues and questions, Ulrike for finding all kinds of bugs in Simstrat, Elisa for the nice talks, Rémy, Alex…

Shout-out to my fellow winter-swimmers Cas, Oli, Bene, Typh (at least until October), Damien and of course Adrien, who was the founding father of this activity.

Thanks to all current and former members of our cooking-group “Ratatouille” and later “KB-cookers” for the culinary surprises (and also the steadily incoming Strudels): Adrien, Rohini, Matthias, Magdi, Oli, Robert, Kathrin, Anna, Bene, Tomy, Cas…

Thanks to all the people who make KB a great working environment, thanks to the organizers of Christmas-parties, the Badehüsliparties, the around-the-lake-cyclists and so on.

Thank you Adrien for motivating people to do what they like. This is how we will remember you.

Finally, thanks to my family Anina, Yann and Milo for your love and your patience (during the last few weeks) and to my parents Ruth and Thomas and my brothers and sisters Oliver, Rebekka and Jana for your support and encouragement now and during the last three decades.

References

Aeschbach-Hertig, W. (1994). Helium und Tritium als Tracer für physikalische Prozesse in Seen (Doctoral dissertation, ETH Zurich).

Bärenbold, F., Boehrer, B., Grilli, R., Mugisha, A., von Tuempling, W., Umutoni, A., & Schmid, M. (2020a) No increasing risk of a limnic eruption at Lake Kivu: intercomparison study reveals gas concentrations close to steady state. *PloS one,* 15(8), e0237836. https://doi.org/10.1371/journal.pone.0237836

Bärenbold, F., Schmid, M., Brennwald, M. S., & Kipfer, R. (2020b). Missing atmospheric noble gases in a large, tropical lake: The case of Lake Kivu, East-Africa. *Chemical Geology*, 532, 119374. https://doi.org/10.1016/j.chemgeo.2019.119374

Beyerle, U., Aeschbach-Hertig, W., Imboden, D. M., Baur, H., Graf, T., & Kipfer, R. (2000). A mass spectrometric system for the analysis of noble gases and tritium from water samples. *Environmental Science & Technology*, 34(10), 2042-2050. https://doi.org/10.1021/es990840h

Boehrer, B., Von Tuempling, W., Mugisha, A., Rogemont, C., & Umutoni, A. (2019). Reliable reference for the methane concentrations in Lake Kivu at the beginning of industrial exploitation. *Hydrology & Earth System Sciences*, 23(11). https://doi.org/10.5194/hess-2019-228

Boehrer, B., Yusta, I., Magin, K., & Sanchez-España, J. (2016). Quantifying, assessing and removing the extreme gas load from meromictic Guadiana pit lake, Southwest Spain. *Science of the Total Environment,* 563, 468-477. https://doi.org/10.1016/j.scitotenv.2016.04.118

Borges, A. V., Abril, G., Delille, B., Descy, J. P., & Darchambeau, F. (2011). Diffusive methane emissions to the atmosphere from Lake Kivu (Eastern Africa). *Journal of Geophysical Research: Biogeosciences,* 116(G3). https://doi.org/10.1029/2011JG001673

Brennwald, M. S., Kipfer, R., & Imboden, D. M. (2005). Release of gas bubbles from lake sediment traced by noble gas isotopes in the sediment pore water. *Earth and Planetary Science Letters*, *235*(1-2), 31-44. https://doi.org/10.1016/j.epsl.2005.03.004

Brennwald, M. S., Schmidt, M., Oser, J., & Kipfer, R. (2016). A portable and autonomous mass spectrometric system for on-site environmental gas analysis. *Environmental Science & Technology,* 50(24), 13455-13463. https://doi.org/10.1021/acs.est.6b03669

Chen, C. T. A., & Millero, F. J. (1986). Thermodynamic properties for natural waters covering only the limnological range 1. *Limnology and Oceanography*, 31(3), 657-662. https://doi.org/10.4319/lo.1986.31.3.0657

Chorowicz, J. (2005). The east African rift system. *Journal of African Earth Sciences*, *43*(1-3), 379-410. https://doi.org/10.1016/j.jafrearsci.2005.07.019

Cogley, J. G. (1979). The albedo of water as a function of latitude. *Monthly Weather Review*, *107*(6), 775-781. https://doi.org/10.1175/1520-0493(1979)107<0775:TAOWAA>2.0.CO;2

Damas, H. (1938). La stratification thermique et chimique des lacs Kivu Édouard et Ndalaga (Congo Belge). *Internationale Vereinigung für theoretische und angewandte Limnologie: Verhandlungen*, 8(3), 51-68.

Degens, E. T., von Herzen, R. P., Wong, H. K., Deuser, W. G., & Jannasch, H. W. (1973). Lake Kivu: structure, chemistry and biology of an East African rift lake. *Geologische Rundschau*, *62*(1), 245-277. https://doi.org/10.1007/BF01826830

Expert Working Group on Lake Kivu Gas Extraction (2009). Management prescriptions for the development of Lake Kivu gas resources. Report prepared for the Ministry of Infrastructure of the Republic of Rwanda and the Ministry of Hydrocarbons of the Democratic Republic of the Congo, 2009 June. https://www.dora.lib4ri.ch/eawag/islandora/object/eawag:19124

Felton, A. A., Russell, J. M., Cohen, A. S., Baker, M. E., Chesley, J. T., Lezzar, K. E., ... & Tiercelin, J. J. (2007). Paleolimnological evidence for the onset and termination of glacial aridity from Lake Tanganyika, Tropical East Africa. *Palaeogeography, Palaeoclimatology, Palaeoecology*, *252*(3-4), 405-423. https://doi.org/10.1016/j.palaeo.2007.04.003

Gaudard, A., Råman Vinnå, L., Bärenbold, F., Schmid, M., & Bouffard, D. (2019). Toward an open access to high-frequency lake modeling and statistics data for scientists and practitioners–the case of Swiss lakes using Simstrat v2.1. *Geoscientific Model Development*, *12*(9), 3955–3974. https://doi.org/10.5194/gmd-12-3955-2019

Gaudard, A., Schwefel, R., Råman Vinnå, C. L. M., Schmid, M., Wüest, A. J., & Bouffard, D. (2017). Optimizing the parameterization of deep mixing and internal seiches in one-dimensional hydrodynamic models: a case study with Simstrat v1.3. *Geoscientific Model Development*, *10*, 3411-3423. https://doi.org/10.5194/gmd-10-3411-2017

Gonfiantini, R. (1986). Environmental isotopes in lake studies. *Handbook of environmental isotope geochemistry*, *2*, 113-168. https://doi.org/10.1016/B978-0-444-42225-5.50008-5

Goudsmit, G. H., Burchard, H., Peeters, F., & Wüest, A. (2002). Application of k-ϵ turbulence models to enclosed basins: The role of internal seiches. *Journal of Geophysical Research: Oceans*, 107(C12), 23-1. https://doi.org/10.1029/2001JC000954

Greinert, J.; McGinnis, D. F.; Naudts, L.; Linke, P.; De Batist, M. (2010). Atmospheric methane flux from bubbling seeps: Spatially extrapolated quantification from a Black Sea shelf area. *Journal of Geophysical Research: Oceans*, *115*, C01002. https://doi.org/10.1029/2009JC005381

Grilli, R., Darchambeau, F., Chappellaz, J., Mugisha, A., Triest, J., & Umutoni, A. (2020). Continuous in situ measurement of dissolved methane in Lake Kivu using a membrane inlet laser spectrometer. *Geoscientific Instrumentation, Methods and Data Systems*, *9*(1), 141-141. https://doi.org/10.5194/gi-9-141-2020

Grilli, R., Triest, J., Chappellaz, J., Calzas, M., Desbois, T., Jansson, P., ... & Romanini, D. (2018). Sub-ocean: Subsea dissolved methane measurements using an embedded laser spectrometer technology. *Environmental Science & Technology*, 52(18), 10543-10551. https://doi.org/10.1021/acs.est.7b06171

Haberyan, K. A., & Hecky, R. E. (1987). The late Pleistocene and Holocene stratigraphy and paleolimnology of Lakes Kivu and Tanganyika. *Palaeogeography, Palaeoclimatology, Palaeoecology*, *61*, 169-197. https://doi.org/10.1016/0031-0182(87)90048-4

Halbwachs, M., Sabroux, J. C., & Kayser, G. (2020). Final step of the 32-year Lake Nyos degassing adventure: Natural CO_2 recharge is to be balanced by discharge through the degassing pipes. *Journal of African Earth Sciences*, 167, 103575. https://doi.org/10.1016/j.jafrearsci.2019.103575

Hirslund, F. (2012). An additional challenge of Lake Kivu in Central Africa-upward movement of the chemoclines. *Journal of Limnology*, *71*(1), e4. https://doi.org/10.4081/jlimnol.2012.e

Hirslund, F. (2020). A single limnic eruption at the origin of today's large-scale density structure of Lake Kivu. *Journal of African Earth Sciences*, *161*, 103614. https://doi.org/10.1016/j.jafrearsci.2019.103614

IAEA/WMO (2020). Global Network of Isotopes in Precipitation. The GNIP Database. Accessible at: http://www.iaea.org/water

Holzner, C. P., McGinnis, D. F., Schubert, C. J., Kipfer, R., & Imboden, D. M. (2008). Noble gas anomalies related to high-intensity methane gas seeps in the Black Sea. *Earth and Planetary Science Letters*, *265*(3-4), 396-409. https://doi.org/10.1016/j.epsl.2007.10.029

Horn, C., Metzler, P., Ullrich, K., Koschorreck, M., & Boehrer, B. (2017). Methane storage and ebullition in monimolimnetic waters of polluted mine pit lake Vollert-Sued, Germany. *Science of the Total Environment*, 584, 1-10. https://doi.org/10.1016/j.scitotenv.2017.01.151

Jansson, P., Triest, J., Grilli, R., Ferré, B., Silyakova, A., Mienert, J., & Chappellaz, J. (2019). High-resolution underwater laser spectrometer sensing provides new insights into methane distribution at an Arctic seepage site. *Ocean Science*, 15(4), 1055-1069. https://doi.org/10.5194/os-15-1055-2019

Katsev, S.; Aaberg; A. A., Crowe; S. A.; Hecky, R. E. (2014). Recent warming of Lake Kivu. *PloS one*, *9*(10), e109084. https://doi.org/10.1371/journal.pone.0109084

Kelley, D. E., Fernando, H. J. S., Gargett, A. E., Tanny, J., & Özsoy, E. (2003). The diffusive regime of double-diffusive convection. *Progress in Oceanography*, 56(3-4), 461-481. https://doi.org/10.1016/S0079-6611(03)00026-0

Kipfer, R.; Aeschbach-Hertig, W.; Peeters, F.; Stute, M. (2002). Noble gases in lakes and ground waters. *Reviews in Mineralogy and Geochemistry*, *47*(1), 615-700.

Kling, G. W., Clark, M. A., Compton, H. R., Devine, J. D., Evans, W. C., Humphrey, A. M., et al. (1987). The 1986 Lake Nyos gas disaster in Cameroon, West-Africa. *Science*, *236*(4798): 169–175. https://doi.org/10.1126/science.236.4798.169

Kusakabe, M. (2017). Lakes Nyos and Monoun gas disasters (Cameroon)—limnic eruptions caused by excessive accumulation of magmatic CO_2 in crater lakes. *Geochem. Monograph Series*, 1, 1-50. https://www.doi.org/10.5047/gems.2017.00101.0001

Lahmeyer, & Osae (1998). Bathymetric survey of Lake Kivu. Final report. Kigali: Republic of Rwanda, Ministry of Public Work, Directory of Energy and Hydrocarbons.

Leifer, I., & Culling, D. (2010). Formation of seep bubble plumes in the Coal Oil Point seep field. *Geo-Marine Letters*, *30*(3-4), 339-353. https://doi.org/10.1007/s00367-010-0187-x

Lorke, A., Tietze, K., Halbwachs, M., & Wüest, A. (2004). Response of Lake Kivu stratification to lava inflow and climate warming. *Limnology and Oceanography, 49*(3), 778-783. https://doi.org/10.4319/lo.2004.49.3.0778

Ma, L., Castro, M. C., & Hall, C. M. (2009). Atmospheric noble gas signatures in deep Michigan Basin brines as indicators of a past thermal event. *Earth and Planetary Science Letters*, *277*(1-2), 137-147. https://doi.org/10.1016/j.epsl.2008.10.015

Majoube, M. (1971). Fractionnement en oxygène 18 et en deutérium entre l'eau et sa vapeur. *Journal de Chimie Physique*, *68*, 1423-1436. https://doi.org/10.1051/jcp/1971681423

Mamyrin, B. A., & Tolstikhin, I. N. (1984). Helium isotopes in nature. Volume 3 of Developments in Geochemistry. 273 pp. Elsevier, Amsterdam.

McGinnis, D. F., Greinert, J., Artemov, Y., Beaubien, S. E., & Wüest, A. (2006). Fate of rising methane bubbles in stratified waters: How much methane reaches the atmosphere?. *Journal of Geophysical Research: Oceans*, *111*, *C09007*. https://doi.org/10.1029/2005JC003183

Mills, R. (1973). Self-diffusion in normal and heavy water in the range 1-45. deg. *The Journal of Physical Chemistry,* 77(5), 685-688. https://doi.org/10.1021/j100624a025

Moore, J. C., Battino, R., Rettich, T. R., Handa, Y. P., & Wilhelm, E. (1982). Partial molar volumbes of gases at infinite dilution in water at 298.15 K. *Journal of Chemical and Engineering Data*, 27(1), 22-24. https://doi.org/10.1021/je00027a005

Morana, C., Borges, A. V., Roland, F. A. E., Darchambeau, F., Descy, J. P., & Bouillon, S. (2015). Methanotrophy within the water column of a large meromictic tropical lake (Lake Kivu, East Africa). *Biogeosciences*, *12*(7), 2077-2088. https://doi.org/10.5194/bg-12-2077-2015

Morana, C., Darchambeau, F., Roland, F., Borges, A., Muvundja, F., Kelemen, Z., ... & Bouillon, S. (2015). Biogeochemistry of a large and deep tropical lake (Lake Kivu, East Africa: insights from a stable isotope study covering an annual cycle. *Biogeosciences*, 12(16), 4953-4963. https://doi.org/10.5194/bg-12-4953-2015

Morville, J., Romanini, D., & Chenevier, M. (2003). Patent WO03031949, Universite J. Fourier, Grenoble, France.

Morville, J., Romanini, D., & Kerstel, E. (2014). Cavity enhanced absorption spectroscopy with optical feedback. In Cavity-Enhanced Spectroscopy and Sensing (pp. 163-209). Springer, Berlin, Heidelberg. https://doi.org/10.1007/978-3-642-40003-2_5

Mugisha, I. R. (2018). British firm searches for oil in Rwanda. *The East African,* 27 February. Available at: https://www.theeastafrican.co.ke/rwanda/Business/British-firm-to-search-for-oil-in-Rwanda/1433224-4322042-ibxqoz/index.html

Muvundja, F. A., Wüest, A., Isumbisho, M., Kaningini, M. B., Pasche, N., Rinta, P., & Schmid, M. (2014). Modelling Lake Kivu water level variations over the last seven decades. *Limnologica*, 47, 21-33. https://doi.org/10.1016/j.limno.2014.02.003

Nagao, K., Kusakabe, M., Yoshida, Y., & Tanyileke, G. (2010). Noble gases in Lakes Nyos and Monoun, Cameroon. *Geochemical Journal*, *44*(6), 519-543. https://doi.org/10.2343/geochemj.1.0101

Newman, F. C. (1976). Temperature steps in Lake Kivu: a bottom heated saline lake. *Journal of Physical Oceanography*, *6*(2), 157-163. https://doi.org/10.1175/1520-0485(1976)006<0157:TSILKA>2.0.CO;2

Pasche, N., Dinkel, C., Müller, B., Schmid, M., Wüest, A., & Wehrli, B. (2009). Physical and biogeochemical limits to internal nutrient loading of meromictic Lake Kivu. *Limnol. Oceanogr*, 54(6), 1863-1873. https://doi.org/10.4319/lo.2009.54.6.1863

Pasche, N., Schmid, M., Vazquez, F., Schubert, C. J., Wüest, A., Kessler, J. D., et al. (2011). Methane sources and sinks in Lake Kivu. *Journal of Geophysical Research: Biogeosciences*, *116*(G3):G001690. https://doi.org/10.1029/2011JG001690

Reichert, P. (1994). AQUASIM-A tool for simulation and data analysis of aquatic systems. *Water Science and Technology*, 30(2), 21. https://doi.org/10.2166/wst.1994.0025

Rettich, T. R., Handa, Y. P., Battino, R., & Wilhelm, E. (1981). Solubility of gases in liquids. 13. High-precision determination of Henry's constants for methane and ethane in liquid water at 275 to 328 K. *The Journal of Physical Chemistry*, *85*(22), 3230-3237. https://doi.org/10.1021/j150622a006

Rooney, G. G., Van Lipzig, N., & Thiery, W. (2018). Estimating the effect of rainfall on the surface temperature of a tropical lake. *Hydrology and Earth System Sciences*, *22*(12), 6357-6369. https://doi.org/10.3929/ethz-b-000312308

Ross, K. A., Gashugi, E., Gafasi, A., Wüest, A., & Schmid, M. (2015a). Characterisation of the subaquatic groundwater discharge that maintains the permanent stratification within Lake Kivu; East Africa. *PloS one*, *10*(3), e0121217. https://doi.org/10.1371/journal.pone.0121217

Ross, K. A., Schmid, M., Ogorka, S., Muvundja, F. A., & Anselmetti, F. S. (2015b). The history of subaquatic volcanism recorded in the sediments of Lake Kivu; East Africa. *Journal of Paleolimnology*, *54*(1), 137-152. www.doi.org/10.1007/s10933-015-9842-6

Schmid, M., Bärenbold, F., Boehrer, B., Darchambeau, F., Grilli, R., Triest, J., & von Tümpling, W. (2019). Intercalibration Campaign for Gas Concentration Measurements in Lake Kivu, Report prepared for the Lake Kivu Monitoring Programme (LKMP) of the Energy Development Corporation Limited (EDCL), Kigali, Rwanda.

Schmid, M., Busbridge, M., & Wüest, A. (2010). Double-diffusive convection in Lake Kivu. *Limnology and Oceanography*, 55(1), 225-238. https://doi.org/10.4319/lo.2010.55.1.0225

Schmid, M., Gerber, C., Bärenbold, F., & Wüest, A. (2019). Assessment of the effect of different scenarios for methane extraction from Lake Kivu based on numerical modelling, Eawag, Kastanienbaum. https://www.dora.lib4ri.ch/eawag/islandora/object/eawag%3A18541

Schmid, M., Halbwachs, M., Wehrli, B., & Wüest, A. (2005). Weak mixing in Lake Kivu: new insights indicate increasing risk of uncontrolled gas eruption. *Geochemistry, Geophysics, Geosystems, 6*(7), Q07009. https://doi.org/10.1029/2004GC000892

Schmid, M., & Köster, O. (2016). Excess warming of a Central European lake driven by solar brightening. *Water Resources Research*, *52*(10), 8103-8116. https://doi.org/10.1002/2016WR018651

Schmid, M., Tietze, K., Halbwachs, M., Lorke, A., McGinnis, D. F., & Wüest, A. (2004). How hazardous is the gas accumulation in Lake Kivu? Arguments for a risk assesment in light of the Nyiragongo volcano eruption of 2002. *Acta vulcanologica*, *14*(1-2), 115-122. http://doi.org/10.1400/19084

Schmid, M., & Wüest, A. (2012). Stratification, mixing and transport processes in Lake Kivu. In Lake Kivu (pp. 13-29). Springer, Dordrecht. https://doi.org/10.1021/j150622a006

Schmitz, D., & Kufferath, J. (1955). Problèmes posés par la présence de gaz dissous dans les eaux profondes du Lac Kivu. *Acad Roy Sci Coloniales. Bull Séances*, 1, 326-356.

Schoell, M., Tietze, K., & Schoberth, S. M. (1988). Origin of methane in Lake Kivu (east-central Africa). *Chemical Geology*, *71*(1-3), 257-265. https://doi.org/10.1016/0009-2541(88)90119-2

Sigurdsson, H., Devine, J. D., Tchoua, F. M., Presser, T. S., Pringle, M. K. W., & Evans, W. C. (1987). Origin of the lethal gas burst from Lake Monoun, Cameroun. *Journal of Volcanology and Geothermal Research*, *31*(1–2):1–16. https://doi.org/10.1016/0377-0273(87)90002-3

Sommer, T., Carpenter, J. R., Schmid, M., Lueck, R. G., Schurter, M., & Wüest, A. (2013). Interface structure and flux laws in a natural double-diffusive layering. *Journal of Geophysical Research: Oceans*, *118*(11), 6092-6106. https://doi.org/10.1002/2013JC009166

Sommer, T., Schmid, M., & Wüest, A. (2019). The role of double diffusion for the heat and salt balance in Lake Kivu. *Limnology and Oceanography*, 64(2), 650-660. https://doi.org/10.1002/lno.11066

Tassi, F., Vaselli, O., Tedesco, D., Montegrossi, G., Darrah, T., Cuoco, E., ... & Delgado Huertas, A. (2009). Water and gas chemistry at Lake Kivu (DRC): geochemical evidence of vertical and horizontal heterogeneities in a multibasin structure. *Geochemistry, Geophysics, Geosystems*, *10*(2). https://doi.org/10.1029/2008GC002191

Tedesco, D., Tassi, F., Vaselli, O., Poreda, R. J., Darrah, T., Cuoco, E., Yalire, M. M. (2010). Gas isotopic signatures (He, C, and Ar) in the Lake Kivu region (western branch of the East African rift system): Geodynamic and volcanological implications. *Journal of Geophysical Research: Solid Earth*, *115*, B01205. https://doi.org/10.1029/2008JB006227

Thiery, W. I. M., Stepanenko, V. M., Fang, X., Jöhnk, K. D., Li, Z., Martynov, A., ... & Van Lipzig, N. P. (2014). LakeMIP Kivu: evaluating the representation of a large, deep tropical lake by a set of one-dimensional lake models. *Tellus A: Dynamic Meteorology and Oceanography*, *66*(1), 21390. https://doi.org/10.3402/tellusa.v66.21390

Tietze, K. (1978). Geophysikalische Untersuchung des Kivusees und seiner ungewöhnlichen Methangaslagerstätte-Schichtung, Dynamik und Gasgehalt des Seewassers (Doctoral dissertation, Christan-Albrechts-Universität zu Kiel).

Triest, J., Chappellaz, J., & Grilli, R. (2017). Patent 08276–01: System for fast and in-situ sampling of dissolved gases in the ocean. CNRS, Grenoble, France.

Tyroller, L., Brennwald, M. S., Mächler, L., Livingstone, D. M., & Kipfer, R. (2014). Fractionation of Ne and Ar isotopes by molecular diffusion in water. *Geochimica et Cosmochimica Acta*, *136*, 60-66. https://doi.org/10.1016/j.gca.2014.03.040

Uveges, B. T., Junium, C. K., Scholz, C. A., & Fulton, J. M. (2020). Chemocline collapse in Lake Kivu as an analogue for nitrogen cycling during Oceanic Anoxic Events. *Earth and Planetary Science Letters*, 548, 116459. https://doi.org/10.1016/j.epsl.2020.116459

Votava, J. E., Johnson, T. C., & Hecky, R. E. (2017). Holocene carbonate record of Lake Kivu reflects the history of hydrothermal activity. *Proceedings of the National Academy of Sciences*, *114*(2), 251-256. https://doi.org/10.1073/pnas.1609112113

Walter, K. M., Zimov, S. A., Chanton, J. P., Verbyla, D., & Chapin, F. S. (2006). Methane bubbling from Siberian thaw lakes as a positive feedback to climate warming. *Nature*, *443*(7107), 71. https://doi.org/10.1038/nature05040

Weiss, R. F. (1970). The solubility of nitrogen, oxygen and argon in water and seawater. In *Deep Sea Research and Oceanographic Abstracts* (Vol. 17, No. 4, pp. 721-735). Elsevier. https://doi.org/10.1016/0011-7471(70)90037-9

Weiss, R. F. (1971). Solubility of helium and neon in water and seawater. *Journal of Chemical & Engineering Data*, *16*(2), 235-241. https://doi.org/10.1021/je60049a019

Weiss, R. (1974). Carbon dioxide in water and seawater: the solubility of a non-ideal gas. *Marine Chemistry*, 2(3), 203-215. https://doi.org/10.1016/0304-4203(74)90015-2

Weiss, R. F.; Kyser, T. K. (1978). Solubility of krypton in water and sea water. *Journal of Chemical and Engineering Data*, *23*(1), 69-72.

Wiesenburg, D. A., & Guinasso Jr, N. L. (1979). Equilibrium solubilities of methane, carbon monoxide, and hydrogen in water and sea water. *Journal of Chemical and Engineering Data*, 24(4), 356-360. https://doi.org/10.1021/je60083a006

Winckler, G., Kipfer, R., Aeschbach–Hertig, W., Botz, R., Schmidt, M., Schuler, S., & Bayer, R. (2000). Sub sea floor boiling of Red Sea Brines: New indication from noble gas data. *Geochimica et Cosmochimica Acta*, *64*(9), 1567-1575. https://doi.org/10.1016/S0016-7037(99)00441-X

Wise, D. L., & Houghton, G. J. C. E. S. (1968). Diffusion coefficients of neon, krypton, xenon, carbon monoxide and nitric oxide in water at 10–60 C. *Chemical Engineering Science*, 23(10), 1211-1216. https://doi.org/10.1016/0009-2509(68)89029-3

Wood, D. A., & Scholz, C. A. (2017). Stratigraphic framework and lake level history of Lake Kivu, East African Rift. *Journal of African Earth Sciences*, *134*, 904-916. https://doi.org/10.1016/j.jafrearsci.2016.06.014

Wüest, A., Jarc, L., Bürgmann, H., Pasche, N., & Schmid, M. (2012). Methane formation and future extraction in Lake Kivu. In: *Lake Kivu* (pp. 165-180). Springer, Dordrecht. http://dx.doi.org/10.1007/978-94-007-4243-7_10

Wüest, A., Jarc, L., & Schmid, M. (2009). Modelling the reinjection of deep-water after methane extraction in Lake Kivu. EAWAG and BTC for the Governments of Rwanda and DR Congo. https://www.dora.lib4ri.ch/eawag/islandora/object/eawag:14884

Wüest, A., Piepke, G., & Halfman, J. D. (1996). Combined effects of dissolved solids and temperature on the density stratification of Lake Malawi. In: The Limnology, Climatology and Paleoclimatology of the East African Lakes (pp. 183 – 202). Gordon and Breach, New York.

Wüest, A., Sommer, T., Schmid, M., & Carpenter, J. R. (2012). Diffusive-type of double diffusion in lakes—a review. *Environmental Fluid Mechanics: Memorial Volume in Honour of Prof. Gerhard H. Jirka, IAHR Monograph*, 271-284.

Zhang, X., Scholz, C. A., Hecky, R. E., Wood, D. A., Zal, H. J., & Ebinger, C. J. (2014). Climatic control of the late Quaternary turbidite sedimentology of Lake Kivu, East Africa: Implications for deep mixing and geologic hazards. *Geology*, *42*(9), 811-814. https://doi.org/10.1130/G35818.1

Ziabakhsh-Ganji, Z., & Kooi, H. (2012). An Equation of State for thermodynamic equilibrium of gas mixtures and brines to allow simulation of the effects of impurities in subsurface CO_2 storage. *International Journal of Greenhouse Gas Control*, 11, S21-S34. https://doi.org/10.1016/j.ijggc.2012.07.025

Appendix A: Supporting information to chapter 2

Table A1. Detailed results of Eawag measurement method. Results and uncertainties using the on-site mass spectrometer method

Depth [m]	CH_4 [mmol/l]	CH_4 err [mmol/l]	CO_2 [mmol/l]	CO_2 err [mmol/l]
11	<0.1		0.03	0.00
32	<0.1		0.05	0.00
50	<0.1		0.05	0.00
71	0.47	0.03	1.54	0.07
91			5.08	0.22
112			7.57	0.33
132			9.30	0.41
152	3.70	1.06	12.86	0.81
172	3.24	1.00	13.07	0.85
192	3.96	0.90	18.50	1.22
212	5.42	0.96	20.64	1.48
242	4.85	0.71	22.34	1.33
254	6.60	0.79	30.48	1.77
270	14.97	2.29	60.13	5.15
289	13.50	1.65	66.37	4.44
309	16.23	1.92	73.86	4.83
335	16.93	1.64	84.05	4.30
355	17.09	1.66	84.79	4.33
375	17.49	1.78	80.94	4.43
394	16.51	1.63	83.72	4.41
414	17.24	1.62	87.78	4.31
453	16.73	1.57	88.82	4.36

Table A2. Temperature data from a Sea and Sun CTD.

Table A3. Salinity data computed using conductivity data.

These tables are not included in this dissertation because they are too long. However, they can be found in the supporting information of the original publication (https://doi.org/10.1371/journal.pone.0237836), or requested from the author.

Appendix A1. Detailed description of on-site measurement method for CO_2 and CH_4

Overview

The measurement approach is schematically summarized in Figure A1. Lake water is pumped to the surface continuously using a 0.75 kW submersible centrifugal pump (UG-18 from Pumpen Lechner) down to a depth of 250 m. Below 250 m, no pump is needed because the outgassing of deep water in the tube sustains the water flow. However, a small peristaltic pump is used to initiate the process by bringing deep water close to the lake surface where the hydrostatic pressure is too low to keep the gases in the water. Relevant data about the pump operation above/below 250 m are shown in Table A4.

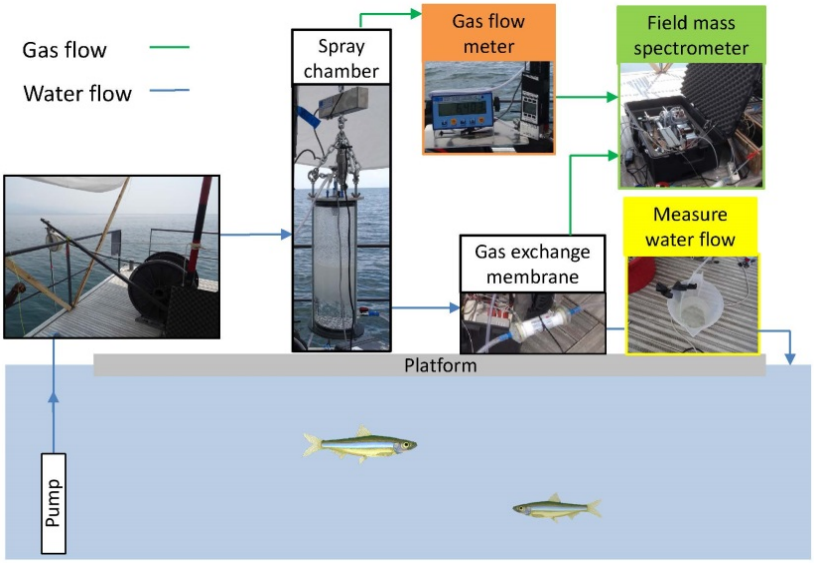

Figure A1. Sketch of measurement approach: lake water is pumped up continuously and dispersed into a spray chamber. The equilibrated gas and water phases flow out of the spray chamber at the top and bottom, respectively. For both phases, partial gas pressures and flows are measured.

A custom-made spray chamber (d = 12 cm, h = 40 cm, V = 4.5 L) is subsequently used to separate water and gas phase of the sampling water by dispersing it through a nozzle at the top. Gas and water phases leave the spray chamber through an outlet at the top and at the bottom, respectively. Pressure (Wika P-30, accuracy: 1 hPa) and temperature (Maxim DS18B20, accuracy: 0.5 °C) are recorded continuously for both gas and water while gas flow is measured using a laminar flow meter (Alicat Scientific MBS-20SLPM-D) and water flow using a simple bucket. Finally, the gas phase components are directly analyzed in the field mass spectrometer. In order to quantify the remaining gas in the sample water, the headspace of a membrane module is equilibrated with the sampling water flowing from the spray chamber and also analyzed using the mass spectrometer.

Table A4. Pump operation data

	Pump	Tube	Flow	Tube flushed
Above 250 m	Yes	polyamide, 6 mm	~ 1.6 L/min	2x
250 – 310 m	No	polyamide, 10 mm	~ 0.5 L/min	2x
Below 310 m	No	polyamide, 10 mm	~ 1 L/min	2x

There are two crucial components in the measurement approach: the portable field mass spectrometer, developed at Eawag (Brennwald et al., 2016, see next section) and the gas flow meter MBS-20SLPM-D made by Alicat Scientific. The gas flow meter forces the gas through a laminar flow element and records the pressure drop across the element. This pressure drop is a linear function of gas flow and thus directly allows the instrument to calculate the gas flow for a given gas mixture. The range of the instrument is from 0.1 to 20 l/min and its accuracy depends on the average flow measured (between 2.5 and 8.5 % below 250 m).

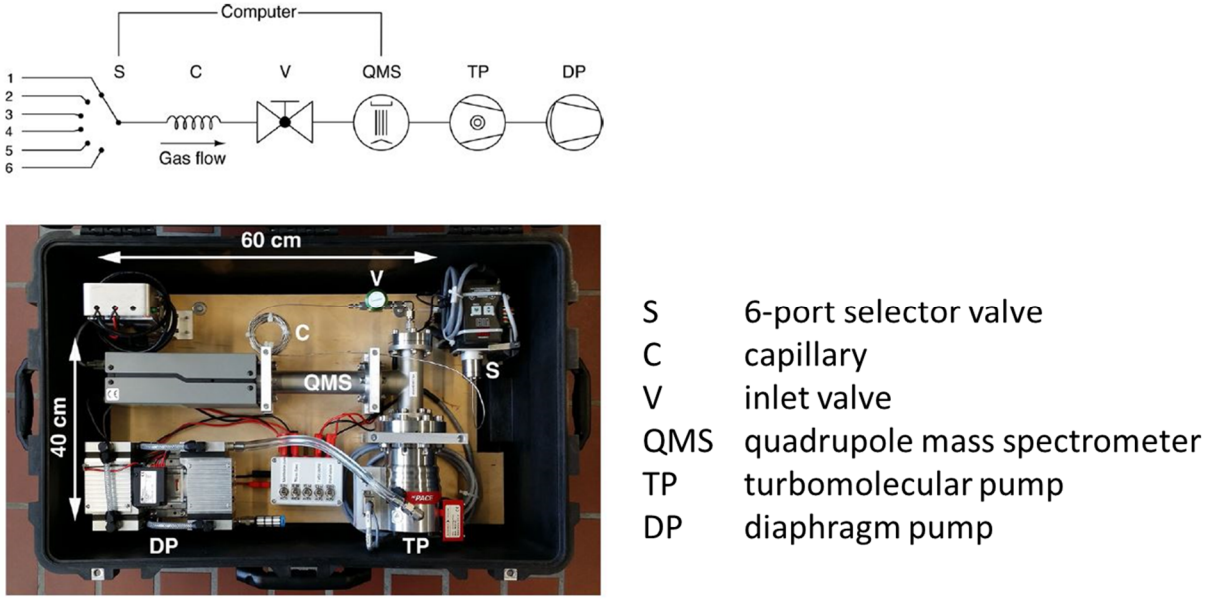

Figure A2. On-site mass spectrometer developed at Eawag (Brennwald et al., 2016)

Figure A2 shows the main components as well as sketch of the mass spectrometric system. Sample or calibration gas enters through one of the ports of the multi-port selector valve and enters the quadrupole mass spectrometer (QMS) through a long capillary. The QMS is evacuated using a low and a high vacuum pump and is suitable for the analysis of any gas between 0 and 200 atomic mass (atm).

If the sample medium is gas (e.g. the gas from deep water in Lake Kivu), the sample can directly enter the QMS. But if water is sampled (down to 130 m in Lake Kivu and for residual gas concentration in water below 130 m), the gas contained in the water needs to be extracted into a headspace. In our approach, this is done using a Liqui-Cel G542 membrane module. Ideally, the water flow through this membrane should be higher than ~ 1 L/min in order to guarantee an equilibrium in the headspace despite the slow consumption by the QMS. Using the equilibrium assumption, the gas concentration in the water can be deduced using the Henry coefficient, and membrane properties do not have to be taken into account.

The device was calibrated several times per day using the following calibration gases (contained in Linde Plastigas bags and permanently attached to two inlets):

- Cal gas 1: 20 % CH_4, 80 % CO_2
- Cal gas 2: 30 % CH_4, 60 % CO_2, 10 % air

Calculations

In order to compute in-situ concentrations from concentrations in the gas and water phase, we use the following equation:

$$C_{in\ situ}\left[\frac{mmol}{L}\right] = \frac{Q_{gas}\left[\frac{L_{gas,SATP}}{min}\right]}{Q_{water}\left[\frac{L}{min}\right]} C_{gas}\left[\frac{mmol}{L_{gas,SATP}}\right] + C_{water}\left[\frac{mmol}{L}\right] \quad (1)$$

where C is concentration and Q is flow. Q_{water} is measured using a bucket and Q_{gas} is the gas flow at standard ambient temperature and pressure SATP (T = 25°C and P = 1013 hPa) computed according to equation (2).

$$Q_{gas}\left[\frac{L_{gas,SATP}}{min}\right] = \frac{V_{out,SATP} + (M_{init} - M_{final}) 1\left[\frac{L}{kg}\right] \frac{P_{ambient}}{P_{SATP}}}{t}, P_{ambient} = 855\ hPa \quad (2)$$

$V_{out,SATP}$ is the total outflow volume (in $L_{gas,SATP}$) measured by the gas flow meter during the time t (in min). M_{init} and M_{final} are the weight (kg) of the spray chamber at the start and at the end of a gas flow measurement (usually 20-30 minutes) to take into account the variation of the gas volume in the spray chamber. Finally, the pressure correction term ensures coherences with the output of the gas flow meter in SATP (temperature correction is negligible). $P_{ambient}$ is the ambient pressure at Lake Kivu, which was always close to 855 hPa.

After calibration, the mass spectrometer gives out relative partial pressure values for every major gas component (CH_4, CO_2, N_2 and O_2). Water vapor is not measured but taken into

account assuming saturation and by calculating saturation pressure (atm) according to the following equation (Robinson, 1954):

$$\ln(pH_2O) = 24.4543 - 67.4509\left(\frac{100}{T}\right) - 4.8489\ln\left(\frac{T}{100}\right) - 0.000544S \quad (3)$$

where T (°K) is water temperature, and S (‰) is salinity, which is calculated from conductivity and ionic composition (Wüest et al., 1996). Finally, the relative pressures are converted to absolute pressures using pressure gauges at the inlet of the mass spectrometer. The partial pressures are subsequently converted to concentrations. For the pure gas phase coming out of the spray chamber, this is done using the molar volume at SATP (24.46 L/mol at 25°C and 1013 hPa) in order to get the concentration in $\left[\frac{mmol}{L_{gas,SATP}}\right]$. For the water phase, we use the Henry coefficients for CH_4 (Yamamoto, 1976) and CO_2 (Weiss 1974) which results in concentration in $\left[\frac{mmol}{L}\right]$.

Individual uncertainties

We first assess the accuracy of the individual concentration and flow measurements in order to conclude on the total uncertainty of our approach.

a) Mass spectrometer

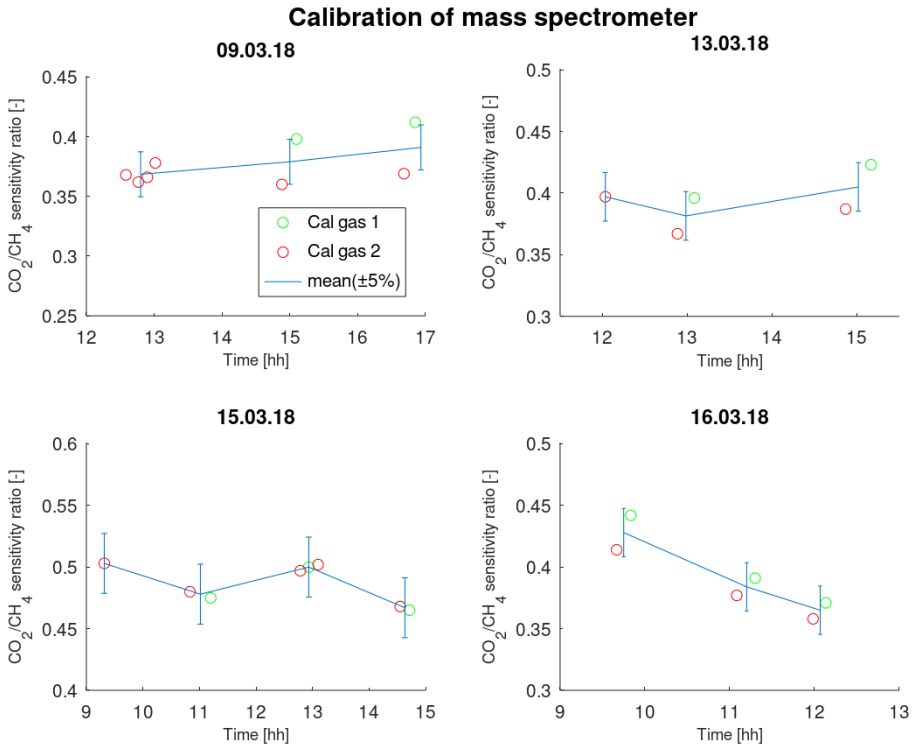

Figure A3. Variability of CO_2 to CH_4 sensitivity ratio of two different calibration gases for different measurement days. The sensitivity ratio of a gas is defined as the signal strength in [A] divided by its partial pressure in the calibration gas in [hPa].

Figure A3 depicts the CO_2/CH_4 sensitivity ratio for two different calibration gases over several measurement days. Most deep water samples were taken on these days. The sensitivity of a gas is given by the detector signal in Ampère divided by its partial pressure in the calibration gas mixture [A/hPa]. On 9, 13 and 16 March, the sensitivity ratio was significantly higher for calibration gas 1 than for calibration gas 2. However, no clear indication was found to discard any of the two calibration gases and therefore both gases were used for calibration purposes. The corresponding uncertainty range of the sensitivity ratio was estimated to 10 % resulting in a deviation of ± 5 % from the mean value (blue error bars in Figure A3).

In the following, the individual uncertainties of the CH_4 and CO_2 measurements are estimated from the uncertainty of the sensitivity ratio

$$E(CO_2\_sens/CH_4\_sens) = \pm 5\ \%$$

where E(…) means uncertainty.

The sensitivities are obtained by dividing the calibration signal [A] by the partial pressure in the calibration gas [hPa]. The calibration signals for both CO_2 and CH_4 (and their uncertainties) are not related to each other. Thus, assuming that CH_4 and CO_2 have the same relative uncertainty, we get:

$$E(CO_2\_sens) = E(CH_4\_sens) = \pm 2.5\ \%$$

(from uncertainty propagation of the ratio of two independent variables for small uncertainty).

To obtain the raw result of a sample, CH_4_sens is multiplied by "CH_4_signal" which is the signal measured at a certain depth in [A]. This raw result is called "CH_4_meas". The uncertainty of CH_4_signal due to the variability of the individual mass peak measurements is ± *1 %*. Therefore:

$$E(CH_4\_meas) = E(CH4\_sens) + E(CH_4\_signal) = 2.5\ \% + 1\ \% = \pm 3.5\ \%.$$

The same is valid for CO_2_meas.

The final result consists of the measured quantity normalized by the ratio of total pressure (uncertainty around 0.1 % which is neglected here) and total gas pressure found by the mass spectrometer. Total gas pressure of the mass spectrometer is very close to CO_2_meas + CH_4_meas below 250 m and therefore: $E(CH_4\_result) = E(CH_4\_meas/(CH_4\_meas + CO_2\_meas))$

$$E(CO_2\_result) = E(CO_2\_meas/(CH_4\_meas + CO_2\_meas))$$

The denominator of these equations not only depends on the error of both CH_4_meas and CO_2_meas but also on the ratio of these measured values. Moreover, the nominator and denominator are not independent, thus making a general assessment difficult. Thus, we proceed with the calculation of "extreme" cases (all errors add up) and we find for a typical CH_4/CO_2 ratio of 0.2/0.8 = 0.25:

E(CH_4_result) ≅ ± 5.5 %

E(CO_2_result) ≅ ± 1.5 %

The ratio of these errors is close to 4 because at the given composition of the gas phase, a 1 % increase in CO_2 concentration roughly results in a 4 % decrease in CH_4 concentration.

Note that in Table 2.2, these uncertainties were calculated using measured CH_4/CO_2 ratios and not the "typical" one.

b) Henry coefficient

In the case of CO_2, a large fraction of the gas remains dissolved in the sample water. For determining its concentration, the measured partial pressure is multiplied by the temperature-dependent Henry coefficient. We adopt a total uncertainty of 3 % to account for the uncertainty of the temperature-dependence of the Henry coefficient and for the fact that the equilibrium in the membrane contactor might not be perfect.

For CH_4, the uncertainty in the Henry coefficient can be neglected, since only a small fraction of the gas remains in the water after degassing.

c) Gas flow

The gas flow is computed using equation (2). According to the manufacturer, the accuracy of the total gas volume $V_{out,SATP}$ which passed through the gas meter in time t is given by

$$\Delta_{V_{out,SATP}}[\%] = \frac{0.8\%\frac{V_{out,SATP}}{t} + 0.2\% Q_{Full\ scale}}{\frac{V_{out,SATP}}{t}}\ ,\ Q_{Full\ scale} = 20\ L/min \qquad (4)$$

With $Q_{Full\ scale}$ the highest gas flow measurable by the device. This error is between 2.5 and 8.5 % in the deep water due to the high full scale value of the gas meter. Thus the contributions of the hanging scales and the pressure gauge (both 0.1 % accuracy) are negligible in comparison and we can state

$$\Delta_{Q_{gas}} = \Delta_{V_{out,SATP}} = 2.5 - 8.5\ \% \qquad (5)$$

d) Water flow

We used a 5 L bucket with labelling every 50 mL, usually filled to 3 to 4 L. Experiments in the laboratory show a positive bias of 3 % and random fluctuations of ± 1 % (Figure A4). The positive bias was corrected by multiplying the measured water flow by 0.97. We estimated the accuracy of the corrected water flow to be ± 1 %.

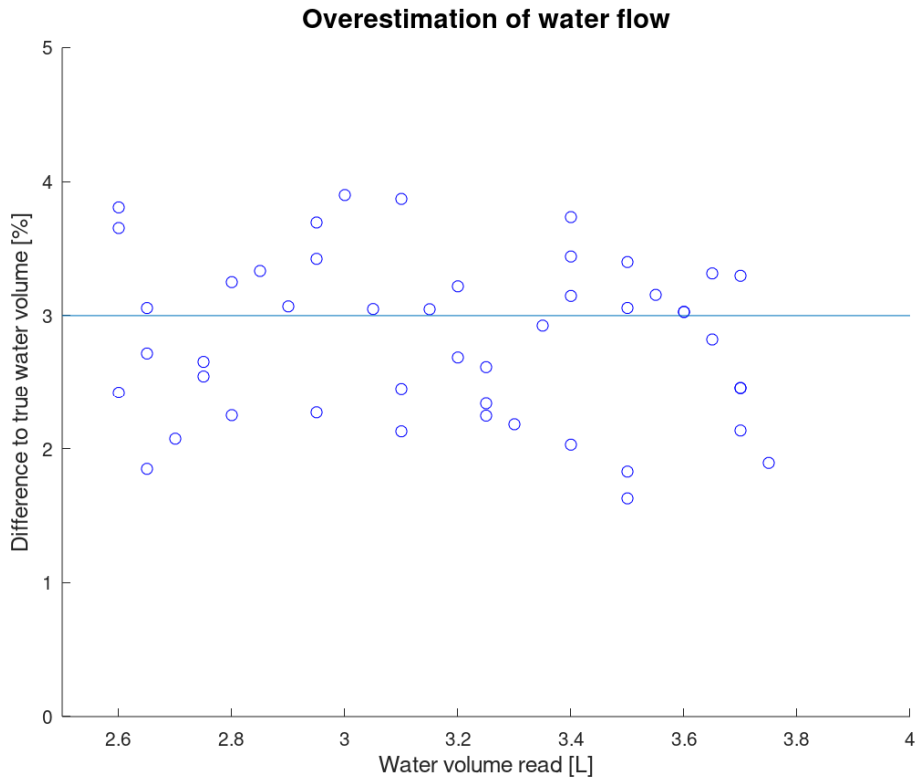

Figure A4: Bias and uncertainty of water flow measurement. A laboratory scale was used to estimate the true water volume.

Total accuracy

We estimated the individual accuracies above, so the true values of the individual measurements (Q_{gas}, Q_{water} and MS measurement) should lie within those limits. In the worst case, we will either underestimate or overestimate the true value of all those individual measurements at the same time. Assuming that all individual errors are small, the maximum uncertainty of the gas amount contained only in the gas phase is given by the sum of the relative errors. We give here an example for the calculation of the uncertainty of CH_4 and CO_2 at 410 m depth.

CH_4:

$$\Delta_{CH_4} = \Delta_{Q_{gas}} + \Delta_{Q_{water}} + \Delta_{Conc.} = 9.2\ \% \quad (6)$$

$$\text{with} \quad \Delta_{Q_{gas}} = 2.7\ \%, \qquad \Delta_{Q_{water}} = 1\ \%, \qquad \Delta_{Conc.} = 5.5\ \%$$

This means that in the worst case, the true value in the gas phase is under- or overestimated by around 9 %. The error contribution from the CH_4 remaining in the water phase is neglected as it is around 1 % of the total CH_4.

CO_2:

The uncertainty of the CO_2 measurement is a weighted sum of the uncertainties in the gas and water phase respectively

$$\Delta_{CO_{2\,gas}} = \Delta_{Q_{gas}} + \Delta_{Q_{water}} + \Delta_{Conc.} = 5.2\ \% \quad (7)$$

$$\text{with} \quad \Delta_{Q_{gas}} = 2.7\ \%,\ \Delta_{Q_{water}} = 1\ \%,\ \Delta_{Conc.} = 1.5\ \%$$

$$\Delta_{CO_{2\,water}} = \Delta_{Conc.} + \Delta_{\mathrm{Henry}} = 4.5\ \% \quad (8)$$

$$\text{with} \quad \Delta_{Conc.} = 1.5\ \%,\ \Delta_{Henry} = 3\ \%$$

Therefore, the accuracy of CO_2 is the weighted average of equations (7) and (8), closer to equation (7) in the deep water and almost equal to equation (8) at the lake surface.

In general, the uncertainty of CH_4 is around 10 % and around 5 % for CO_2 in the deep water (below 250 m).

References:

Brennwald, M. S., Schmidt, M., Oser, J., and Kipfer, R. (2016). A portable and autonomous mass spectrometric system for on-site environmental gas analysis. *Environmental Science & Technology*, *50*(24), 13455-13463.

Moore, J. C., Battino, R., Rettich, T. R., Handa, Y. P., and Wilhelm, E. (1982). Partial molar volumbes of gases at infinite dilution in water at 298.15 K. *Journal of Chemical and Engineering Data*, *27*(1), 22-24.

Rettich, T. R., Handa, Y. P., Battino, R., and Wilhelm, E. (1981). Solubility of gases in liquids. 13. High-precision determination of Henry's constants for methane and ethane in liquid water at 275 to 328 K. *The Journal of Physical Chemistry*, *85*(22), 3230-3237.

Robinson R. A. (1954). The vapour pressure and osmotic equivalence of sea water. *Journal of the Marine Biological Association of the United Kingdom* 33(2): 449-455.

Ross, K. A., Gashugi, E., Gafasi, A., Wüest, A., & Schmid, M. (2015). Characterisation of the subaquatic groundwater discharge that maintains the permanent stratification within Lake Kivu; East Africa. *PloS one*, *10*(3), e0121217.

Weiss, R. (1974). Carbon dioxide in water and seawater: the solubility of a non-ideal gas. *Marine Chemistry*, *2*(3), 203-215.

Wüest, A., G. Piepke, and J. D. Halfman (1996), Combined effects of dissolved solids and temperature on the density stratification of Lake Malawi, in *The Limnology, Climatology and Paleoclimatology of the East African Lakes*, edited by T. C. Johnson and E. O. Odada, pp. 183–202, Gordon and Breach, New York.

Yamamoto, S., Alcauskas, J. B., and Crozier, T. E. (1976). Solubility of methane in distilled water and seawater. *Journal of Chemical and Engineering Data*, *21*(1), 78-80.

Appendix A2. Calculation of salinity effect of Lake Kivu dissolved solids

The dependence on salinity of the Henry coefficient has been derived for sea salt. However, the dissolved salts in Lake Kivu mainly consist of bicarbonates of Na, Mg, K, and Ca. We assume that the salinity effect mainly depends on the ionic strength of the solution. For seawater, the ionic strength I (mol/kg) can be calculated from unit less (i.e., kg/kg) salinity as $I = C_2 * \frac{S}{1-S}$ (IOC et al., 2010) with C_2 = 19.8272 mol/kg. Since both the salinity correction of the Henry coefficient and the ionic strength in Lake Kivu are small, we can neglect the denominator and replace S in equation (2) by 1000 g/kg * I/C_2. The ionic strength in Lake Kivu was calculated as a function of conductivity, based on the observed average concentrations of the main dissolved ions and conductivities given in Tables 2 and 3 of Ross et al. (2015). A linear regression forced through the zero point resulted in an equation of I = C_3 κ_{25} (R^2 = 0.985), where κ_{25} (mS/cm) is the conductivity corrected to a standard temperature of 25 °C, and C_3 = 0.0173 (mol/kg)/(mS/cm). In summary, this results in the following equation for the Henry coefficients of CO_2, CH_4 and N_2 in Lake Kivu:

$$ln(K_i) = A_1 + A_2(100/T) + A_3\, ln(T/100) + C_1\kappa_{25}[B_1 + B_2(T/100) + B_3(T/100)^2]$$

where C_1 = 1000*C_3 /C_2 = 0.8725 (g/kg)/(mS/cm). Altogether, water with a conductivity of 1 mS/cm in Lake Kivu has about the same ionic strength as seawater with a salinity of 0.8725 g/kg. Finally, it should be noted that for CO_2, this Henry coefficient is the ratio between the fugacity of CO_2 and the concentration of the dissolved undissociated aqueous CO_2, often referred to as H_2CO_3 . For calculating the total dissolved CO_2, the concentration of bicarbonate (HCO_3^-) and carbonate (CO_3^{2-}) would have to be added.

Appendix A3. Octave scripts for conversion of concentration to partial pressure

This appendix is a long document full with octave code. Therefore, it is not included in this dissertation. However, it can be found in the supporting information of the original publication (https://doi.org/10.1371/journal.pone.0237836), or requested from the author.

Appendix B: Supporting information to chapter 4

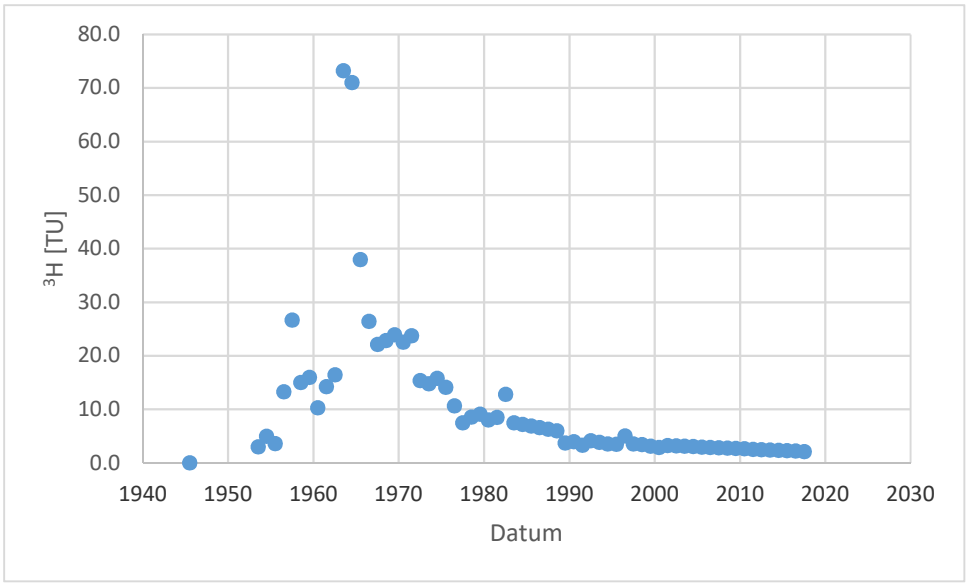

Figure B1. ^{3}H input function used for Lake Kivu. The data shown is aggregated from several stations across Africa due to scarce availability of data in the Lake Kivu region

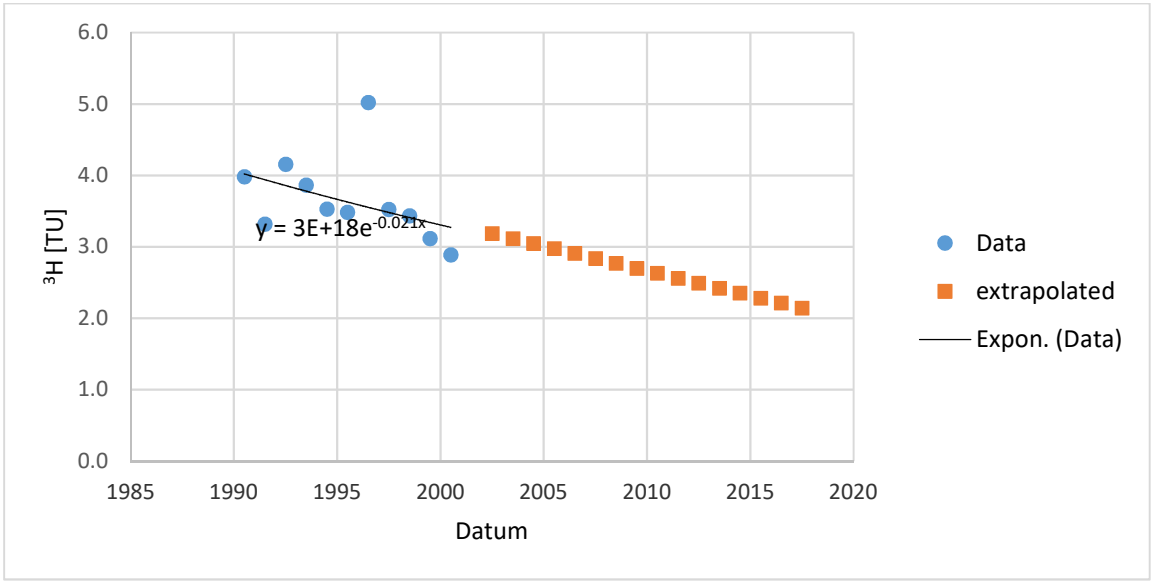

Figure B2. Extrapolation of ^{3}H concentrations in precipitation to 2018

Table B1. Simstrat-AED2 configuration parameters used throughout this work

Simstrat configuration	Name in config file	Value
k-epsilon closure model	Turbulence model	1
Fluxes are parameterized below 120 m	Apparent diffusivity	1
Seiche parameter is constant in time	Split seiche parameter	False
Quasi-equilibrium	Stability function	2
No-flux condition	Flux condition	1
Wind, temperature, solar radiation, vapor pressure and incoming long wave	Forcing	5
No wind filtering	UseFilteredWind	False
Integral normalization	SeicheNormalization	2
According to Wüest and Lorke, 2003	WindDragModel	3
Inflow plunges according to density	InflowMode	2
To avoid resonance due to low latitude	PressureGradients	2
Albedo is computed according to Grishchenko in Cogley, 1979	UserDefinedWaterAlbedo	False
No feedback by bioshading on light absorption	Bioshading	0
Sediment flancs also interact with water column	Benthic interaction mode	1

Table B2. Simstrat model parameters used throughout this work. Calibrated parameters are tuned manually with the goal of producing a steady-state simulation which matches today's observations of temperature, salinity and gas concentrations.

Simstrat Parameter	Name in config file	Value	Units	Calibrated
Number of grid cells	Grid	243	-	-
Simulation timestep	Timestep s	300	s	-
Light absorption coefficient	"read from file"	0.27	m^{-1}	No
Latitude	lat	-2	°N	No
Air pressure	p_air	855	mbar	No
Fraction of wind that goes into seiche energy	a_seiche	0.0027	-	Yes
Parameter for distribution of seiche energy	q_nn	1.6	-	Yes
Wind correction factor	f_wind	2.4	-	Yes
Wind drag parameter	c10	1.0	-	No
Bottom drag coefficient	cd	0.002	-	No
Geothermal heat flux	hgeo	0.13	W m^{-2}	Yes
Fit parameter for incoming short wave radiation	p_sw	0.95	-	Yes
Fit parameter for incoming long wave radiation	p_lw	0.95	-	Yes
Fit parameter for convective and latent heat fluxes	p_windf	1.0	-	No
Fraction of short wave radiation absorbed as heat	beta_sol	0.35	-	No

Table B3. Selected AED2 model parameters used throughout this work. Calibrated parameters are tuned manually with the goal of producing a steady-state simulation which matches today's observations of temperature, salinity and gas concentrations.

Selected AED2 parameters	Name in AED2 config file	Value	Units	Calibrated
Atmospheric CO_2 mixing ratio	Atm_co2	410e-6	-	No
Atmospheric CH_4 mixing ratio	Atm_ch4	1.9e-6	-	No
CH_4 sediment flux	Fsed_ch4	3.2	mmol m^{-2} d^{-1}	Yes
Half saturation O_2 for CH_4 flux	Ksed_ch4	100	mmol m^{-3}	No
Temperature multiplier of CH_4 flux	theta_sed_ch4	1	-	No
Maximum rate of CH_4 oxidation	Rch4ox	0.01	mmol m^{-3} d^{-1}	No
Half saturation O_2 concentration for CH_4 oxidation	Kch4ox	10	mmol m^{-3}	No
Temperature multiplier of CH_4 oxidation	vTch4ox	1	-	No

Table B4. Main properties of inflowing groundwater. All properties are manually calibrated to reach a steady-state after a simulation duration of around 500 years. "CH_4 a)" is used in Figures 4.5d) and 4.7d), and "CH_4 b)" in Figures 4.5e) and 4.7e).

Description	Inflow depth m	Discharge $m^3\ s^{-1}$	Temperature °C	Salinity $g\ kg^{-1}$	CO_2 $mmol\ L^{-1}$	CH_4 a) $mmol\ L^{-1}$	CH_4 b) $mmol\ L^{-1}$
Surface tributaries	0	63	21.5	0.1	0	0	0
Distributed inflow	90 – 195	23.6	21.0	2.2	6.8	0	0
Point source	190	6	21.0	2.2	6.8	0	0
Point source	253	11	22.6	2.6	11.7	0	0
Point source	310	1.5	26.0	4.4	45.6	0	7
Point source	330	0.6	26.0	5.6	76.5	0	7
Point source	400	1	25.6	5.7	86.2	0	10
Point source	430	1.2	25.7	6.0	91.1	0	10

Table B5. Hydrogen isotope and neon concentrations of inflowing groundwater. For ^3H, the concentrations are adjusted to match the observed profile in 2018, with the inflows at 190 and 253 m being a mixture of young groundwater with atmospheric ^3H and old groundwater with a background concentration of 0.5 TU. δ^2H and Ne values are adjusted to produce a steady-state simulation within ~500 years.

Description	Inflow depth m	Discharge $m^3\ s^{-1}$	^3H TU	δ^2H ‰ VSMOW	Ne ccSTP g^{-1}	Ne % of ASW
Surface tributaries	0	63	Input function	-4.5	1.55e-7	100
Distributed inflow	90 – 195	23.6	45 % * Input function 60 % * 0.5	30	1.47e-7	95
Point source	190	6	45 % * Input function 60 % * 0.5	30	1.47e-7	95
Point source	253	11	20% * Input function 80% * 0.5	23.5	1.39e-7	90
Point source	310	1.5	0.5	22	9.0e-8	58
Point source	330	0.6	0.5	13	9.0e-8	58
Point source	400	1	0.5	11	8.0e-8	52
Point source	430	1.2	0.5	11	7.5e-8	48